5-1-2010

The aortic valve endothelial cell: a multi-scale study of strain mechanobiology

Scott Andrew Metzler

THE AORTIC VALVE ENDOTHELIAL CELL:

A MULTI-SCALE STUDY OF STRAIN

MECHANOBIOLOGY

By

Scott Andrew Metzler

A Thesis
Submitted to the Faculty of
Mississippi State University
in Partial Fulfillment of the Requirements
for the Degree of Doctor of Philosophy
in Biomedical Engineering
in the Department of Agricultural and Biological Engineering

Mississippi State, Mississippi

May 2010

THE AORTIC VALVE ENDOTHELIAL CELL:

A MULTI-SCALE STUDY OF STRAIN

MECHANOBIOLOGY

By

Scott Andrew Metzler

Approved:

James N. Warnock Assistant Professor Committee Chair	Jerome A. Gilbert Provost Committee Member
Shane C. Burgess Associate Dean, CVM Director, LSBI Committee Member	Jun Liao Assistant Professor Committee Member
Allen Crow Assistant Professor Committee Member	
Steve Elder Associate Professor Graduate Coordinator	Sarah Rajala Dean of Bagley College of Engineering

Name: Scott Andrew Metzler

Date of Degree: 84BMay 2010

Institution: Mississippi State University

Major Field: Biomedical Engineering

Major Professor: James N. Warnock

Title of Study: THE AORTIC VALVE ENDOTHELIAL CELL: A MULTI-SCALE STUDY OF STRAIN MECHANOBIOLOGY

Pages in Study: 162

Candidate for Degree of Doctor of Philosophy

The aortic valve (AV) functions in arguably the most demanding mechanical environment in the body. The AV experiences fluid shear stress, cyclic pressure and mechanical strain in vivo. Recent evidence has shown the progression of degenerative aortic valve disease (AVD) to be an active cellular mediated process, altering the conception of the AV as a passive tissue. AVD has shown a strong correlation with altered hemodynamics and tissue mechanics. Aortic valve endothelial cells (AVECs) line the fibrosa (aortic facing) and ventricularis (left ventricle facing) surfaces of the valve. AVECs sense and respond to circulating stimuli in the blood stream while maintaining a non-thrombogenic layer. AVEC activation has been implicated in the initiation and progression of AVD, but the role of cyclic strain has yet to be elucidated.

The hypothesis of this dissertation is that altered mechanical forces have a causal relationship with aortic valvular endothelial cell activation. To test this hypothesis 1) the role of in vitro cyclic strain in regulating expression of pro-inflammatory adhesion molecule was elucidated 2) cyclic strain-dependent activation of side-specific aortic valve

endothelial cells was investigated 3) a novel stretch bioreactor was developed to dramatically increase the ability to correlate valvular endothelium response to physiologically relevant applied planar biaxial loads.

The results from this study further the field of heart valve mechanobiology by correlating AVEC physiological and pathophysiological function to cellular and tissue level strain. Elucidating the AVEC response to an altered mechanical environment may result in novel clinical diagnostic and therapeutic approaches to the initiation and progression of degenerative AVD. Furthermore, a cardiovascular health outreach program, Bulldogs for Heart Health, has been designed and implemented to combat the startling rise in childhood obesity in the state of Mississippi. It is the hope that these results, novel methods, and outreach initiatives developed will significantly impact the study of the mechanobiology of the aortic valve endothelial cell and potential treatment and prevention of cardiovascular disease.

DEDICATION

This work is dedicated to my mother, Christine, my father, Larry, and my brother Brian. They are my best friends and undoubtedly the source of my inspiration. My deep and sincere gratitude for the role of my extended family in Arizona, California, Colorado, Hawaii, and Minnesota, could be the subject of another dissertation entirely. My Aunt Susan deserves great appreciation and special recognition for masterminding my academic career, and my Aunt Wendy for lending me the sanity and perspective to see it through. To Candace, your patience and support in finishing this dissertation was nothing short of remarkable and saying thank you merely scratches the surface. To my network of truly remarkable friends in South Tampa, La Jolla, San Francisco, Starkville, and Nashville; challenging each other to grow has been the honor of my life.

ACKNOWLEDGEMENTS

I would like to acknowledge the incredible students and staff of Mississippi State University. The entire Agricultural and Biological Engineering Department, Bill Monroe and Amanda Lawrence at the Electron Microscope Center, the gifted researchers at the College of Veterinary Medicine and the Life Sciences and Biotechnology Institute, all have been instrumental to this work. Steven Waller, Lester Jones, Chris Digesu, and Joel Howard, deserve special recognition for their dedication and effort. Kimberly Schipke has been an incredible contributor to this work, especially Bulldogs for Heart Health, and needs a standing ovation for her brilliance and perseverance.

TABLE OF CONTENTS

Page

LIST OF TABLES

LIST OF FIGURES

LIST OF ACRONYMNS

AV=Aortic Valve

AVD=Aortic Valve Disease

CVD= Cardiovascular Disease

CAS= Calcific Aortic Stenosis

PAVIC=Porcine Aortic Valve Interstitial Cell

PAVEC= Porcine Aortic Valve Endothelial Cell

FEC=Fibrosa Aortic Valve Endothelial Cell

VEC= Ventricularis Aortic Valve Endothelial

ICAM-1= Intracellular Adhesion Molecule 1

VCAM-1= Vascular Cellular Adhesion Molecule 1

MCP-1= Monocyte Chemoattractant Protein 1

PECAM-1= Platelet Endothelial Cell Adhesion Molecule 1

ROS= Reactive Oxygen Species

TVP=Transvalvular Pressure

LSM=Laser Scanning Microscopy

CHAPTER I

INTRODUCTION

1.1 The Human Heart

The human heart functions to circulate oxygenated blood throughout the body. The heart accepts deoxygenated blood from the systemic circulation and directs it to the lungs. Oxygenated blood returns to the heart and is consequently ejected to the body. This is accomplished by the concerted action of four chambers. Two chambers accept blood, the atria, while two chambers expel blood, the ventricles. The left and right side of the heart each consist of two chambers. The path of directional blood flow begins in the right atrium, which collects blood from the body, and in turn directs flow into the right ventricle. The right ventricle then sends blood through the pulmonary artery to the lungs. Oxygenated blood returns to the heart via the left atrium. The left atrium directs the blood into the left ventricle, where it is ejected through the aorta to the systemic circulation via the great arteries, or returns to the heart through the coronary circulation. A diagram of the human heart is seen in Figure 1.

The unidirectional flow of blood through the heart is made possible by the function of the heart valves (HV). Heart valves are fibrous structures that passively move in response to mechanical cues in the form of blood flow and pressure. The four HV are classified as atrioventricular valves or semilunar valves. The atrioventricular valves, deemed for their residence between the atria and ventricles, consist of the mitral valve

(MV) and tricuspid valve (TV). The semilunar valves are composed of three half-moon shaped cusps. The aortic valve (AV) functions between the left ventricle and aorta, while the pulmonary valve (PV) is situated between the right ventricle and the pulmonary artery.

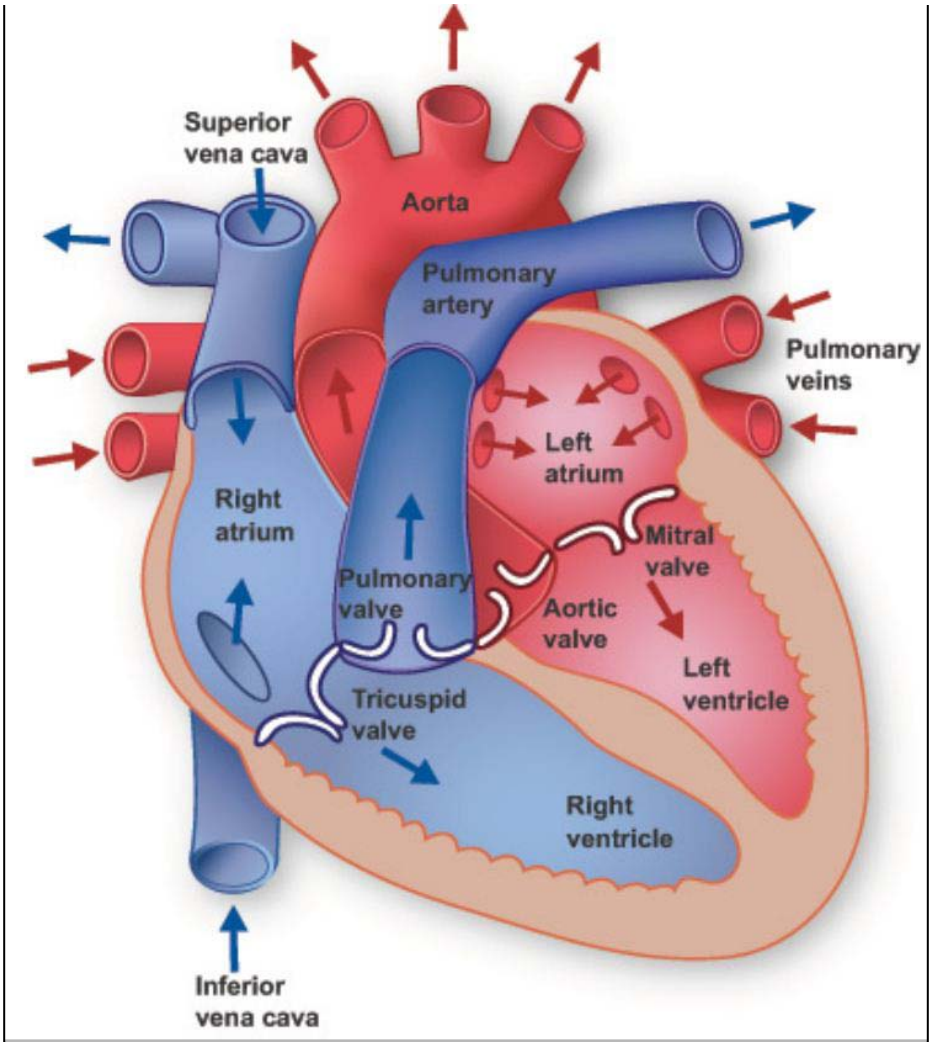

Figure 1 The anatomy of the human heart. The right side of the heart is depicted in blue and the left side in red. From (texasheartinstitute).

The cardiac cycle is the term given to the bi-phasic function of the heart. The stages, systole and diastole, are most often characterized in regard to ventricular function. Systole represents ventricular contraction and subsequent ejection of blood. During this phase, the atrioventricular valves are closed, and blood freely passes through the semilunar valves out of the pulmonary artery and aorta (Figure 2A). The closure of the AV valves prevents blood from entering the atria. As the ventricles conclude their ejection, systole ends, and diastole begins. Diastole, or ventricular filling, causes the semilunar valves to close, while the atrioventricular valves are open to allow blood to pass from the atria and fill the ventricles (Figure 2B).

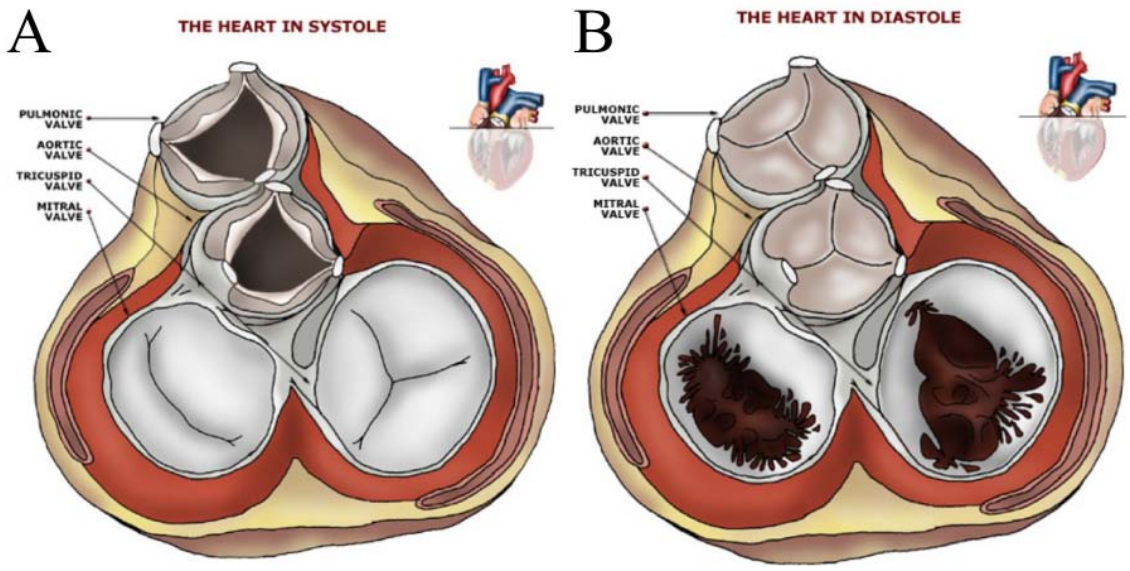

Figure 2 The heart in systole (A) and diastole (B). Note the open (A) configuration and closed (B) position of the semilunar valves. From (prenhall.com).

1.2 The Aortic Valve

1.2.1 Structure and Function

The aortic valve (AV) functions to allow for unimpeded ejection of blood out of the left ventricle during systole while preventing retrograde blood flow during ventricular filling, or diastole. The AV must fully open and close each cardiac cycle, which can occur in excess of 3 billion times over the average lifespan. Blood volume that passes through the aortic valve can vary from 1-20L per minute (1). Average blood flow volume through the aortic valve at rest is 5L/min. The AV function relies on the intricate relationship with the aortic root, the structure that connects the heart to the systemic circulation. The aortic root consists of the annulus, sinotubular junction, sinuses of Valsalva, inter-leaflet triangles, and the aortic valve leaflets. The dynamic interaction of the aortic root structures dictates left ventricular function and coronary perfusion. The situation of the AV in relation to the aortic root can be seen in Figure 3. The AV is a tricuspid structure, or consisting of three leaflets or cusps. The terminology of the valve cusps remains debatable, hence, both 'leaflet' and 'cusp' will be used throughout this dissertation to denote the portion of the aortic valve extending out from the commissure point to the aortic root and extending into the lumen of the aorta. Two of the AV leaflets have coronary ostia initiating from the sinus of Valsalva, or a bulge distal to the AV. These coronary ostia are the passageway to the coronary arteries, and the AV leaflets have developed their nomenclature based on relation to the ostia. The three leaflets are the non-coronary, the left coronary, and the right coronary cusp. Slight structural and functional differences have been found between the leaflets. The non-coronary leaflet tends to be the largest in size, followed by the left and right coronary cusps (2), although

the differences were not found to be statistically significant. Individual valve leaflets can be characterized by four primary structural domains. The hinge region physically joins the AV leaflet to the aortic root. The belly region is suspended freely during diastole, while the coapting surface of each leaflet creates a seal that prevents diastolic regurgitation. Extending slightly above the coapting region is the lanula, which contains a small triangle of fibrous tissue, the nodule of Arantii. These structures have all been associated with efficient and complete closure in healthy AV.

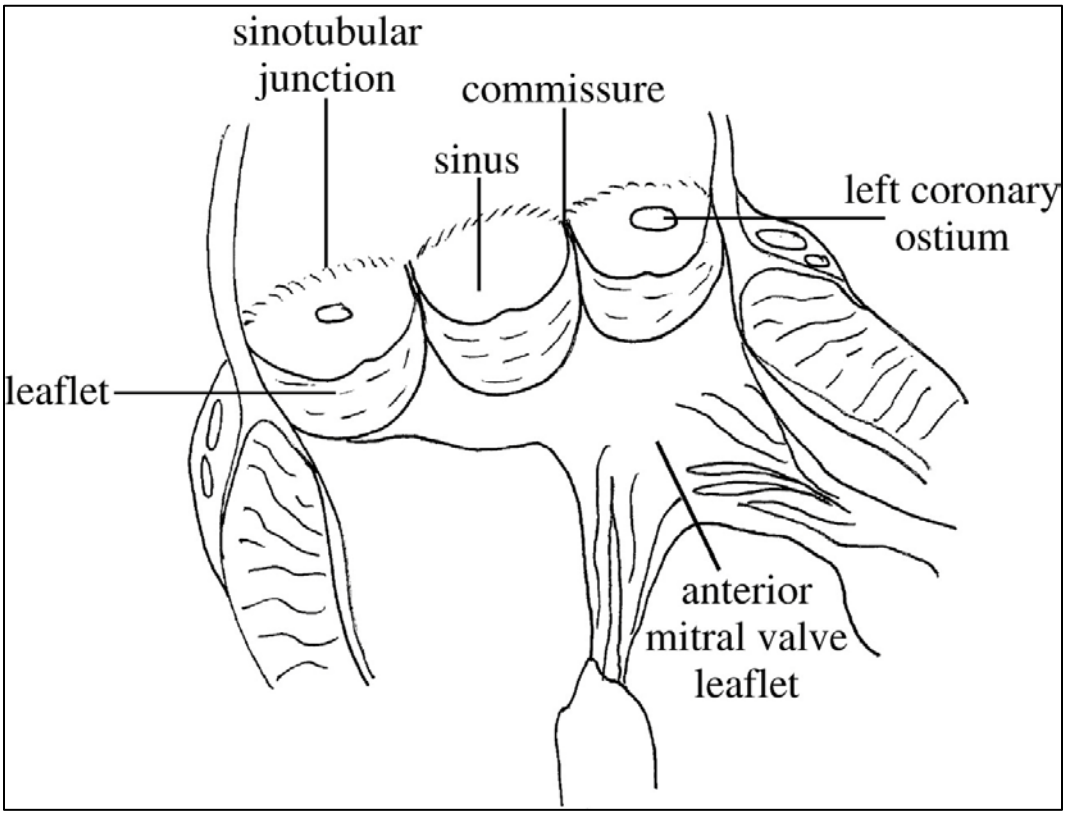

Figure 3 The aortic valve cusps and aortic root structures. The AV leaflets are shown following longitudinal opening of the aortic root through a commissure point. From (1).

The nutrient supply of the AV is derived from passive diffusion from the blood stream, and can be considered predominantly avascular. Evidence for vascularization exists in the hinge region, where the leaflet is thicker than 0.5mm. The belly and commissure regions range from 0.36 to 0.48mm in thickness, decreasing in thickness from the aortic root to the free edge, and lack any signs of vascularization (3;4).

The aortic valve has an elegant and complex structure optimized for a relatively simple function of regulating unidirectional flow. The fibrous components of the valve allow for remarkable tissue flexibility while exhibiting tremendous mechanical strength. The AV is a tri-layered structure, consisting of the aortic facing fibrosa, internal spongiosa, and ventricularis on the left ventricle facing surface (5).

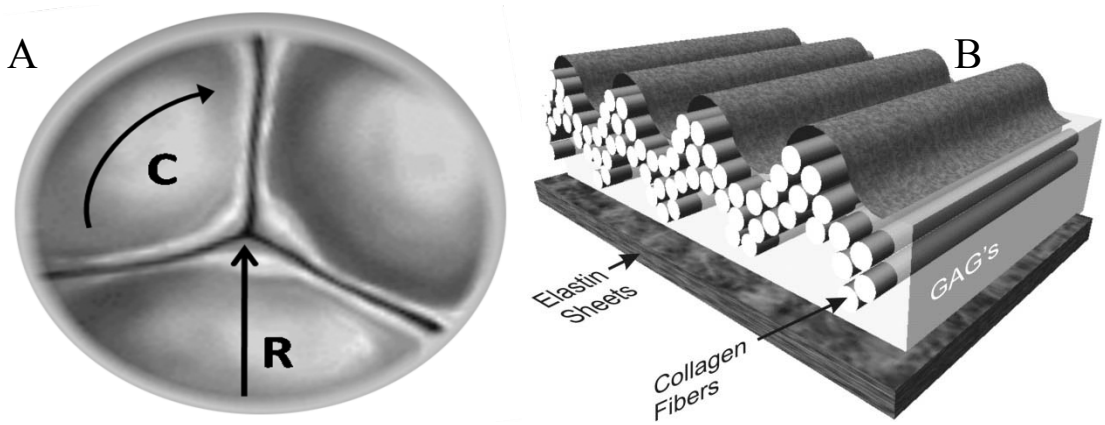

Figure 4 (A) Aerial view of AV during diastole depicting common directional nomenclature, circumferential (C) and radial (R). Schematic of structural hierarchy of AV (B). Collagen fibers are oriented circumferentially and compose the bulk of the fibrosa, while the elastin meshwork makes up the majority of the ventricularis. Adapted from (6).

The extracellular matrix of the valve is composed of directionally oriented collagen and elastin fibers. Directional notation and a schematic of the AV extracellular matrix is shown in Figure 4. The collagen fibers are dominant in the fibrosa, and bear most of the mechanical stresses in the AV during diastole. The fibrosal collagen dominates the mechanical response of the AV to loads applied in the circumferential direction. The spongiosa consists of glycosaminoglycans, primarily serving to connect the two surface layers while providing force reduction and dissipation properties (7). The ventricularis dictates the force-transition state of the AV in the radial direction. The layers of the valve are in a preloaded state, where the fibrosa is under compression and the ventricularis is under tension (8). The preload can be attributed to the intrinsic mechanical characteristics of collagen and elastin. Collagen is extremely resistant to tensile stress but shows no resistance to compression, instead adopting a crimped or wavy structure. In contrast, elastin is properly named for its highly elastic response, and can be thought of as a coiled spring in compression. The ventricularis is believed to serve in maintaining the spatial configuration of collagen fibers during the cardiac cycle. The valve is also composed of 60-70% water by weight and is assumed to be incompressible, evidenced by the fact that compressing the valve does not expel any fluid(14;15) .

1.2.2 Mechanical Environment

The aortic valve functions in a dynamic, complex, and demanding mechanical environment. Left ventricular ejection during systole imposes a fluid shear stress on the AV via blood flowing through the valve at a peak rate of 1.35+/-0.35m/s (9). The wall shear stress experienced by the surfaces of the leaflet have been reported as low as 20

dynes cm^{-2} and as high as 1000 dynes cm^{-2} (10-12). The fluid shear on the ventricularis is characterized as pulsatile and unidirectional, in contrast to the fibrosa, where local vortices are formed behind the leaflet. The disturbed flow pattern creates a recirculating shear stress on the fibrosa. The magnitude of fluid shear is far lower on the fibrosa, although the flow pattern is much more complex.

The AV also experiences a significant transvalvular pressure (TVP) when the leaflets coapt following systole. 80mmHg represents a physiological TVP, while 100 and 120mmHg represent the classification of diastolic blood pressure for stage I and stage II hypertension, respectively. A pressure gradient is sufficient for closure of the valves, independent of blood flow. This is most likely due to the radial orientation of the elastin fibers on the ventricularis, which extend inward when the inertial force of blood flowing through the valve has receded.

The relationship between stress and strain in the AV is one of the more complex in the human body. The TVP dictates the strain state of the AV. Strain levels are reported in two directions, the radial and circumferential, and vary greatly in magnitude. The variant response of a biological soft tissue to stress in two different directions is classified as anisotropic. The anisotropic strain response can be attributed to the aligned fibers that make up the extracellular matrix. The valve is significantly stiffer in the circumferential direction, due to the high tensile strength of collagen, see Figure 5. A study of collagen fibril response to strain at the molecular level by Liao et al has elucidated the intrinsic elasticity of collagen fibrils(13). The study found that collagen fibrils underwent strain at the end of the non-linear region of the stress-strain curve only. The study suggested that valvular collagen fibrils are intrinsically elastic, and therefore only experience loading

after the larger collagen fibers are fully straightened. The graph of the stress strain curve becomes non-linear at this transition point. Thus, the mechanical response of aortic valves is termed as anisotropic non-linear.

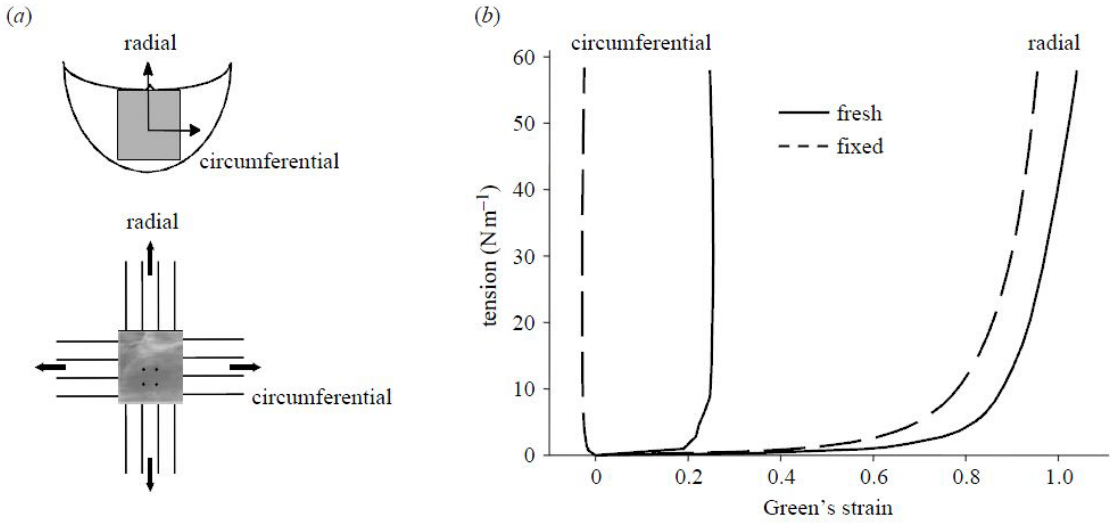

Figure 5 (A) Biaxial testing setup and (B) strain versus membrane tension graph of an aortic valve under planar biaxial stretch. Note the marked anisotropy displayed by the dramatic differences in radial and circumferential extensibility. From (16).

1.2.3 Aortic Valve Interstitial Cells

The AV consists of two cell types, the endothelial cells that line the surface, and the interstitial cells which populate the interstitium of the valve. The aortic valve interstitial cells (AVICs) are a heterogenous population, consisting of fibroblasts, smooth muscle cells, and myofibroblasts. The majority of interstitial cells in a non-remodeling AV are characterized as quiescient fibroblasts, and do not express smooth muscle actin, an indication of a smooth muscle phenotype. The interstitial cells are responsible for the remodeling of the AV by regulating the production and degradation of extracellular matrix components. AVIC has been shown to be plastic and reversible, with the activated

myofibroblast phenotype being implicated in aortic valves that are developing, remodeling, or diseased(17;18). An actively remodeling AVIC have been shown to be responsive to mechanical cues by altering the cellular stiffnes in response to local tissue stresses(19).

1.2.4 Aortic Valve Endothelial Cells

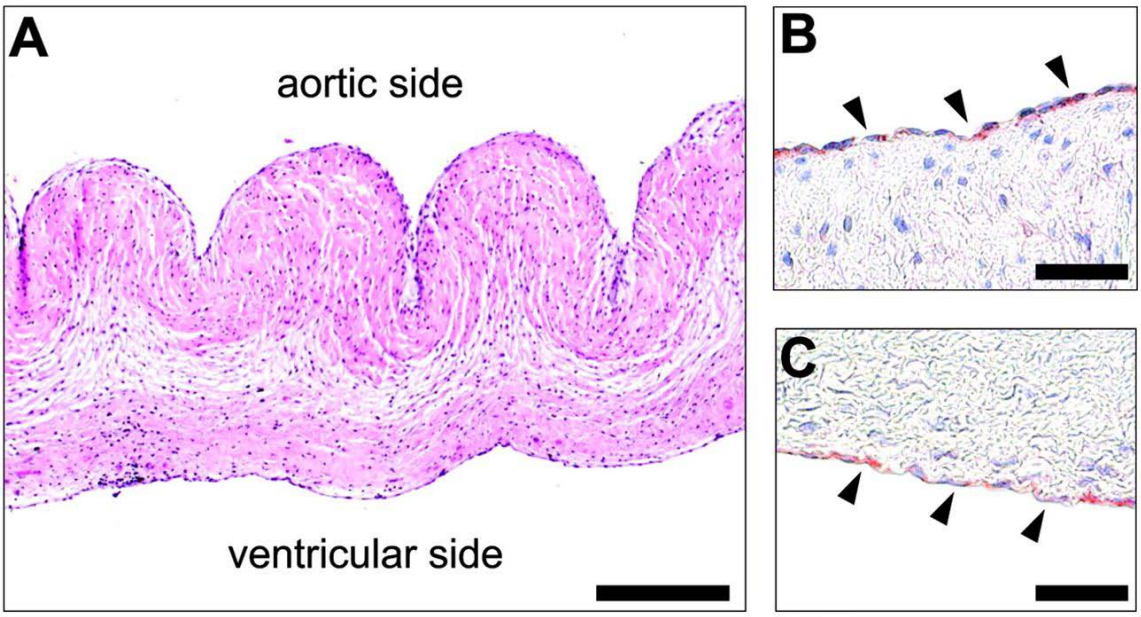

Figure 6 Endothelial cell monolayer on the aortic and ventricularis surfaces of the aortic valve are shown in cross section (A), and positively staining for von Willebrand factor on the fibrosa (B) and ventricularis (C) surfaces. From(20).

Endothelial cells (ECs) line all of the surfaces in the body that directly contact the blood. Primary functions of ECs include maintaining a non-thrombogenic surface and sensing and responding to circulating stimuli in the blood stream. ECs are inherently sensitive to changes in their hemodynamic and mechanical environments.The ECs of the

aortic valve line both the fibrosa and ventricularis surfaces. The ECs are maintained on a sub-endothelial layer consisting of fibronectin and collagen type IV(21). The sub-endothelium has been shown to be characteristically similar on both sides of the valve, with respect to height, pore diameter, pore depth, and fiber diameter.

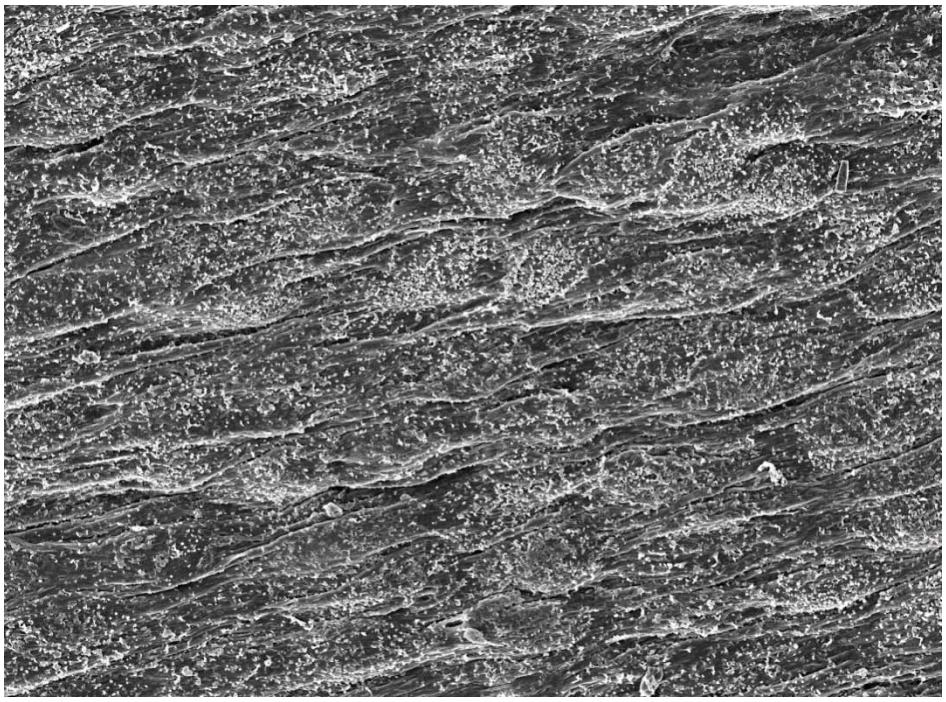

Figure 7 SEM micrograph of AVEC on the fibrosa surface creating a monolayer and oriented in the circumferential (left to right) direction.

AVECs have been shown to be incredibly mechanoresponsive to the effects of fluid shear stress, cyclic pressure, as well as cyclic strain(22). The assumption that endothelial cells from various origins along the vascular tree behave similarly when exposed to an isolated mechanical stimulus was disproved in the presence of laminar flow. Aortic endothelial cells, like most all endothelial cells, were seen to align with the direction of flow. However, aortic valvular endothelial cells were shown to align

perpendicularly to flow, indicating a distinct phenotype(23). This seminal study in the field of valvular endothelial cell mechanobiology has led to a recent surge in the study of valvular endothelial cells to mechanical forces. While the role of shear stress has been investigated thoroughly, the response of AVECs to cyclic strain has been a recent undertaking.

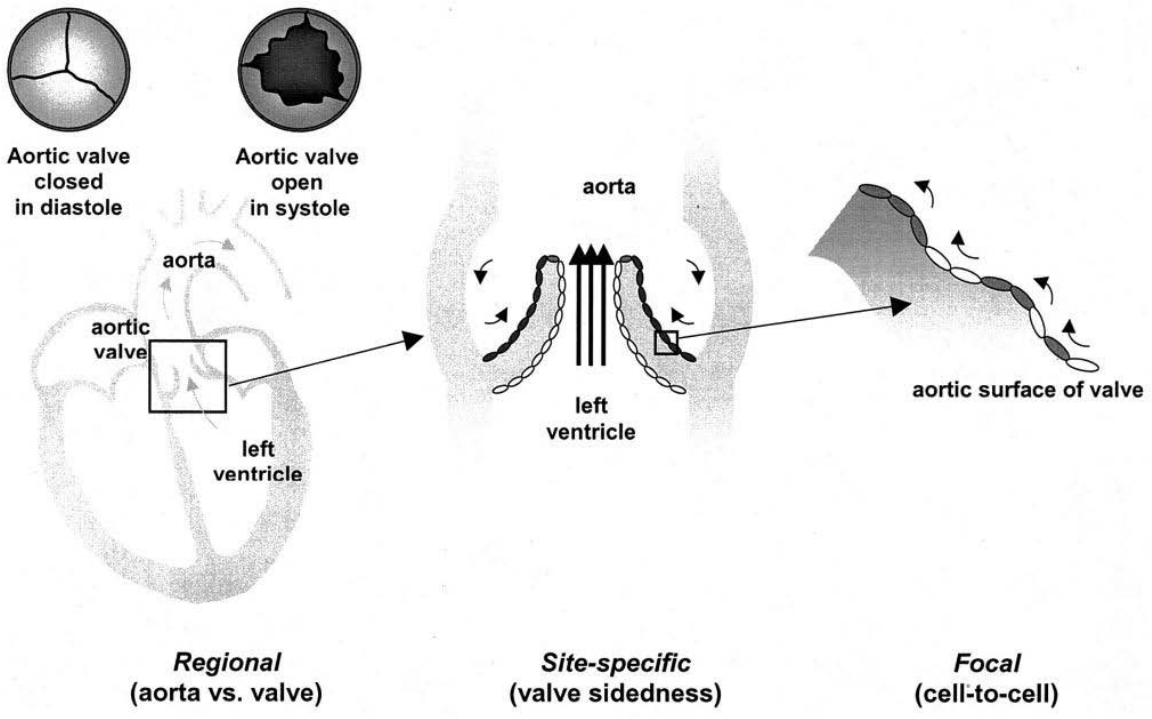

Figure 8 Schematic of the mechanical environment scale of aortic valvular endothelial cells. From (24).

1.2.5 Endothelial Cell Activation

Endothelial cells possess inherent mechanisms to become activated, or in a heightened state capable of mediating a disease process. The hallmarks of endothelial activation include generation of adhesion molecules, production of reactive oxygen species (ROS), and increased proliferation and apoptosis. The activated endothelial layer

generates specific surface molecules involved in monocyte and T-cell migration, adhesion, and congregation. The pro-inflammatory proteins include intercellular adhesion molecules (ICAM), vascular cell adhesion molecules (VCAM), and endothelial leukocyte adhesion molecules (E-Selectin or ELAM). These proteins act concurrently with chemotactic molecules, such as monocyte chemoattractant protein 1 (MCP-1), expressed by the endothelium and smooth muscle cells, to attract monocytes into the tissue. Once monocytes have migrated to the sub-endothelial space, macrophage differentiation occurs. Monocyte derived macrophages dictate the cellular inflammatory response through cytokine and chemokine secretion, and also express growth regulating factors and metalloproteinases. An aortic valve subject to a chronic inflammatory response may develop calcific lesions, similar to atherosclerotic plaques. Non-sclerotic post-mortem valves fail to express the adhesion molecules ICAM-1, VCAM-1 and E-Selectin, while the pro-inflammatory proteins are present on the endothelium of excised non-rheumatic degenerative diseased valves, as seen in Figure 10 (25;26).

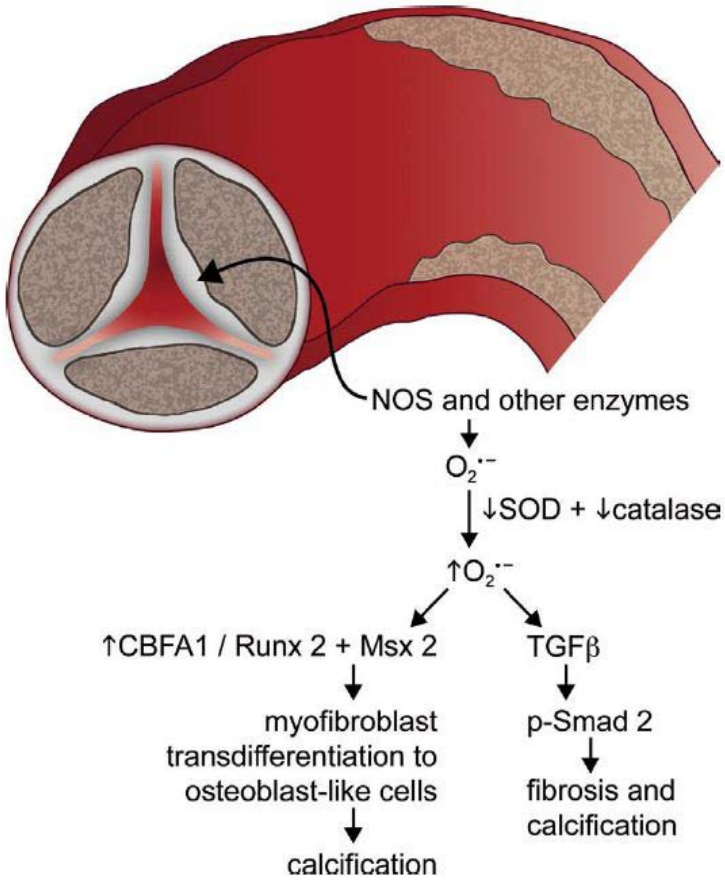

Figure 9 Oxidative stress pathway involved in calcific aortic stenosis, initiated with endothelial dysfunction(27).

The generation of reactive oxygen species (ROS) is critical to the pathophysiology of endothelial cells in the vasculature. The mechanisms for generation of ROS appear to be different in AVECs than in vascular endothelial cells(28). It is known that levels of superoxide are elevated in aortic valve stenosis, and has been shown in hypercholesterolemic mice prone to AV stenosis, as well as humans(28;29). Regulation of oxidative stress differs mechanistically between atherosclerosis and aortic valve stenosis. While NAD(P)H oxidase activity appears to be the main contributor to generation of ROS in atherosclerosis, there has been no evidence showing increased

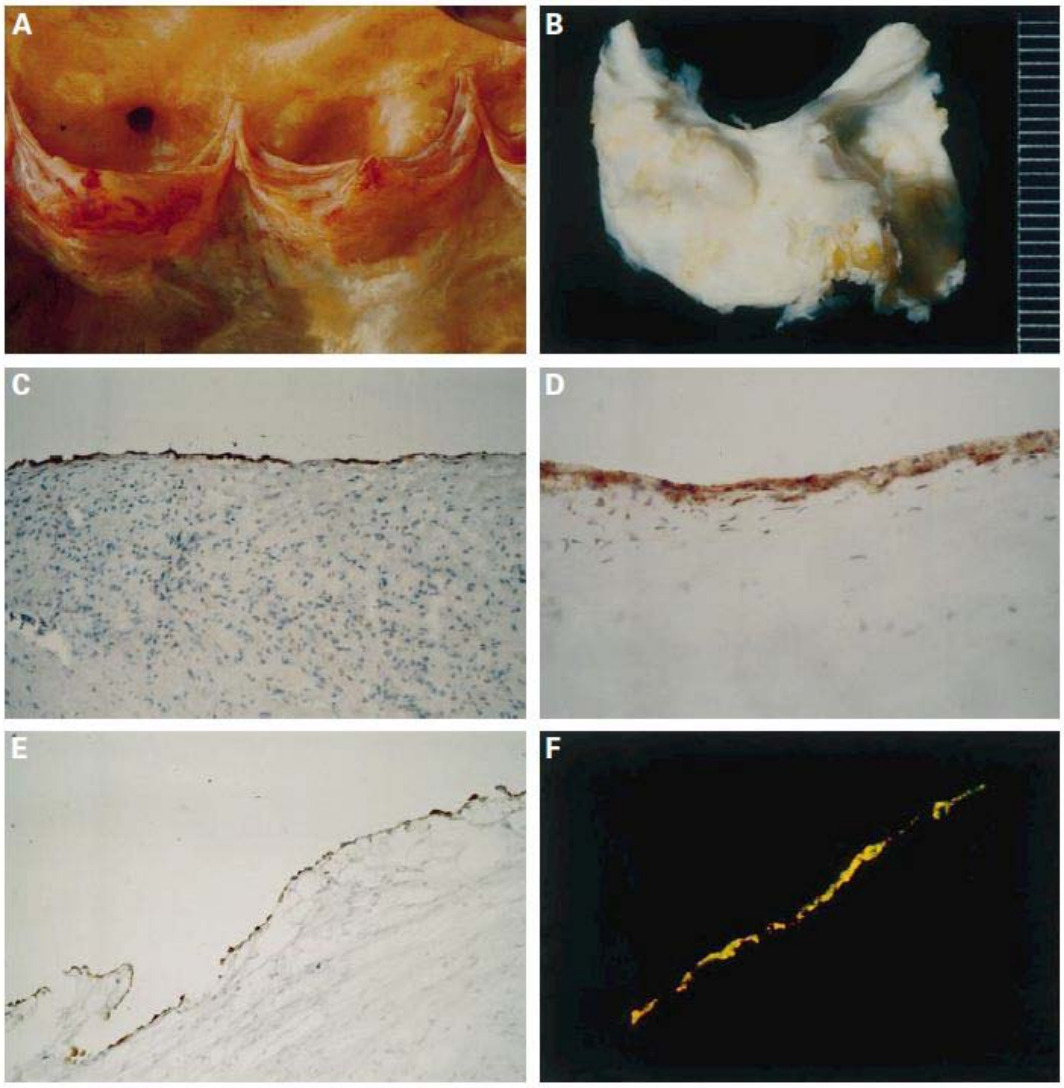

Figure 10 Diseased aortic valves depicting (A) endocarditis and (B) degenerative calcific valve disease. Both valves show an endothelium staining positive for ICAM-1 (C), E-Selectin(D), and VCAM-1 (E). E-Selectin is co-localized with FVIII, an endothelial marker (F). From(32).

NAD(P)H activity in AV stenosis(30;31). The presence of oxidative stress generally results in an increased level of superoxide dismutase (SOD), and a subsequent protection against high levels of superoxide, however, stenotic aortic valves show no such mechanism. Many fibrotic and calcific genes are regulated by oxidative stress,

typically by activation of the NF-κB pathway. The NF-κB pathway has been shown to be mechanically and biochemically regulated in vascular ECs. NF-κB and valvular EC activation could likely contribute to the initiation of degenerative aortic valve disease in a mechanical stress related manner. However, the role of the endothelial cells in regulating progression of AVD is not well known and has only recently been appreciated.

1.3 Aortic Valve Disease

The pathologies and clinical states that fall under the umbrella term of cardiovascular disease include heart failure, hypertension, stroke, myocardial infarction, angina pectoris congenital cardiovascular defects, and valve defects. 79,400,000, or 1 in 3, American adults have been diagnosed with some form of cardiovascular disease (CVD). CVD is the most common form of death in the United States. The number of deaths from all types of CVD is greater than the combined forms of cancer (Figure 11). The death rate from cardiovascular disease has declined in recent decades, however, diseases associated with increased age have seen dramatic increases in prevalence. Coronary artery bypass grafting is the most commonly performed cardiovascular operation in the United States and has been recently declining. However, the penultimate CVD related surgery in the US is replacement of the heart valves and the most commonly diseased valve is the aortic valve (AV) (33).

1.3.1 Prevalence

Total mention mortality from valvular heart disease was 43,900 in 2005. Aortic valve disorders were implicated in 27,390 of these deaths. In addition, 49,000 hospital

discharges were attributed to aortic valve disease, more than half of the 93,000 hospital discharges for all forms of valvular disease(34). The risk of a myocardial infarction and death from cardiovascular related diseases increased by 50% when aortic sclerosis was present(35). Prevalence of AV stenosis has shown a strong positive correlation with advancing age.

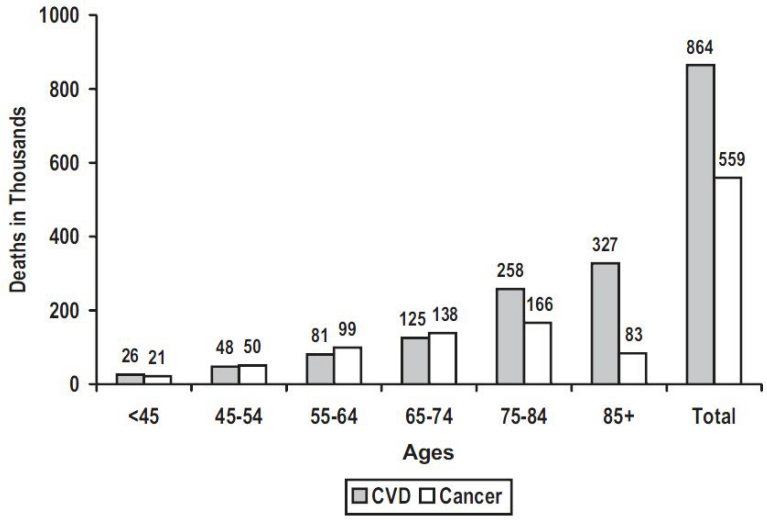

Figure 11 Deaths in the United Stated in 2005 from combined forms of cardiovascular disease compared to all forms of cancer by age. Taken from (34).

1.3.2 Aortic Valve Pathology

Aortic valve abnormalities can manifest during development (congenital valve disease) or acquired over time on a previously healthy valve (acquired degenerative valve disease). Two states of degenerative AV disease exist, aortic sclerosis and aortic stenosis. A sclerotic aortic valve shows signs of fibrosis and thickening, while not presenting an obstruction to blood flow. Aortic stenosis represents a progression of aortic sclerosis, with a significant obstruction to blood flow. The accepted model for the disease

progression is parallel to atherosclerosis. The model begins with an endothelial injury and recruitment of monocytes to the site, through production of pro-inflammatory adhesion molecules, as seen in Figure 10. Monocytes migrate to the interstitium to the valve and differentiate into macrophages. The macrophages then dictate the pathological remodeling of the valve by secreting cytokines and chemokines that lead to calcification and fibrosis of the valve. Surgical aortic valve replacement is the only current treatment for severe AV stenosis. The risk factors for valvular heart disease parallel those for atherosclerosis(36). Advanced age, male sex, hypertension, smoking, high LDL and total cholesterol levels are all known risk factors for aortic valve stenosis.

1.4 Motivation, Rationale, And Specific Aims

Aortic valve disease poses to be a significant health risk for millions of Americans today, and shows no signs of abating in the near future. Surprisingly little is known about the mechanisms underlying the disease process in aortic valves. Current methods that are adequate for vascular disease research are not directly applicable to the study of AVD, with particular regard to the valvular endothelium. This is due to the fact the AVECs are in one of the most unique environments in the vasculature. No pharmaceutical or therapeutic treatments exist for AVD specifically, instead requiring surgical intervention of end stage valve disease. The valvular endothelium is only recently getting the attention it deserves as a distinct phenotype from vascular ECs. Studies have been conducted investigating the role of fluid shear stress on the function of AVECs, and have yielded intriguing results. However, cyclic stretch is also an integral force experienced by the valve endothelium. The role of cyclic stretch and AVEC

function remains largely unexplored. *In vitro* models for application of cyclic stretch are useful in elucidating certain cellular responses, yet fail to encompass a physiological mechanical and native tissue environment. The most widely accepted method for application of cellular level stretch will be investigated for its role in EC activation, as well as to investigate the side specificity and phenotypic heterogeneity of the valvular endothelium. No methods exist for the study of the valvular endothelium in response to applied cyclic stretch on a tissue level. Given that AVECs are known to play an increasingly important role in the initiation and progression of valvular disease, there is a critical need for novel methods to observe the relationship of AVEC function and cyclic stretch. The valvular endothelium poses one of the most experimentally difficult cell types to replicate their native environment and mechanical milieu. The cells are constantly exposed to fluid shear stress, cyclic pressure, and a cyclic stretch as a function of transvalvular pressure. The cells never experience a true stress-free or static state, and *in vitro* studies have shown that statically cultured endothelial cells have an activated phenotype. Thus, dynamic in vitro and appropriate ex vivo models are necessary for investigating the endothelial response to mechanical forces.

The goals of this study are as follows: 1) elucidate the role of *in vitro* cyclic strain in regulating expression of pro-inflammatory adhesion molecules 2) investigate cyclic strain-dependent activation of side-specific aortic valve endothelial cells 3) develop a novel biaxial stretch bioreactor to dramatically increase the ability to correlate valvular endothelium response to physiologically relevant applied planar loads.

Specific Aim 1) Elucidate the role of in vitro cyclic strain on pro-inflammatory adhesion molecule expression in aortic valve endothelial cells. The valvular endothelium

has been implicated in the initiation and progression of degenerative aortic valve disease. Aortic valve disease has been associated with altered hemodynamics and tissue mechanics. Thus, the hypothesis that an altered mechanical environment has a causal relationship with valvular endothelial cell activation was tested. Isolated porcine aortic valvular endothelial cells will be subject to various *in vitro* cyclic strain regimens and the production of adhesion molecules known to be involved in degenerative valve disease was investigated.

Specific Aim 2) Investigate the cyclic-strain dependent activation of side-specific aortic valve endothelial cells. The aortic valve is lined with endothelial cells on the fibrosa (aortic facing) and ventricularis (left ventricular facing) surfaces, which function in unique mechanical environments. Calcific aortic valve disease is known to occur preferentially on the fibrosa. *In vivo* transcription profiles suggest the valvular endothelial populations are heterogeneous sub-phenotypes with differential expression of genes related to inflammation, anti-oxidation and calcification. The hypothesis that the valvular endothelial cells are unique phenotypes preferentially functioning in their respective mechanical environment was tested by isolating side specific valvular endothelial cells and subjecting them to *in vitro* cyclic strain regimens. The strain response was compared by quantifying pro-inflammatory gene expression, generation of reactive oxygen species, expression of endothelial nitric oxide synthase and role of the NF kappa B inflammatory pathway.

Specific Aim 3) Develop a novel biaxial stretch bioreactor to investigate endothelial cell response to tissue level anisotropic biaxial cyclic strain. Valvular endothelial cell response to altered mechanics has been investigated *in vitro*. However, *in*

vitro studies are severely limited by a lack of physiological relevance with regard to maintenance of native biological and mechanical environments. *Ex vivo* studies pose a considerable improvement in the field of heart valve mechanobiology. This section will detail the design, construction, and validation of a cyclic stretch bioreactor for the specific function of applying physiologically relevant cyclic strains, while allowing for live cell imaging of the AV endothelium.

Chapter V outlines the design and implementation of a cardiovascular health outreach program, Bulldogs for Heart Health. Founded by the author and a group of biomedical engineering graduate students in the Fall of 2007, the goals of BH^2 focused on combating the rise of childhood obesity in Mississippi. Mississippi State campus outreach has also been conducted and detailed in this chapter. The underlying theme being that the majority of heart disease is preventable with the combination regular physical activity and conscious dietary decisions.

1.5 References

(1) Misfeld M, Sievers HH. Heart valve macro- and microstructure. Philos Trans R Soc Lond B Biol Sci 2007 Aug 29;362(1484):1421-36.

(2) Kunzelman KS, Grande KJ, David TE, Cochran RP, Verrier ED. Aortic root and valve relationships. Impact on surgical repair. J Thorac Cardiovasc Surg 1994 Jan;107(1):162-70.

(3) Weind KL, Ellis CG, Boughner DR. Aortic valve cusp vessel density: relationship with tissue thickness. J Thorac Cardiovasc Surg 2002 Feb;123(2):333-40.

(4) Weind KL, Ellis CG, Boughner DR. The aortic valve blood supply. J Heart Valve Dis 2000 Jan;9(1):1-7.

(5) Schoen FJ. Evolving concepts of cardiac valve dynamics: the continuum of development, functional structure, pathobiology, and tissue engineering. Circulation 2008 Oct 28;118(18):1864-80.

(6) Doehring TC, Kahelin M, Vesely I. Mesostructures of the aortic valve. J Heart Valve Dis 2005 Sep;14(5):679-86.

(7) Stephens EH, Chu CK, Grande-Allen KJ. Valve proteoglycan content and glycosaminoglycan fine structure are unique to microstructure, mechanical load and age: Relevance to an age-specific tissue-engineered heart valve. Acta Biomater 2008 Sep;4(5):1148-60.

(8) Vesely I. The role of elastin in aortic valve mechanics. J Biomech 1998 Feb;31(2):115-23.

(9) Yoganathan AP, He Z, Casey JS. Fluid mechanics of heart valves. Annu Rev Biomed Eng 2004;6:331-62.

(10) Dwyer HA, Matthews PB, Azadani A, Jaussaud N, Ge L, Guy TS, et al. Computational fluid dynamics simulation of transcatheter aortic valve degeneration. Interact Cardiovasc Thorac Surg 2009 May 4.

(11) Nakamura M, Wada S, Yamaguchi T. Quantitative evaluation of intra-aortic flow disturbance by the fluid momentum index: Effect of the left ventricular systolic function on the hemodynamics in the aorta. Technol Health Care 2007;15(2):111-20.

(12) Nandy S, Tarbell JM. Measurement of wall shear stress distal to a tri-leaflet valve in a rigid model of the aortic arch with branch flows. J Biomech Eng 1988 Aug;110(3):172-9.

(13) Liao J, Yang L, Grashow J, Sacks MS. The relation between collagen fibril kinematics and mechanical properties in the mitral valve anterior leaflet. J Biomech Eng 2007 Feb;129(1):78-87.

(14) HVIDBERG E. Investigations into the effect of mechanical pressure on the water content of isolated skin. Acta Pharmacol Toxicol (Copenh) 1960;16:245-9.

(15) HVIDBERG E. Water-binding by connective tissue and the acid mucopolysaccharides of the ground substance. Acta Pharmacol Toxicol (Copenh) 1960;17:267-76.

(16) Billiar KL, Sacks MS. Biaxial mechanical properties of the natural and glutaraldehyde treated aortic valve cusp--Part I: Experimental results. J Biomech Eng 2000 Feb;122(1):23-30.

(17) Rabkin-Aikawa E, Farber M, Aikawa M, Schoen FJ. Dynamic and reversible changes of interstitial cell phenotype during remodeling of cardiac valves. J Heart Valve Dis 2004 Sep;13(5):841-7.

(18) Rabkin E, Hoerstrup SP, Aikawa M, Mayer JE, Jr., Schoen FJ. Evolution of cell phenotype and extracellular matrix in tissue-engineered heart valves during in-vitro maturation and in-vivo remodeling. J Heart Valve Dis 2002 May;11(3):308-14.

(19) Merryman WD, Youn I, Lukoff HD, Krueger PM, Guilak F, Hopkins RA, et al. Correlation between heart valve interstitial cell stiffness and transvalvular pressure: implications for collagen biosynthesis. Am J Physiol Heart Circ Physiol 2006 Jan;290(1):H224-H231.

(20) Simmons CA, Grant GR, Manduchi E, Davies PF. Spatial heterogeneity of endothelial phenotypes correlates with side-specific vulnerability to calcification in normal porcine aortic valves. Circ Res 2005 Apr 15;96(7):792-9.

(21) Brody S, Anilkumar T, Liliensiek S, Last JA, Murphy CJ, Pandit A. Characterizing nanoscale topography of the aortic heart valve basement membrane for tissue engineering heart valve scaffold design. Tissue Eng 2006 Feb;12(2):413-21.

(22) Butcher JT, Nerem RM. Valvular endothelial cells and the mechanoregulation of valvular pathology. Philos Trans R Soc Lond B Biol Sci 2007 Aug 29;362(1484):1445-57.

(23) Butcher JT, Penrod AM, Garcia AJ, Nerem RM. Unique morphology and focal adhesion development of valvular endothelial cells in static and fluid flow environments. Arterioscler Thromb Vasc Biol 2004 Aug;24(8):1429-34.

(24) Davies PF, Passerini AG, Simmons CA. Aortic valve: turning over a new leaf(let) in endothelial phenotypic heterogeneity. Arterioscler Thromb Vasc Biol 2004 Aug;24(8):1331-3.

(25) Ghaisas NK, Shahi CN, Foley B, Goggins M, Crean P, Kelly A, et al. Elevated levels of circulating soluble adhesion molecules in peripheral blood of patients with unstable angina. Am J Cardiol 1997 Sep 1;80(5):617-9.

(26) Ghaisas NK, Foley JB, O'Briain DS, Crean P, Kelleher D, Walsh M. Adhesion molecules in nonrheumatic aortic valve disease: endothelial expression, serum levels and effects of valve replacement. J Am Coll Cardiol 2000 Dec;36(7):2257-62.

(27) Heistad DD, Wakisaka Y, Miller J, Chu Y, Pena-Silva R. Novel aspects of oxidative stress in cardiovascular diseases. Circ J 2009 Feb;73(2):201-7.

(28) Miller JD, Chu Y, Brooks RM, Richenbacher WE, Pena-Silva R, Heistad DD. Dysregulation of antioxidant mechanisms contributes to increased oxidative stress in calcific aortic valvular stenosis in humans. J Am Coll Cardiol 2008 Sep 2;52(10):843-50.

(29) Weiss RM, Ohashi M, Miller JD, Young SG, Heistad DD. Calcific aortic valve stenosis in old hypercholesterolemic mice. Circulation 2006 Nov 7;114(19):2065-9.

(30) Griendling KK, FitzGerald GA. Oxidative stress and cardiovascular injury: Part I: basic mechanisms and in vivo monitoring of ROS. Circulation 2003 Oct 21;108(16):1912-6.

(31) Papaharalambus CA, Griendling KK. Basic mechanisms of oxidative stress and reactive oxygen species in cardiovascular injury. Trends Cardiovasc Med 2007 Feb;17(2):48-54.

(32) Muller AM, Cronen C, Kupferwasser LI, Oelert H, Muller KM, Kirkpatrick CJ. Expression of endothelial cell adhesion molecules on heart valves: up-regulation in degeneration as well as acute endocarditis. J Pathol 2000 May;191(1):54-60.

(33) Rajamannan NM, Bonow RO, Rahimtoola SH. Calcific aortic stenosis: an update. Nat Clin Pract Cardiovasc Med 2007 May;4(5):254-62.

(34) Lloyd-Jones D, Adams R, Carnethon M, De SG, Ferguson TB, Flegal K, et al. Heart disease and stroke statistics--2009 update: a report from the American Heart Association Statistics Committee and Stroke Statistics Subcommittee. Circulation 2009 Jan 27;119(3):480-6.

(35) Otto CM, Lind BK, Kitzman DW, Gersh BJ, Siscovick DS. Association of aortic-valve sclerosis with cardiovascular mortality and morbidity in the elderly. N Engl J Med 1999 Jul 15;341(3):142-7.

(36) Stewart BF, Siscovick D, Lind BK, Gardin JM, Gottdiener JS, Smith VE, et al. Clinical factors associated with calcific aortic valve disease. Cardiovascular Health Study. J Am Coll Cardiol 1997 Mar 1;29(3):630-4.

CHAPTER II

CYCLIC STRAIN REGULATES PRO-INFLAMMATORY PROTEIN EXPRESSION IN AORTIC VALVE ENDOTHELIAL CELLS

For nearly a decade, cardiovascular research has put to rest the notion that valve disease is a passive degenerative process. While a breadth of research in vascular disease mechanisms exists, the task of elucidating valve pathology on a cellular and molecular level has been a relatively recent undertaking. Inflammation has been implicated in the instigation and progression of atherosclerosis, with the vascular endothelium critically involved in homeostasis and pathology. Histological similarities between early sclerotic vascular lesions and calcific aortic valve lesions imply parallel cellular level pathogenesis (1). The role of the aortic valve endothelium in valve sclerosis remains poorly understood. However, the initiation of aortic valve stenosis has shown a strong correlation with a pro-inflammatory response (2). The inflammatory reaction is most often associated with endothelial injury and the resultant cascade of cell mediated inflammatory events (3). The activated endothelial layer generates specific surface molecules involved in monocyte and T-cell migration, adhesion, and congregation. The pro-inflammatory proteins include intercellular adhesion molecules (ICAM), vascular cell adhesion molecules (VCAM), and endothelial leukocyte adhesion molecules (E-Selectin or ELAM). These proteins act concurrently with chemotactic molecules, such as

monocyte chemoattractant protein 1 (MCP-1), expressed by the endothelium and smooth muscle cells, to attract monocytes into the tissue. Once monocytes have migrated to the sub-endothelial space, macrophage differentiation occurs. Monocyte derived macrophages dictate the cellular inflammatory response through cytokine and chemokine secretion, and also express growth regulating factors and metalloproteinases. An aortic valve subject to a chronic inflammatory response may develop calcific lesions, similar to atherosclerotic plaques. Non-sclerotic post-mortem valves fail to express the adhesion molecules ICAM-1, VCAM-1 and E-Selectin, while the pro-inflammatory proteins are present on the endothelium of excised non-rheumatic degenerative diseased valves (4).

Regions of valvular calcification show a strong correlation with increased mechanical forces and abnormal hemodynamics (5). The aortic valve is subject to cyclic stretch as a function of diastolic transvalvular pressure, as well as fluid shear stress and hydrostatic pressure. A valve withstands physiological stresses through constant renewal of the extracellular matrix. A disrupted mechanical environment may be responsible for the initiation and/or acceleration of aortic stenosis and calcification. Hypertensive conditions result in an increased transvalvular pressure and thus, higher strains are imparted on the leaflets during diastole. In systole, the transvalvular pressure is essentially zero. Thus, throughout the cardiac cycle, cyclic surface strain on aortic valve leaflets are imparted to the endothelium. However, the cellular response of the aortic valve endothelium to altered mechanical forces has yet to be fully characterized. Previous studies have shown that cyclic stretch induces oxidative stress in arterial ECs and can also initiate an up-regulation in E-Selectin, ICAM-1, and VCAM-1 expression in a time-dependent manner

and consequently mediate monocyte adhesion (6;7). It is not currently known if valvular ECs respond in a similar fashion.

The aim of this study was to determine if cyclic strain would regulate a pro-inflammatory reaction in porcine aortic valvular endothelial cells in vitro. Cells were exposed to equibiaxial cyclic strains of 0-5%, 0-10%, and 0-20% for 24 hours. Expression of adhesion molecules E-Selectin, ICAM-1, VCAM-1 was determined through fluorescent assisted cell sorting (FACS) and confirmed with laser scanning confocal microscopy (CLSM).

Table 1. Primary endpoint rationale for Specific Aim 1.

Primary Endpoint	Methodology	Rationale
Pro-Inflammatory Protein Expression	Confocal Microscopy	Spatial distribution of protein expression, cellular integrity
	Flow Cytometry	Quantitative Protein Expression

2.1 Methods

2.1.1 Cell Source and Culture

Aortic valves for specific aim 1 were obtained from adult female pigs within 30 minutes of slaughter (Holifield's Farm, Covington, GA, Specific Aim 2 Pigs from Maben, MS) and transported to the laboratory in ice-cold Dulbecco's Phosphate Buffered Saline (PBS; Sigma, St. Louis, MO). Cells were isolated as previously described(9). In brief, tissue was digested with collagenase II (~600 U/ml; Worthington Biochemical Corp., Lakewood, NJ) for 10 minutes at 37oC and 5% CO_2. The leaflet surface was gently scraped with sterile cotton swabs and the resulting cell solution was centrifuged

and the pelleted cells were plated onto tissue culture flasks pre-coated with collagen type I (Becton-Dickson, Rat tail, 50 μg/mL). Porcine Aortic Valve Endothelial Cells (PAVEC) pooled from both surfaces of the AV leaflet were cultured in Dulbecco's Modified Eagle Medium (DMEM; Sigma, St. Louis, MO) supplemented with 10% Fetal Bovine Serum (FBS; Mediatech Inc., Herndon, VA) and 1% Anti-biotic/Anti-mycotic solution (Sigma), using standard tissue culture methods. Cells used in all experiments were between passage 3 and 8. The cell line used for the adhesion molecule study were isolated and characterized by Dr. Jonathan Butcher. These cells have been a source of a number of seminal publications in the field of valvular endothelial mechanobiology. They have been shown to align perpendicular to laminar shear stress, have distinct transcriptional profiles from aortic endothelial cells, and have been utilized in a co-culture model(9-11).

2.1.2 FX-4000T™ Flexercell® Tension Plus™

Numerous studies have been conducted to observe the response of endothelial cells to cyclic strain. The role of oxidative stress and the expression of nitric oxide synthase has been correlated to cyclic strain in vascular cells(12-14). However, no studies have been conducted on the valvular endothelial cell type with particular regard to cyclic strain. The commercially available Flexcell system is the most commonly used apparatus to impart dynamic strain on cells cultured on a deformable substrate. Negative vacuum pressure is applied to custom culture plates with a flexible silicone membrane.

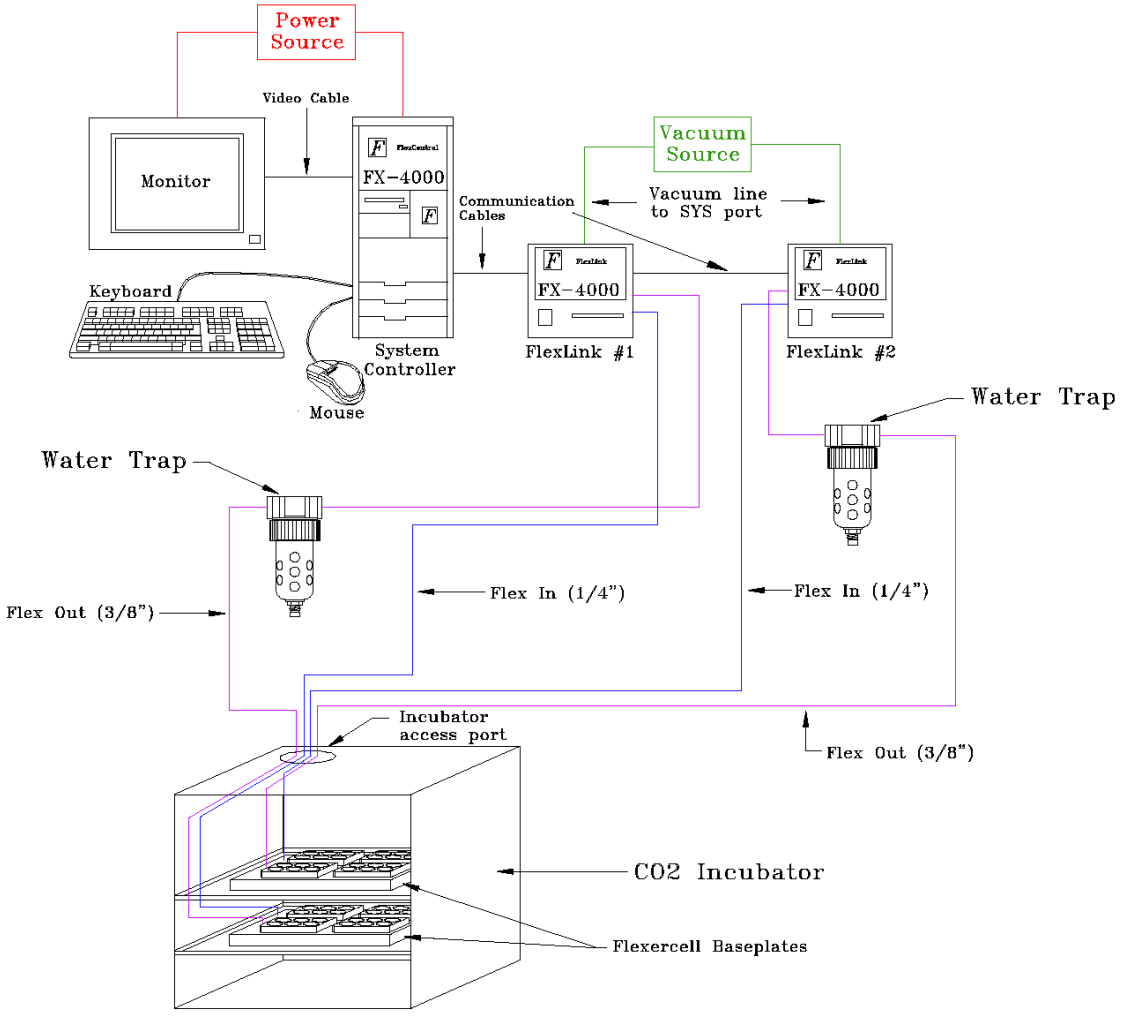

Figure 12 Schematic of the FX-4000T™ Flexercell® Tension Plus™ system. Collagen Type I Bioflex™ plates are seeded with cells and stretched in an incubator via application of cyclic negative vacuum pressure.

PAVEC were centrally seeded (~60,000/well) into 6-well BioFlex™ culture plates pre-coated with collagen type I (Flexcell International, Hillsborough, NC) and grown to confluence. The medium was completely changed to contain 0.1% FBS for 48 hours prior to stretching to induce cell cycle arrest. The plates were then placed into the Flexcell® FX4000-T™ Tension Plus system (Flexcell International, Hillsborough, NC). This device applies negative pressure beneath the BioFlex™ plate wells via a vacuum

pump, which is monitored by a pressure transducer, permitting precisely defined, equibiaxial stretch of up to 30%. The stretch can be applied with any waveform and frequency; a sinusoidal waveform at 1Hz was chosen to most accurately mimic the cardiac cycle. 25mm loading posts were utilized to give a uniform equibiaxial strain, which has been previously characterized (15).

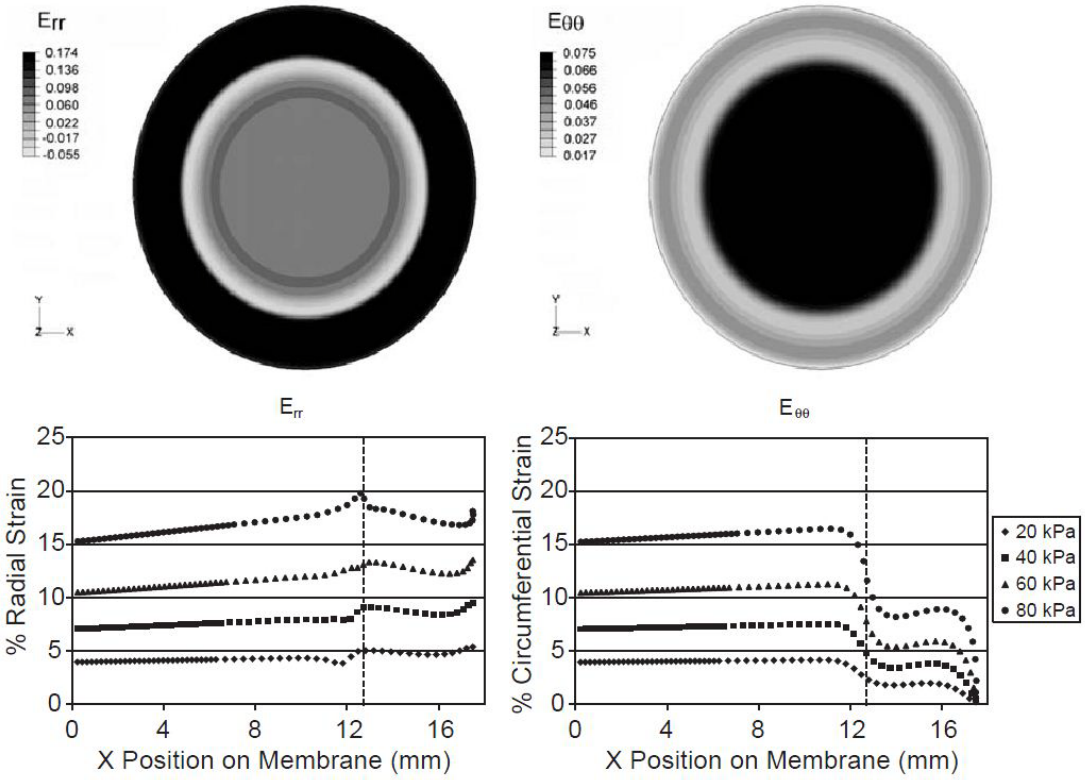

Figure 13 Stress distribution in the Flexcell membranes being stretched by negative vacuum pressure over a loading post. Endothelial cells are centrally seeded for uniform radial and circumferential strain profiles. From (17).

Cells were stretched for 24 hours at cyclic strains of 0-5, 0-10, and 0-20%. The duration correlates to previous studies where ECs elicited a biological response to cyclic

strains over a 24 hour time period(16). The applied cyclic strains were chosen to represent a range that would mimic physiological and pathological strain conditions.

2.1.3 Flow cytometry

Flow cytometry was used to quantify relative antigen expression. One well per plate was used to detect each pro-inflammatory protein, in addition to a control well. PAVEC were removed from the plates by adding 2 mL Trypsin-EDTA (Sigma) per well for 5 minutes. DMEM was added to the cell suspension and centrifuged for 8 minutes at 1000 rpm. The cell pellet was re-suspended in 1mL PBS with 1% Bovine Serum Albumin (Sigma). The cells were then fixed in 2% Paraformaldehyde (Sigma) for 5 minutes. 200µL Fluorescein isothiocyanate (FITC) conjugated monoclonal antibodies were added (VCAM-1 Biolegend, San Diego, CA; E-Selectin, ICAM-1 US Biological, Swampscott, MA) in 1:100 dilution and incubated in the dark at room temperature for 45 minutes. Mouse Anti-Human IgG primary Ab's were used, thus, a secondary Anti-Mouse IgG Ab conjugation was performed to screen the samples for primary Ab. Secondary biotinylated antibodies were utilized in a 1:250 dilution and incubated with each sample for 20 minutes in 200 µL solution. The samples were washed then immersed in 200µL Avidin D for 10 minutes. A control sample consisted of performing only the biotinylated anti-mouse Ab and Avidin D conjugation. Flow cytometry was performed with a FACSCalibur flow cytometer (Becton-Dickinson, San Jose, CA) and 5000 events were collected per sample. The density plot for the control sample was gated for viable cells based on forward scatter and side scatter. Mean fluorescence intensity (MFI; FL-1H) of the antigen positive cells was quantified. Using FCS Express 3 (De Novo Software, Los

Angeles, CA), the control for each experimental strain was divided by two markers; M1, indicating low MFI, and M2, representing high MFI, or positively stained cells. To ensure continuity between strains and eliminate day to day variations in FACSCalibur calibration, control levels of M2 cells were set at 3.29, 3.33, and 3.33% of gated cells for cyclic strains of 5, 10, and 20% respectively. These levels were chosen due to the presence of assorted autofluorescent cellular phenomena, and additionally to yield a MFI difference from M1 to M2 exceeding ten-fold for each sample. The percentage of the target sample's M2 cells was normalized to the control for each strain, yielding a fold change in positively stained cells. Each experiment was conducted in triplicate, and a paired t-test was used to determine significance differences between strains for each inflammatory molecule. Significance was determined at values of $p \leq 0.05$ unless stated otherwise.

2.1.4 Laser Scanning Confocal Microscopy

Upon completion of the strain experiments, cells were retained in the BioFlex™ plate and rinsed twice with PBS with 1% BSA, and fixed with 2% paraformaldehyde in PBS. Cells underwent primary Ab conjugation for 45 min in the dark, biotinylated secondary Ab conjugation for 20 min in the dark, and incubation with Avidin D for 10 min. Cell membranes were then permeabilized with 0.1% Triton X-100 in PBS, and stained with 300µL propidium iodide. Cells were washed twice with PBS with BSA prior to and following each stain. The collagen membrane was excised from the Bioflex plate with a razor blade, placed on a microscope slide, and fixed with a coverslip immediately prior to viewing. A Zeiss LSM 510 confocal microscope (Carl Zeiss,

Thornwood NY) was used with a 10X or 20X objective. FITC and Rhodamine filters were used to observe the fluorescein conjugated antibodies, and the propidium iodide stain, respectively. Carl Zeiss LSM Imaging Software Version 3.5.0.223 was used for image processing. Images were captured depicting the monolayer integrity and cellular environment following cell cycle arrest and immediately prior to stretching (Figure 15A). Also, a control sample image was taken with only a secondary conjugation performed to verify the absence of non-specific biotinylated Ab staining (Figure 15B).

The Zeiss LSM 510 confocal microscope was used in the plane scanning mode to acquire each image at a single focal z-plane. Plane scanning mode was used to create an 1024X1024 8-bit image with a scale of 0.9µmX0.9µmX1.0 µm. The objective used was an EC Plan-Neofluar 10X, with a numerical aperture (NA) of 0.30. Beam splitters split the laser lines at 405, 488, and 543 nm for the red, green, and blue channels, respectively. Filters for fluorescent detection were a band pass 420-480 (blue), band pass 505-530 (green) and a long pass 615 for the red channel.

Adobe Photoshop CS4 (Adobe Systems Incorporated, San Jose, CA) was used to post-process images according to guidelines from the Microscopy Association of America (John Mackenzie, NC State, Confocal Microscopy Workshop). This method is used to avoid data manipulation from conventional "brightness/contrast" methods that have become abundantly abused. Light and dark levels are set using the histogram of pixel values of individual channels. For instance, the dark levels of the blue channel are set at the level where individual nuclei outlines are first seen, hence, the first relevant pixels in the blue channel are set in the histogram and all background not indicating nuclei is set to a histogram level of zero, or "true black". Light levels, or saturation point,

a level of 255 in an 8-bit image or 4095 in a 12-bit image, is set to the first discernible pixels in each channel individual. This assures that the brightest pixel level is now set to the saturation point. This is a process known as histogram stretching, a method that spreads your data from each channel across the 256 or 4096 level spectrum, enhancing contrast of your data, while taking care not to over-represent bright spots, or have data on the dark side of the spectrum set to black artificially. Next, gamma levels are set sequentially in the red, blue, and green channels. Identical gamma levels are used for the green channel to give a proper comparison between images. Images are then saved in the TIFF format to avoid any loss of image quality due to compression.

2.2 Results

2.2.1 Flow Cytometry and CLSM

Flow cytometry and laser scanning confocal images demonstrate the presence of pro-inflammatory molecules at cyclic strains of 0-5 and 0-20% for 24 hours. Conversely, there is an absence of adhesion and chemotactic molecules at a cyclic strain of 0-10%. Cells stained for the adhesion molecule E-Selectin (high MFI) significantly increased 2.84 fold and 6.97 fold at strains of 5 and 20%, respectively, compared to secondary Ab controls (Figure 14). High MFI cells decreased for E-Selectin at 10% strain to a normalized level of 0.37. The laser scanning confocal images taken of PAVEC with FITC conjugated antibodies demonstrate a similar E-Selectin rich environment at strains of 5 and 20% (Figure 13 A,B,C). PAVEC stained red in Figure 13A were clearly present in a disrupted and non-viable monolayer, when contrasted to the cellular environment observed prior to stretching (Figure 12). Fluorescent E-Selectin antibodies, seen in green,

are prevalent at 5 and 20% strain, in Figure 13**A** and Figure 13C, respectively. Expression of the adhesion molecule, ICAM-1, significantly increased by 2.19 fold ($p < 0.10$) and 6.21 fold ($p \leq 0.05$) at strains of 5 and 20%, respectively (Figure 14). ICAM-1 expression at 10% strain was downregulated compared to the control, with a normalized level of 0.67. CLSM images taken of PAVEC with FITC conjugated antibodies depict an ICAM-1 positive environment at strains of 5 and 20% **(**Figure 14). PAVEC seen in Fig 13 are clearly present in a perturbed non-confluent layer. Fluorescent ICAM-1 Ab, in green, exists substantially at 5 and 20% strain, as seen in Figure 13D and Figure 13F, respectively. Cells staining positively for the adhesion molecule VCAM-1 significantly increased 4.49 fold ($p<0.05$) at a strain of 20%, when compared to 5 and 10% cyclic strain (Figure 14). High MFI cells for VCAM-1 at 10% strain decrease to a normalized level of 0.23. CLSM images taken of PAVEC with FITC Ab show VCAM-1 expression at strains of 5 and 20% (Figure 13). PAVEC stained red in Figure 13G lack monolayer integrity. Fluorescent VCAM-1 Ab was seen clearly at 5 and 20% strain (Figure 13A and Figure 13C, respectively).

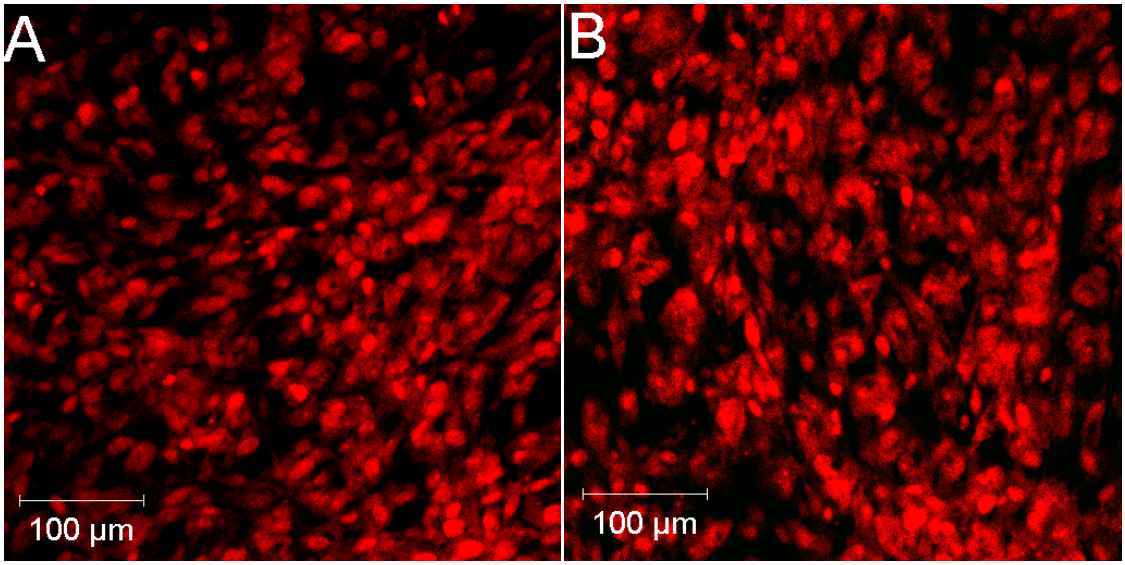

Figure 14 Laser scanning confocal microscopy images of PAVEC seeded onto BioFlex plates. A) PAVECs under static conditions prior to stretching; B) Static culture of PAVECs stained with secondary antibody only. Red: propidium iodide nucleic acid stain. Green: Secondary Mouse Biotinylated IgG

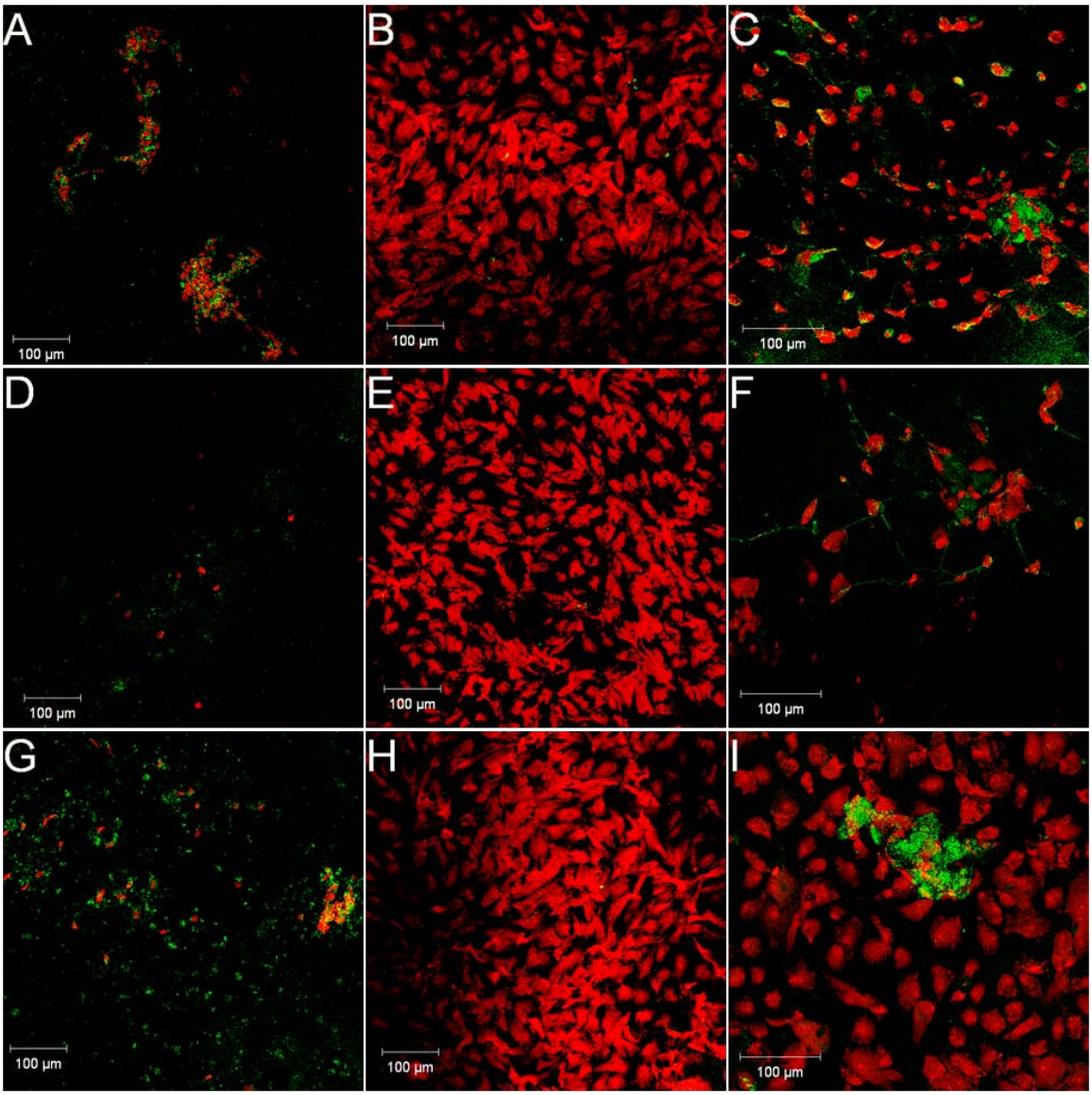

Figure 15 Laser scanning confocal microscopy images of E-Selectin (A,B,C) , ICAM-1 (D,E,F), and VCAM-1 (G,H,I) expression in PAVECs exposed to various levels of cyclic strain for 24h A,D,G) 0-5% cyclic strain; B,E,H) 0-10% cyclic strain; C,F,I) 0-20% cyclic strain. Red: Propidium Iodide; Green: FITC-Avidin Biotinylated Conjugated Mouse Anti-Human E-Selectin, ICAM-1, and VCAM-1.

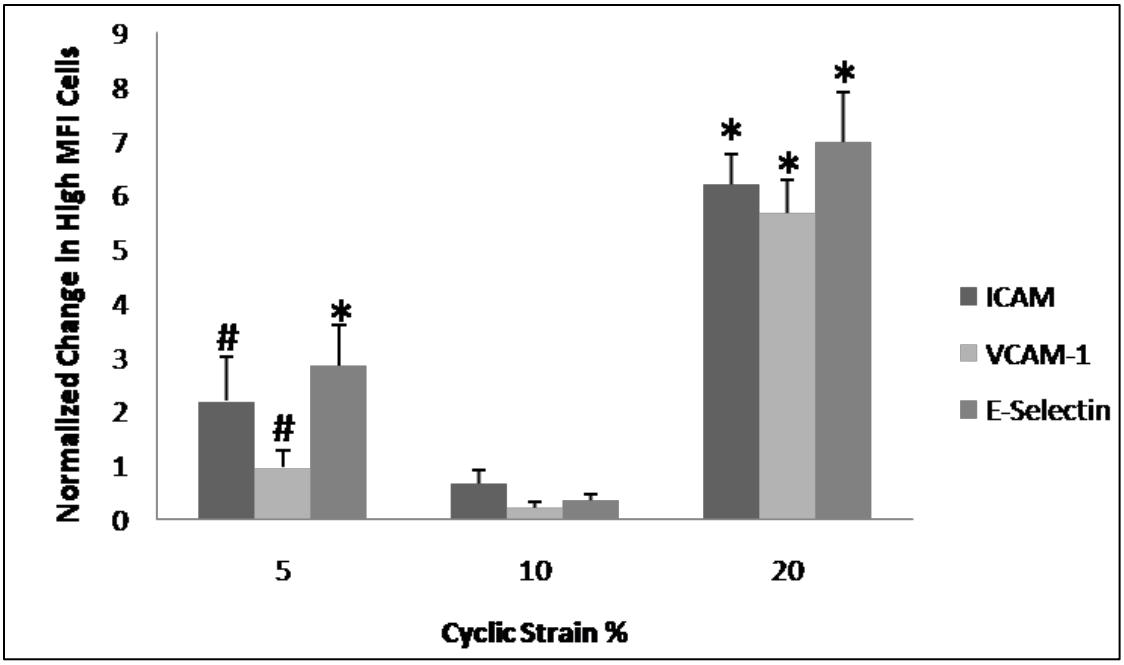

Figure 16 FACS analysis of E-Selectin, ICAM-1, and VCAM-1 expression in PAVEC exposed to various levels of cyclic strain for 24h. Bars represent the fold change in High Mean Fluorescent Intensity Positive Cells normalized to the control. Error Bars represent standard error of the mean (n=3). * denotes statistically significant up-regulation when compared to 10% cyclic strain ($p \leq 0.05$), while # denotes significance ($p \leq 0.10$).

2.3 Discussion

This study has demonstrated that cyclic strain regulates the pro-inflammatory behavior of porcine aortic valvular endothelial cells (PAVEC) *in vitro*. The endothelial layer serves in the mechanosensation of an abnormal mechanical environment in both the vasculature and heart valve leaflets. The aortic valve endothelium, subject to cyclic strain *in vivo* via diastolic transvalvular pressure, has been suspect in playing an initiating role in valvular disease pathogenesis. The complex relationship between mechanical forces and the vascular endothelium has been investigated thoroughly (19-21) and has led to much speculation about the valvular endothelium. Histological similarities between vascular and valvular lesions lend credence to the belief that inflammation, and the subsequent cellular reaction cascade, remains a mitigating factor in aortic valve disease. However, the assumption that valvular and vascular cell physiology and pathogenesis are parallel has become outdated as distinctions between the cell populations mount (10;22-24). Thus, we have established that a correlation exists between equibiaxial cyclic strain and pro-inflammatory protein expression in aortic valve endothelial cells.

Both uniaxial and biaxial strain analyses have been performed to approximate *in vivo* deformations in the porcine aortic valve (25;26). Aortic valve leaflets experience an array of strains, varying in the radial and circumferential directions, while exhibiting side specificity. Higher strains are seen in the radial direction, especially on the smooth ventricularis. The fibrosa experiences diastolic radial strain that, in part, serves to flatten corrugations that arise from leaflet bending in systole. Isolated PAVEC for the experiments were pooled from the fibrosa and ventricularis, however, side specific inflammatory response may be a future research topic. Aortic valvular circumferential

strain of 10% has been cited consistently and therefore chosen as a baseline strain. Strains capable of inducing pathological states may arise in the presence of vasoactive agents, hypertension, and degeneration due to aging (27-29).

The 24 hour duration gave PAVEC ample time to increase gene transcription and translation while maintaining pro-inflammatory protein detection prior to degradation. Confocal laser scanning microscopic (CLSM) images depict the PAVEC on excised collagen membranes from BioFlex™ plates following 24 hours of exposure to each cyclic strain. The use of monoclonal Ab in conjunction with FITC conjugated secondary Ab clearly depicts the presence, in green, of the adhesion molecules, E-Selectin, ICAM-1, and VCAM-1. Due to the observation that diseased valves alone express adhesion molecules, and hypertension is a risk factor for aortic valve disease, one would expect a threshold to exist where elevated strain would lead to endothelial adhesion molecule expression. Hypertension simulating PAVEC protein expression was verified at a cyclic strain of 0-20%. Each image depicts the presence of the target inflammatory molecule as well as the cellular monolayer environment. If a threshold existed for strain induced adhesion molecule expression, we may have observed increasing pro-inflammatory proteins as strain increased from 5 to 10 to 20% cyclic strain. An interesting and promising observation involves abundant pro-inflammatory protein expression at 0-5% strain, yet negligible evidence of an inflammatory reaction at 0-10% cyclic strain. The lack of mAB presence at this strain implies similarity to a physiological mechanical stretch environment, where pro-inflammatory proteins also lack expression. The initial choice of strains was aimed to cover a variety of *in vivo* states, and may have yielded a

reliable in vitro model to observe a broad array of strain regulated behavior in the aortic valve endothelium.

PAVEC nuclei were stained red with Propidium Iodide. The 0-20% cyclic strain images show an incomplete PAVEC monolayer, which appears to be uninterrupted in pre-stretch controls. A significant loss of cells is seen in all 0-5% strain images (Figures 16 A, D, G), indicating cell death, or simulating a denudation of the endothelial layer *in vivo*. The few remaining spots of red appear individually smaller than PAVEC at other strains, possibly indicating cell fragments attached to the collagen membrane. The PAVEC monolayer at 10% strain (Figures 16 B, E, H) yields an additional promising observation. The intact and generally undisturbed monolayer supports the argument that 10% equibiaxial cyclic strain mimics physiological stretch, in conjunction with the lack of adhesion and chemotaxis molecules. Additionally, the flexible collagen membrane becomes more pliant after 24 hours of stretching, and the confocal lens periodically failed to capture a flat surface, as is somewhat the case in Figures 16B and 16H.

The FACS results aid in elucidating the cellular response captured by the CLSM images. One might expect the images to correspond directly to the FACS data, however, on account of the FACS live cell control gating, many adhesion molecules existed on dead cells and were not included in the fluorescence shifts, with particular regard to 5% strain. M2 levels for 10% cyclic strain are less than the control for E-Selectin, ICAM-1, and VCAM-1. This may be attributed to the additional staining step and subsequent washes where viable autofluorescent cells were lost, and not replaced by M2 cells contributing Ab induced fluorescence, as is the case in 5 and 20% strains. The representative histograms yield visual conformation increased expression of

inflammatory proteins at 5 and 20% cyclic strain, as evinced by the shift of the gated cell populations to higher fluorescence in FL-1H.

In conclusion, we have demonstrated the cyclic strain regulated pro-inflammatory behavior of valvular endothelial cells. Through application of varied equibiaxial cyclic strains, we observed the target adhesion molecule and chemotactic protein expression at a lower level of strain, 0-5%, in addition to an elevated strain, 0-20%. Our results suggest that a pro-inflammatory reaction may occur *in vivo* when the valve endothelium is exposed to higher than physiological stretch, as is the case in hypertension. The data also implicate a pro-inflammatory state may exist when endothelial cells are subject to less than physiological stretch, as may be the case in an aging valve. We have observed a cyclic strain, 0-10%, which appears to mimic a physiological aortic valve endothelium surface strain environment, with respect to PAVEC monolayer integrity and the absence of adhesion molecules and chemotactic proteins. Cyclic strain, in addition to laminar shear stress and cyclic pressure, contributes to the makeup of the mechanical environment imposed on aortic valve leaflets. Characterization of the individual forces with regard to valve disease pathogenesis will lead to establishing a comprehensive model with diagnostic and therapeutic clinical implications.

Several limitations exist for *in vitro* studies of AVEC strain response. Apparent differences exist in cell source used for cell strain studies. The Flexcell system is useful for applying an equibiaxial strain, however, the native valve endothelium does not function in an equibiaxial strain state. The endothelium is on a highly aligned substrate, with structural differences between the fibrosa and the endothelium. The strain environment is highly anisotropic, with the valve experiencing radial and circumferential

strains that differ in magnitude up to 3X over the cardiac cycle. The native-subendothelial layer consists of collagen type IV and fibronectin. The BioFlex plates are made of collagen type I. Endothelial cells must also be isolated, passaged, and cultured in static conditions prior to cyclic stretching**.** It has been shown that endothelial cells in static culture may be in an activated state. Subjecting a cell type that had previously been subjected to various mechanical forces in vivo, fluid shear, pressure, and stretch, to a cyclic strain following days and often times weeks in static culture prior to stretching is a severe limitation.

2.4 References

(1) Mohler ER, III. Mechanisms of aortic valve calcification. Am J Cardiol 2004 Dec 1;94(11):1396-402, A6.

(2) Agmon Y, Khandheria BK, Jamil TA, Seward JB, Sicks JD, Fought AJ, et al. Inflammation, infection, and aortic valve sclerosis; Insights from the Olmsted County (Minnesota) population. Atherosclerosis 2004 Jun;174(2):337-42.

(3) Ross R. Atherosclerosis is an inflammatory disease. Am Heart J 1999 Nov;138(5 Pt 2):S419-S420.

(4) Ghaisas NK, Foley JB, O'Briain DS, Crean P, Kelleher D, Walsh M. Adhesion molecules in nonrheumatic aortic valve disease: endothelial expression, serum levels and effects of valve replacement. J Am Coll Cardiol 2000 Dec;36(7):2257-62.

(5) Thubrikar MJ, Aouad J, Nolan SP. Patterns of calcific deposits in operatively excised stenotic or purely regurgitant aortic valves and their relation to mechanical stress. Am J Cardiol 1986 Aug 1;58(3):304-8.

(6) Yun JK, Anderson JM, Ziats NP. Cyclic strain effects on human monocyte interactions with endothelial cells and extracellular matrix proteins. Tissue Eng 1999 Feb;5(1):67-77.

(7) Yun JK, Anderson JM, Ziats NP. Cyclic-strain-induced endothelial cell expression of adhesion molecules and their roles in monocyte-endothelial interaction. J Biomed Mater Res 1999 Jan;44(1):87-97.

(8) Ghaisas NK, Shahi CN, Foley B, Goggins M, Crean P, Kelly A, et al. Elevated levels of circulating soluble adhesion molecules in peripheral blood of patients with unstable angina. Am J Cardiol 1997 Sep 1;80(5):617-9.

(9) Butcher JT, Penrod AM, Garcia AJ, Nerem RM. Unique morphology and focal adhesion development of valvular endothelial cells in static and fluid flow environments. Arterioscler Thromb Vasc Biol 2004 Aug;24(8):1429-34.

(10) Butcher JT, Tressel S, Johnson T, Turner D, Sorescu G, Jo H, et al. Transcriptional profiles of valvular and vascular endothelial cells reveal phenotypic differences: influence of shear stress. Arterioscler Thromb Vasc Biol 2006 Jan;26(1):69-77.

(11) Butcher JT, Nerem RM. Valvular endothelial cells regulate the phenotype of interstitial cells in co-culture: effects of steady shear stress. Tissue Eng 2006 Apr;12(4):905-15.

(12) Awolesi MA, Sessa WC, Sumpio BE. Cyclic strain upregulates nitric oxide synthase in cultured bovine aortic endothelial cells. J Clin Invest 1995 Sep;96(3):1449-54.

(13) Awolesi MA, Widmann MD, Sessa WC, Sumpio BE. Cyclic strain increases endothelial nitric oxide synthase activity. Surgery 1994 Aug;116(2):439-44.

(14) Howard AB, Alexander RW, Nerem RM, Griendling KK, Taylor WR. Cyclic strain induces an oxidative stress in endothelial cells. Am J Physiol 1997 Feb;272(2 Pt 1):C421-C427.

(15) Vande Geest JP, Di Martino ES, Vorp DA. An analysis of the complete strain field within Flexercell membranes. J Biomech 2004 Dec;37(12):1923-8.

(16) Sung HJ, Yee A, Eskin SG, McIntire LV. Cyclic strain and motion control produce opposite oxidative responses in two human endothelial cell types. Am J Physiol Cell Physiol 2007 Jul;293(1):C87-C94.

(17) Vande Geest JP, Di Martino ES, Vorp DA. An analysis of the complete strain field within Flexercell membranes. J Biomech 2004 Dec;37(12):1923-8.

(18) Simmons CA, Grant GR, Manduchi E, Davies PF. Spatial heterogeneity of endothelial phenotypes correlates with side-specific vulnerability to calcification in normal porcine aortic valves. Circ Res 2005 Apr 15;96(7):792-9.

(19) Chien S. Molecular basis of rheological modulation of endothelial functions: importance of stress direction. Biorheology 2006;43(2):95-116.

(20) Vanhoutte PM. Role of calcium and endothelium in hypertension, cardiovascular disease, and subsequent vascular events. J Cardiovasc Pharmacol 1992;19 Suppl 3:S6-10.

(21) Zhao S, Suciu A, Ziegler T, Moore JE, Jr., Burki E, Meister JJ, et al. Synergistic effects of fluid shear stress and cyclic circumferential stretch on vascular endothelial cell morphology and cytoskeleton. Arterioscler Thromb Vasc Biol 1995 Oct;15(10):1781-6.

(22) Butcher JT, Nerem RM. Porcine aortic valve interstitial cells in three-dimensional culture: comparison of phenotype with aortic smooth muscle cells. J Heart Valve Dis 2004 May;13(3):478-85.

(23) Roy A, Brand NJ, Yacoub MH. Molecular characterization of interstitial cells isolated from human heart valves. J Heart Valve Dis 2000 May;9(3):459-64.

(24) Taylor PM, Allen SP, Yacoub MH. Phenotypic and functional characterization of interstitial cells from human heart valves, pericardium and skin. J Heart Valve Dis 2000 Jan;9(1):150-8.

(25) Lo D, Vesely I. Biaxial strain analysis of the porcine aortic valve. Ann Thorac Surg 1995 Aug;60(2 Suppl):S374-S378.

(26) Adamczyk MM, Vesely I. Characteristics of compressive strains in porcine aortic valves cusps. J Heart Valve Dis 2002 Jan;11(1):75-83.

(27) Grande KJ, Cochran RP, Reinhall PG, Kunzelman KS. Mechanisms of aortic valve incompetence in aging: a finite element model. J Heart Valve Dis 1999 Mar;8(2):149-56.

(28) Hafizi S, Taylor PM, Chester AH, Allen SP, Yacoub MH. Mitogenic and secretory responses of human valve interstitial cells to vasoactive agents. J Heart Valve Dis 2000 May;9(3):454-8.

(29) Poggianti E, Venneri L, Chubuchny V, Jambrik Z, Baroncini LA, Picano E. Aortic valve sclerosis is associated with systemic endothelial dysfunction. J Am Coll Cardiol 2003 Jan 1;41(1):136-41.

CHAPTER III

CYCLIC STRAIN ACTIVATES AORTIC VALVE ENDOTHELIAL CELLS IN A SIDE-SPECIFIC MANNER

Healthy aortic valves (AV) function within the confines of a dynamic and demanding mechanical environment. Hemodynamic forces dictated by left ventricular performance impose a fluid shear stress and cyclic mechanical stretch as a function of diastolic blood pressure on the AV leaflets. Two distinct AV cell phenotypes sense and respond to mechanical cues as well as circulating biochemical stimuli (1). Aortic valvular endothelial cells (AVEC) and valvular interstitial cells (VIC) engage in a complex interplay with the predominantly fibrous extracellular matrix (ECM), creating an actively remodeling tissue with mechanical characteristics unique from the vasculature. Altered hemodynamics and tissue mechanics have been implicated in the initiation and progression of an array of cardiovascular diseases(2;3).

The mechanisms and risk factors associated with calcific aortic valve disease (CAVD) have been shown to be highly analogous with atherosclerosis; however, mounting data suggest the existence of cellular and molecular events unique to valvular pathogenesis (4). Endothelial cell activation has been implicated in the initiation of CAVD (5). The hallmarks of AVEC activation include activation of the transcription factor NF-κB, disrupted anti-oxidant mechanisms, and pro-inflammatory cell adhesion

molecule (CAM) expression (6;7). Mechanical forces may play a significant role in instigating the focal development of CAVD, a result of the pro-inflammatory cascade dictated by an activated valvular endothelium. Sclerotic AV develop calcific lesions, occurring preferentially on the aortic facing surface (fibrosa), coincidental with EC activation and monolayer disruption (8;9). *In vivo* transcription profiles suggest the valvular endothelial populations are heterogeneous sub-phenotypes with differential gene expression related to inflammation, anti-oxidation and calcification(10) . It is not currently known whether differential transcription *in vivo* can be attributed to unique mechanical environments, or truly distinct AVEC sub-phenotype populations.

The aim of this study was to assess side-specific AVEC activation in response to physiological and pathophysiological cyclic strains. This information could be used to determine if the *in vivo* transcriptional profiles were different as a result of the mechanical environment or if two distinct sub-phenotypes exist on opposing sides of the AV. A more comprehensive understanding of the valvular endothelium is critical in developing more effective preventative practices, as well as novel therapeutic approaches to CAVD.

Table 2 Primary Endpoints for Specific Aim 2.

Activation Indicator	Methodology	Rationale
Pro-Inflammatory Gene Expression	qRT-PCR	ICAM-1, VCAM-1, E-Selectin, P-Selectin, PECAM-1
ROS generation	CLSM(Carboxy-H_2DCFDA)	Detection of (O_2^-), H_2O_2
eNOS protein expression	CLSM(Mab, AF488	NO indicator
NF-κB	CLSM Phosphorylated Iκ-B (Ser32) intracellular location	Mechanoresponsive, regulate inflammatory CAMs

3.1 Methods

3.1.1 Cell Isolation and Culture

Porcine hearts were obtained directly following slaughter from a local abattoir (Sansing Meat Service Maben, MS). Female Yorkshire/Hampshire pigs were slaughtered before 6 months of age with a post-slaughter weight of no more than 120 lbs. Cell culture and isolation were conducted as previously described (11;12). Briefly, freshly excised AV leaflets were pinned fibrosa (concave up) or ventricularis (concave down) side up on paraffin coated dishes. AVEC were swabbed following a brief collagenase type II digestion (~600 U/ml; Worthington Biochemical Corp., Lakewood, NJ) and plated on fibronectin coated plates (BD Biosciences, San Jose, CA). Cobblestone morphology, contact inhibition, and positive vWF expression confirmed EC phenotype characterization. Fibrosa endothelial cells (FEC) and ventricularis endothelial cells (VEC) were between passage 4 and 6. Unique cell lines were used for transcription and microscopy studies.

3.1.2 Cyclic Straining of Cultured Cells

Cells were centrally seeded ($5x10^5$/well) into 6-well BioFlex™ culture plates pre-coated with collagen type I (Flexcell International, Hillsborough, NC) and grown to ~75% confluence in 3ml Dulbecco's Modified Eagle Medium (DMEM, Sigma, St. Louis, MO) supplemented with 10% Fetal Bovine Serum (FBS; Hyclone, Logan, UT) and 1% Anti-Mycotic/Anti-Biotic (ABAM, Sigma). The medium was completely changed to contain 0.1% FBS for 24 hours prior to stretching to induce cell cycle arrest. The plates were then placed into the Flexcell® FX4000-T™ Tension Plus system (Flexcell International, Hillsborough, NC). Negative pressure is applied under the BioFlex™ plate wells with a vacuum pump, monitored by a pressure transducer, imparting precisely defined equibiaxial stretch. A sinusoidal waveform at 1Hz was chosen to most accurately imitate the cardiac cycle. 25mm loading posts were utilized to give a previously characterized uniform equibiaxial strain (13). Cells were stretched for 24 hours at cyclic strains of 5, 10, and 20%. The duration correlates to previous studies where ECs elicited a biological response to cyclic strains over a 24 hour time period (14). The applied cyclic strains were chosen to represent a range that would mimic physiological and pathological strain conditions (15). As not all pro-inflammatory CAMs are constitutively expressed by AVEC *in vitro*, a positive activation control for transcription was performed by biochemical activation. Thus, FEC and VEC static controls were incubated with 5ng/µl tumor necrotic factor α (TNF-α, human recombinant, Sigma) in Bioflex plates for 24hr. Each condition was repeated in triplicate (n=3) for qRT-PCR, and experiments were independently repeated for the qualitative eNOS, ROS, and Iκ-B studies.

3.1.3 Quantification of mRNA Transcription

Immediately following cyclic stretching protocols, total RNA was isolated using the Qiagen RNEasy Total RNA isolation kit (Qiagen, Valencia, CA). RNA purity and quality was assessed on the Agilent Bioanalyzer (Agilent Technologies, Santa Clara, CA). The Agilent RNA 6000 Nanoassay confirmed high quality RNA with narrow 18s and 28s peaks. RNA quantification was performed on the Nanodrop 1000 (Thermo Scientific, Wilmington, DE). Total RNA concentration and 260/280nm absorbance ratios were measured, with only RNA samples with a 260/280 ratio of 1.8-2.1 used. Working dilutions of 100 ng/µl RNA in DEPC treated water were stored at -80°C until transcription quantification. Primers were designed to detect expression levels of E-selectin, P-selectin, PECAM-1, ICAM-1 and VCAM-1 using Primer3 software (16). These particular adhesion molecules have all been implicated in endothelial mediated inflammatory response in aortic valve stenosis, or involved in endothelial mechanosensation (17;18). Primer sets spanned intron-exon boundaries and amplification products were 100-200bp in length. Primer sequences and accession numbers are given in Table 1. A Stratagene Mx3005P (Agilent) was used for quantification of mRNA transcripts using the SuperScript III Platinum SYBR Green One-Step qRT-PCR kit (Invitrogen, Carlsbad, CA**).** Reactions were optimized for template quantity, primer concentration and cycling conditions. Final template concentration of total RNA used was 100ng/µl. A primer concentration of 10µM per 20 µl reaction was used for a final primer concentration of 200nM. The reaction components were as follows: 1µl Superscript III RT/Platinum Taq Mix with RNAse Out, 25µl SYBR Green Reaction Mix, 1µl of 10µM for forward and reverse primers, 1µl of ROX reference dye,

1µl of template RNA at a concentration of 100ng/µl, and 20µl of DEPC treated water. 19µl of the reaction mix was used with 1µl of template RNA for a final reaction volume of 20µl. Cycling conditions were as follows: 50°C for 3 minutes for cDNA synthesis, 5min at 95°C, followed by 40 cycles of 95°C for 15s and 60°C (primer specific binding temp, most primers were designed to have a binding temperature of 60°C) for 30s. Samples were then held at 40°C for 60s to begin the melting curve analysis. Melting curves were generated by holding at 95°C for 60s followed by 55°C for 30s and ramping to 95°C with data collection. Primers used all had melting curves with a single peak above 75°C, indicating specific DNA products were created and detected by the SYBR green fluorophore. HPRT1 was used as the housekeeping gene. Briefly, the machine was first RNAse decontaminated using RNase ZAP. The gel was prepared by allowing all components to equilibrate to room temperature. 550µl of Agilent RNA 6000 Nano gel matrix was loaded into the spin filter. The spin filter was spun at 1500g for 10 minutes. 1µl of RNA 6000 dye concentrate was added to a 65µl aliquot of filtered gel. The gel-dye mix was vortexed thoroughly and spun for 10min at 13000g. 9µl of the gel-dye was loaded into a RNA Nano chip and loaded into the Priming Station. The RNA Nano chip was pressurized for 30 seconds with a syringe plunger, followed by loading 9µl of the gel-dye mix into each of the wells on the chip. Figure 17 depicts 18s and 28s rRNA obtained from RNA samples in the Agilent Bioanalyzer, while Figure 18 shows the actual bands of extremely high quality RNA.

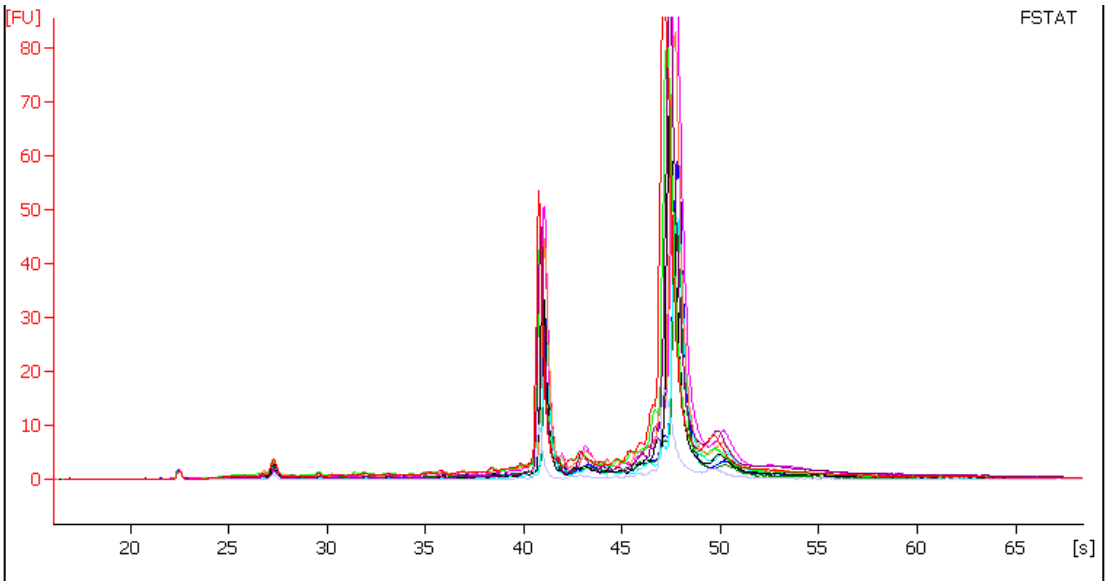

Figure 17 Overlay of AVEC total RNA isolated following Flexercell stretching protocols. RNA analysis used the Agilent Bioanalyzer depicting 18s and 28s rRNA peaks

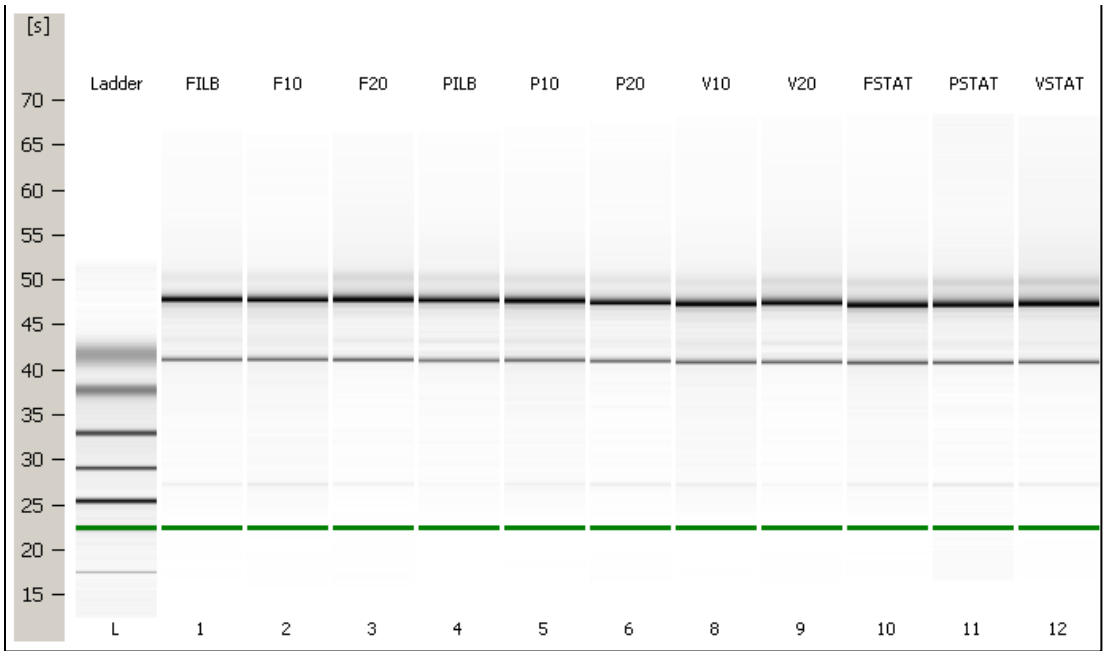

Figure 18 Agilent Bioanalyzer 18s and 28s bands depicting high quality AVEC RNA isolated from Bioflex™ plates.

Table 3 Primer sequences used for qRT-PCR

Gene	Primer Sequence	GenBank Accession No.
E-Selectin	5'-AGGGCTGAATGCGTATTGG-3'(F)	NM_214268
	5'-CCTCTGCTATTCTGATCTTC-3'(R)	
P-Selectin	5'-AGCTTCAGAACTGTCCAA-3'(F)	NM_214078
	5'-GCGAAGTATTCCATGAGTAAG-3'(R)	
PECAM-1	5'-CTCCTGTCAAGCTAATGTC-3'(F)	NM_213907
	5'-GATGTGGAACTTGGGATT-3'(R)	
ICAM-1	5'-AGGCCGCCACTAACAATC-3'(F)	NM_213816
	5'-AGGTGGGAAGCTGTAGAAG-3'(R)	
VCAM-1	5'-GAGAATGAACACTCCTATC-3'(F)	NM_213891
	5'-AGGCTACTCCAGTGAATC-3'(R)	
HPRT-1	5'-GGACTTGAATCATGTTTGTG-3'(F)	DQ845175
	5'-CAGATGTTTCCAAACTCAAC-3'(R)	

3.1.4 Statistical Analysis

Samples were run in triplicate, and relative expression was determined by using HPRT1 gene expression as the reference, or housekeeping gene. Gene expression levels were calculated using $2^{-\Delta Ct}$, while assuming 100% PCR efficiency. ΔCt resulted from the difference in threshold cycle between the gene of interest and HPRT1. qRT-PCR results are reported as mean ± 95% confidence interval. One-way analysis of variance (ANOVA) was performed using SAS analysis software to determine significant differences (p value ≤ 0.05) between FEC and VEC in each condition.

3.1.5 Confocal Laser Scanning Microscopy

Following cyclic stretching, staining for endothelial nitric oxide synthase (eNOS), reactive oxygen species (ROS), and phosphorylated Iκ-B and subsequent image acquisition and processing were conducted as previously described (19). The redox and NF-κB mechanisms were investigated due to their mechanosensitive nature, and ability to control inflammatory cell adhesion molecule transcription. Membranes were incubated in primary antibody dilutions ((1:100 eNOS, Mouse Anti-Human $I_gG_{2\alpha,}$Calbiochem, in PBS with 1% BSA, 1:1000 Iκ-Bα (phosphorylated at Ser32) Rabbit Anti-Human IgG_1, Biosource, Camarillo, CA,) overnight with gentle agitation at 4° C. Cells were rinsed twice for 15 min in PBS with 1% BSA. Secondary antibodies (Alexa Fluor 488 goat anti-mouse $I_gG_{2\alpha}$ and Alexa Fluor 488 goat anti-rabbit IgG_1, Invitrogen, 1:200 in PBS with 1%BSA) were incubated for 2 hours at 37°C. F-actin staining utilized AlexaFluor 635 Phalloidin (3µg/ml, Invitrogen) Membranes were cut out of the Bioflex plates with a razor blade and a drop (~25µl) of Vectashield Fluorescent Mounting Medium with DAPI (Vector Laboratories, Burlingame, CA) was allowed to spread over the membrane. The Image-IT live Reactive Oxygen Species kit (Invitrogen) was used to investigate the presence of ROS. The kit utilizes carboxy-H_2DCFDA, which fluoresces in the presence of reactive oxygen species (20;21). Upon completion of stretching experiments, cells were labeled with 25µM carboxy-H_2DCFDA, 1µl Hoechst 33342, rinsed, and imaged in warm Hanks Balanced Salt Solution (Gibco) according to manufacturer's instructions. Positive controls were conducted for ROS with the addition of hydrogen peroxide to normalize levels of fluorescence in the green channel prior to sample image acquisition.

3.2 Results

3.2.1 Gene Expression

Differential adhesion molecule gene transcription was performed using qRT-PCR. Data presented in Figs. 1-5 show the relative levels of mRNA expression for E-Selectin, P-Selectin, PECAM-1, ICAM-1, and VCAM-1, respectively. FECs were more susceptible to biochemical activation under static conditions than VECs. Incubation with TNF-α resulted in significantly greater expression E-selectin, P-selectin, ICAM-1, and VCAM-1 in FEC. The ratio of relative expression (FEC/VEC) of E-selectin and P-selectin was 11.30 ($p=0.037$) and 32.0 ($p\leq0.001$) times higher in FEC, respectively, while ICAM-1 and VCAM-1 were 2.22 ($p=0.019$) and 1.77 ($p=0.036$) times greater, respectively. However, PECAM-1 expression was not significantly different between cell types upon biochemical activation.

When cells were subjected to 5 or 10% strain, there was no significant difference in the level of gene expression between FEC and VEC, with the exception of E-selectin. E-Selectin expression was significantly higher in FEC at 5% (72.49, $p=0.021$) and 20% (3.09, $p=0.03$), and while expression was 25.88 times higher at 10% ($p=0.065$), the result was only considered statistically significant at $p<0.1$ (Fig.1). Statistically significant differences were also observed at 20% strain in PECAM-1 (10.67, $p\leq0.001$; Fig.3) and ICAM-1 mRNA levels. In contrast to the other genes, ICAM-1 expression was significantly greater in VEC exposed to 20% strain (1.80, $p=0.03$; Fig.4). P-Selectin showed no significantly different expression between AVEC types at any applied strain (Fig.2), and levels suggest neither FEC or VEC differentially express P-Selectin in a magnitude dependent manner. VCAM-1 gene expression was not significantly different

at any applied strain, although transcription levels declined with increasing magnitude in FEC (Fig.5). HPRT1, an enzyme in the purine salvage pathway, was less variant than a host of other potential reference genes tested (RPL4, TPB, 18s, data not shown), in accordance with a reference gene selection study in pig tissue (22).

3.2.2 Confocal Laser Scanning Microscopy

To investigate potential mechanosensitive mechanisms responsible for regulating adhesion molecule transcription in AVECs, CLSM was used to visualize expression of endothelial nitric oxide synthase (eNOS), reactive oxygen species (ROS), and phosphorylated Iκ-B.

Fig.6 demonstrates the lack of eNOS production at 5% strain in both cell types (Fig. 6A and 6B). Applied cyclic strain of 10% resulted in eNOS expression (green) in FEC, while eNOS was undetectable in VEC (Fig. 6C and 6D). However, eNOS expression is readily apparent and cytoplasmically diffuse in both cell types at 20% strain.

ROS were visualized in live AVEC immediately following cyclic straining, as seen in Fig. 7. A 5% strain resulted in localized, bright ROS staining (green) in both cell types (Fig. 7A and 7B). An applied strain of 10% resulted in much weaker staining, in a more diffuse pattern throughout the cytoplasm in both cell types (Fig. 7C and 7D). The most drastic side specific ROS production occurred following 24h of 20% cyclic strain. FEC display a somewhat bright and localized ROS production that is markedly non-nucleocentric (Fig. 7E). In contrast, VEC display much more prevalent and brighter ROS staining, diffuse across the entire cytoplasm, including nuclei (blue) co-localization (Fig. 7F).

The effect of cyclic strain on the intracellular location of phosphorylated Iκ-B was visualized in Fig. 8. Iκ-B staining (green) is stronger in VEC at 5% strain and also found in the cytoplasm, whereas Iκ-B remains in the nucleus (blue) in FEC (Fig. 8A and 8B). Strain of 10% resulted in similar Iκ-B staining in both cell types, although slightly more pronounced in VEC (Fig. 8C and 8D). A 20% strain yielded nuclear and cytoplasmic location of phosphorylated Iκ-B in both cell types. However, Iκ-B staining is much more prevalent in VEC than FEC, and distinctly brighter in the cytoplasm (Fig. 8E and 8F).

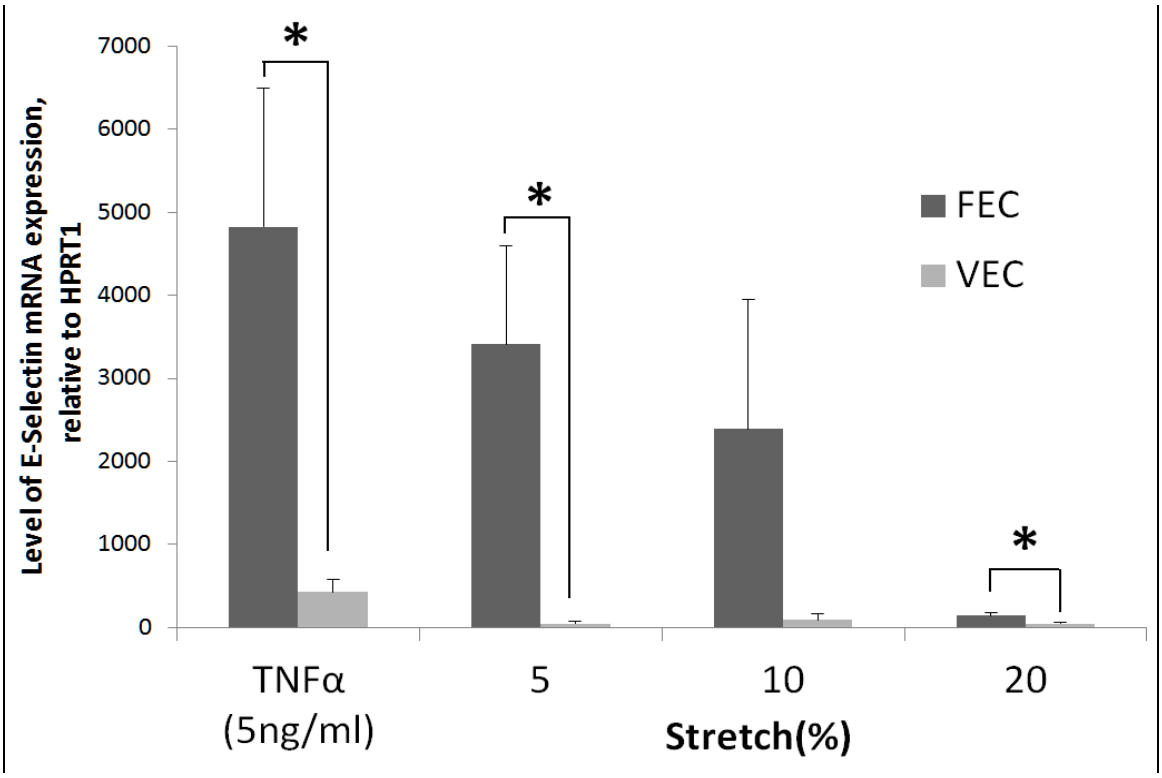

Figure 19 Level of E-Selectin mRNA expression, relative to HPRT1, in VECs exposed to cyclic strain or statically incubated in TNFα for 24h. Bars represent mean values + 95% confidence interval; n=3. * denotes significance of $p<0.05$.

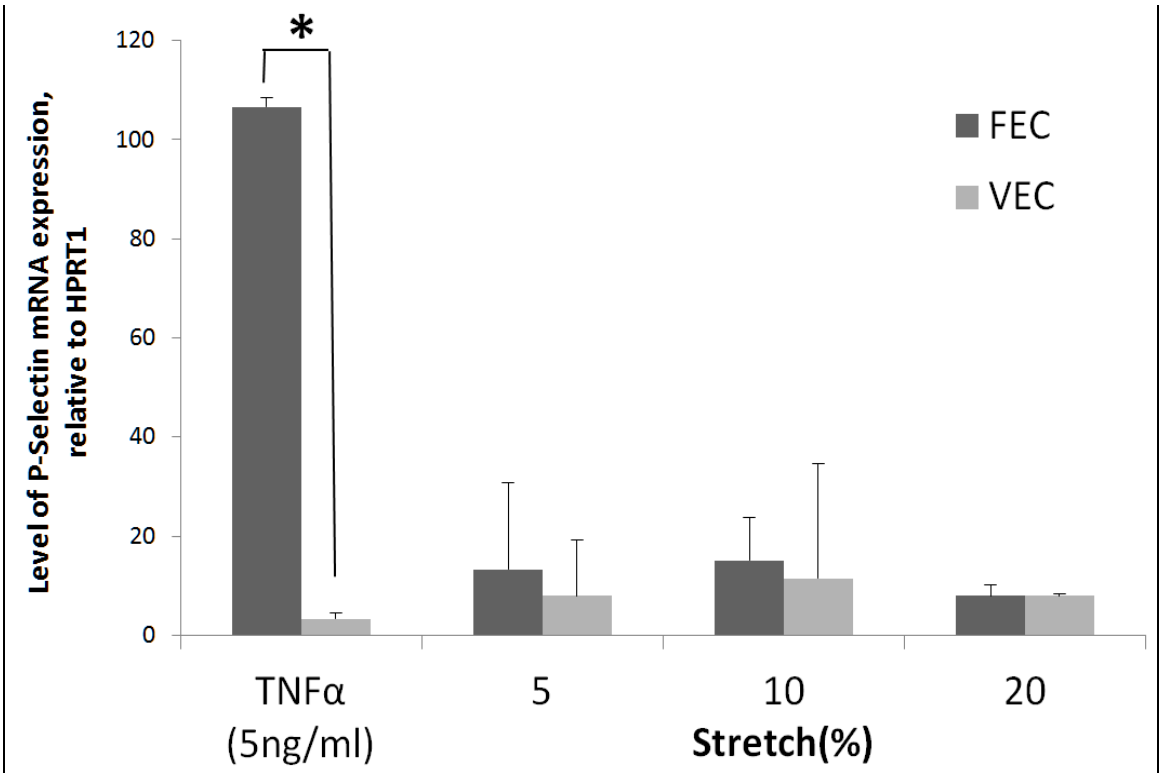

Figure 20 Level of P-Selectin mRNA expression, relative to HPRT1, in VECs exposed to cyclic strain or statically incubated in TNFα for 24h. Bars represent mean values + 95% confidence interval; n=3. * denotes significance of $p<0.05$.

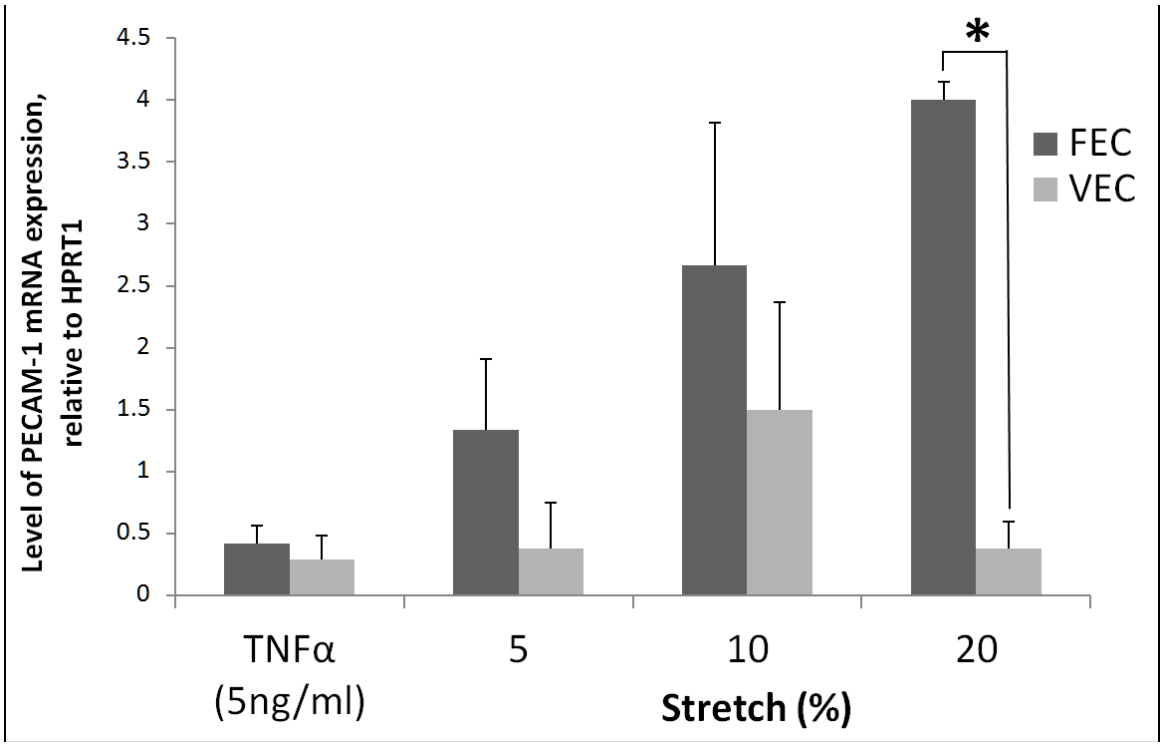

Figure 21 Level of PECAM-1 mRNA expression, relative to HPRT1, in VECs exposed to cyclic strain or statically incubated in TNFα for 24h. Bars represent mean values + 95% confidence interval; n=3. * denotes significance of $p<0.05$.

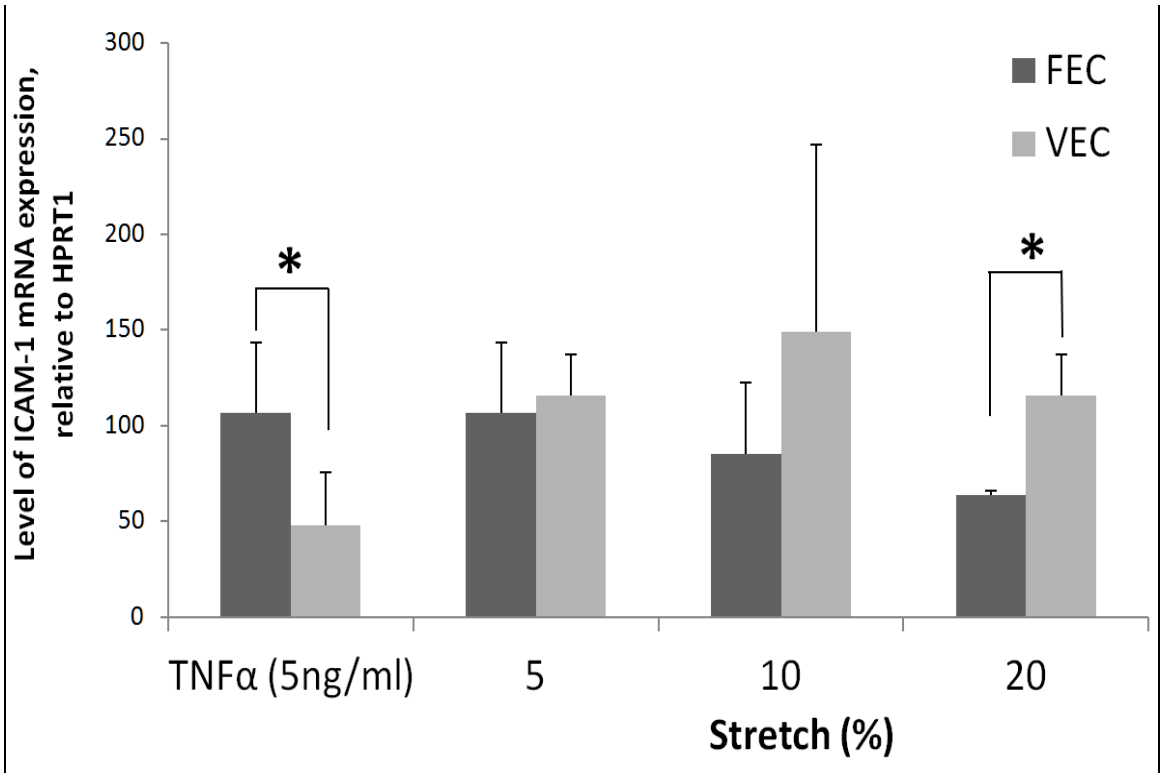

Figure 22 Level of ICAM-1 mRNA expression, relative to HPRT1, in VECs exposed to cyclic strain or statically incubated in TNFα for 24h. Bars represent mean values + 95% confidence interval; n=3. * denotes significance of $p<0.05$.

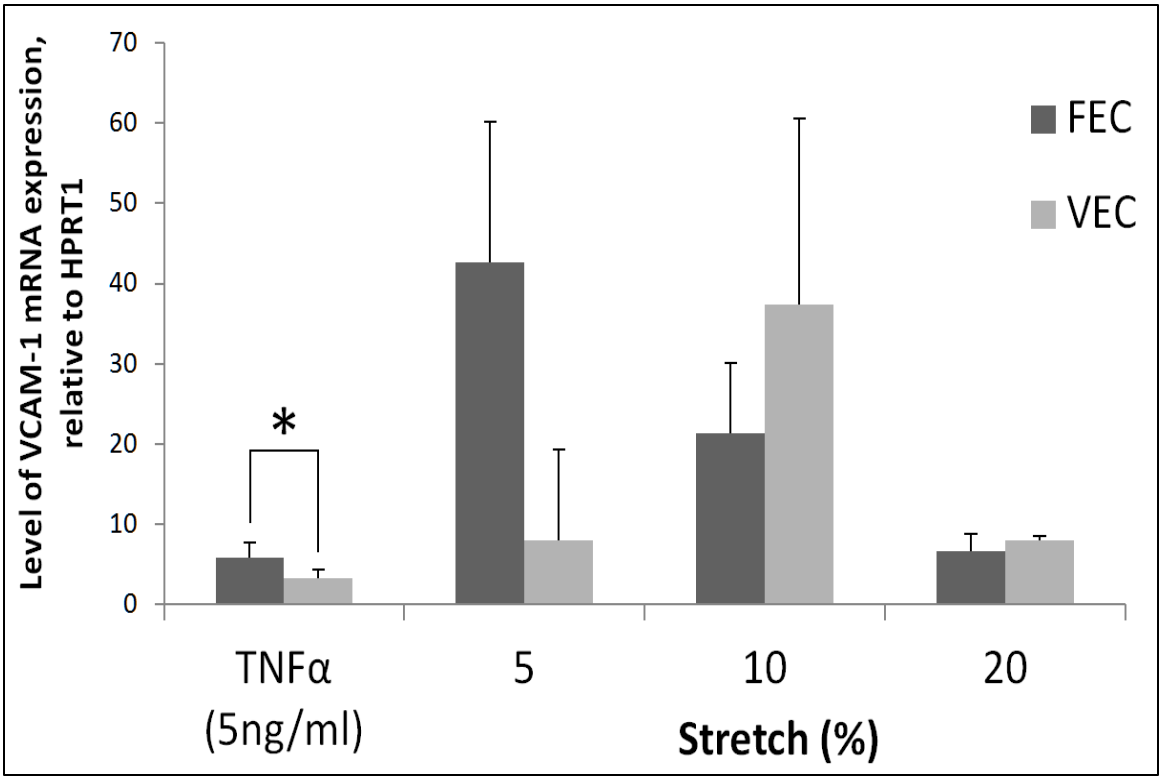

Figure 23 Level of VCAM-1 mRNA expression, relative to HPRT1, in VECs exposed to cyclic strain or statically incubated in TNFα for 24h. Bars represent mean values + 95% confidence interval; n=3. * denotes significance of $p<0.05$.

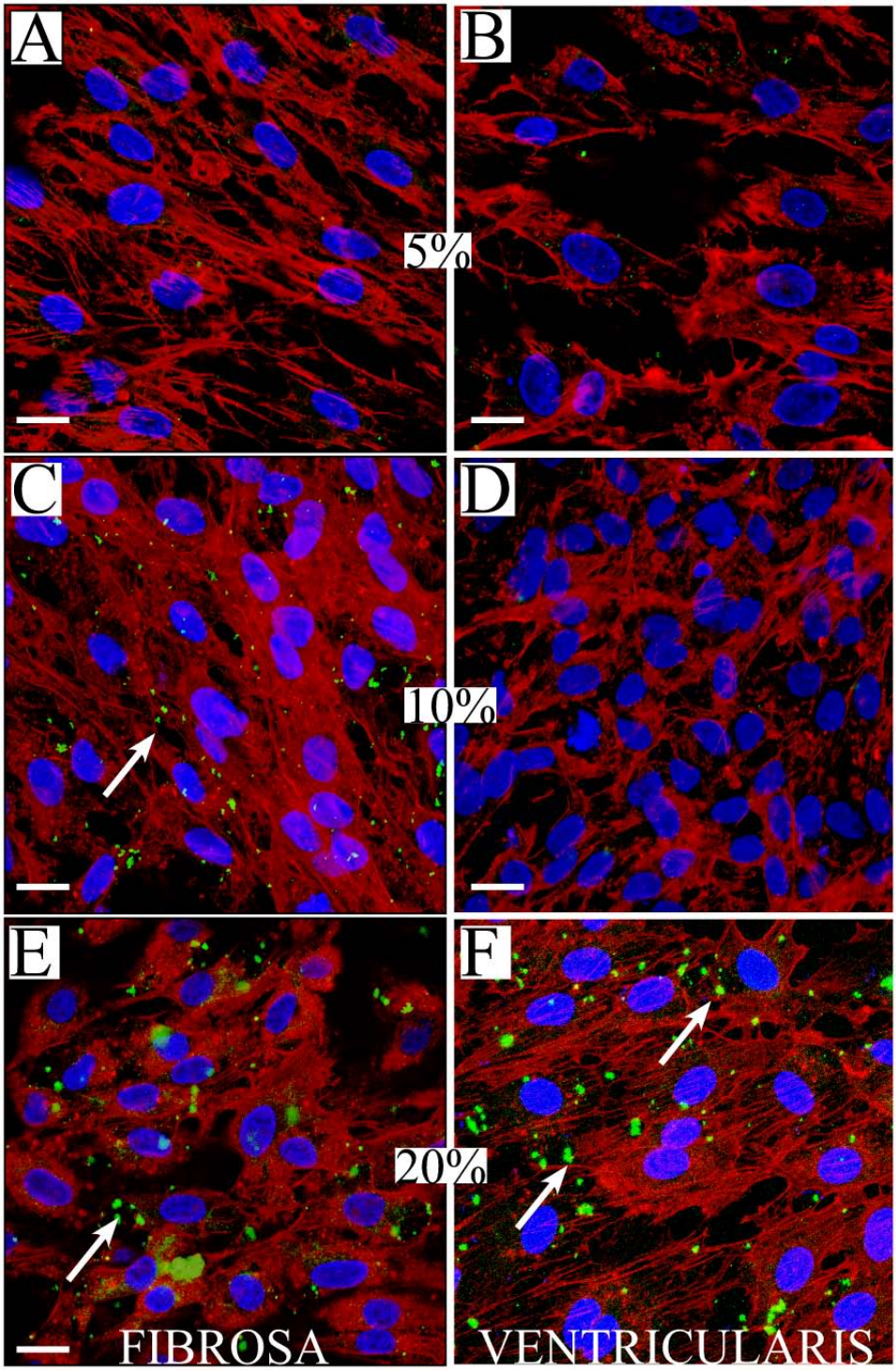

Figure 24 Confocal laser scanning microscopy images of FEC (A, C, E) and VEC (B, D, F) exposed to 24hr of cyclic stretch at 5 (A, B), 10 (C, D), and 20% (E, F). *Blue* cell nuclei, *red* F-actin, and *green* endothelial nitric oxide synthase (eNOS). Scale bars represent 10μm.

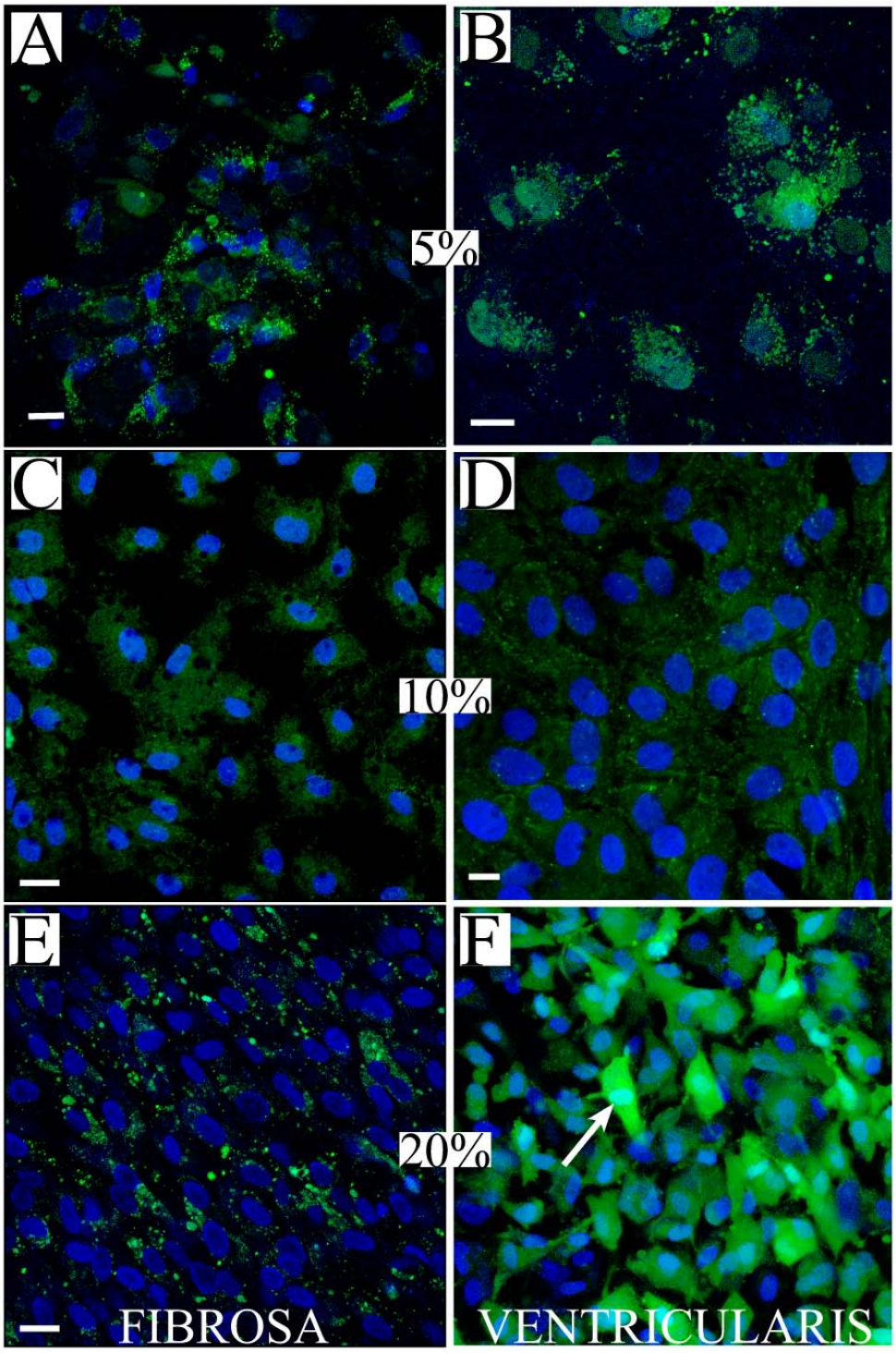

Figure 25 Confocal laser scanning microscopy images of FEC (A, C, E) and VEC (B, D, F) exposed to 24hr of cyclic stretch at 5 (A, B), 10 (C, D), and 20% (E, F). *Blue* cell nuclei and *green* carboxy-H_2DCFDA fluorescence in the presence of reactive oxygen species (ROS). Scale bars represent 10μm.

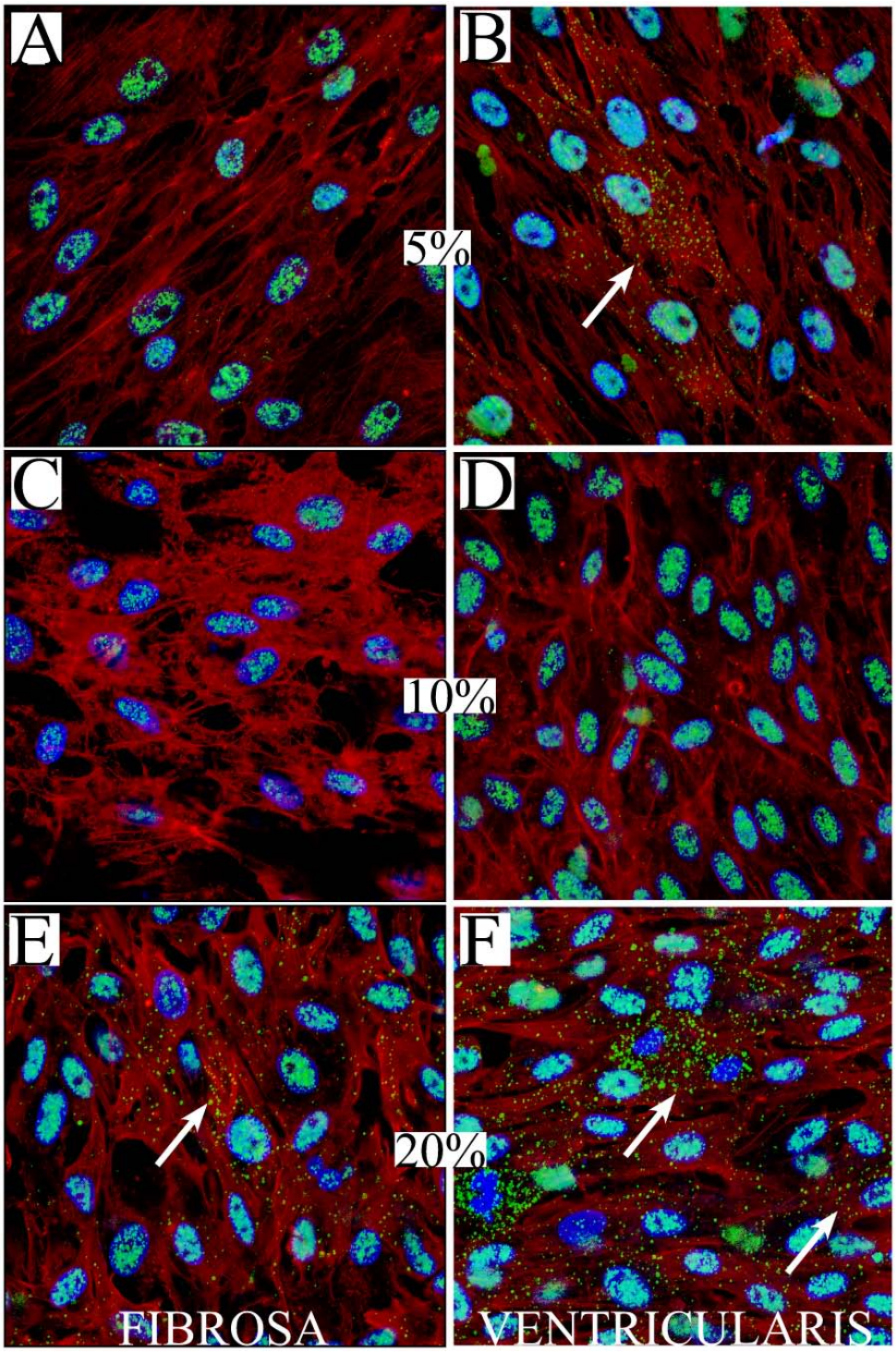

Figure 26 Confocal laser scanning microscopy images of FEC (A,C,E) and VEC (B,D,F) exposed to 24hr of cyclic stretch at 5(A,B), 10(C-D), and 20%(E,F). *Blue* cell nuclei, *red* F-actin and *green* phosphorylated (Ser32) Iκ-B. Scale bars represent 10μm.

3.3 Discussion

Nearly half a century of cardiovascular research has emphasized the crucial role the endothelium plays in mitigating vascular disease progression. Surprisingly, there exists a relatively recent appreciation of the pathophysiological mechanisms inherent to the valvular endothelium. The absence of effective non-surgical therapeutic strategies specifically targeting calcific valve disease underscores the imperative to achieve a more comprehensive understanding of valve biology. Diseased aortic valves exhibit inflammatory markers, concurrent with systemic endothelial dysfunction(5;23). Spatially distinct, or side-specific, valvular endothelial sub-phenotypes may contribute to the focal nature of AV calcific lesion development(10;24). CAVD is known to develop lesions preferentially on the fibrosa surface of the valve. The valvular endothelium becomes activated in early stages of CAVD, coincidental with alterations in the mechanical environment, most notably disrupted flow profiles and tissue mechanics (25;26). In the presence of a variety of mechanical and biochemical stimuli, activated aortic valve endothelial cells (AVEC) can elicit behavior consistent an athero-protective response, in addition to initiating pathogenesis(27). This study exposed spatially distinct (FEC and VEC) cell populations to an *in vitro* mechanical stimulus, in the form of cyclic stretch, and investigated the EC activation response.

The results from the study elucidated two primary functional differences between FEC and VEC. The first exposed a heightened sensitivity to biochemical stimuli on the disease susceptible side of the valve. The second demonstrated cyclic strain-induced anti-oxidant and anti-inflammatory activity in FEC, suggesting a protective phenotype. Differential expression of PECAM-1 and ICAM-1 at 20% strain, and of E-selectin at 5

and 20% strain indicates that FEC and VEC are distinct endothelial sub-phenotypes. This assertion is supported further by the data obtained from positive activation controls. Four of the five genes were differentially expressed between FEC and VEC after activation with TNF-α. The significantly different high strain (20%) expression levels of E-Selectin and PECAM-1 seen in FEC were indicative of an athero-protective response, due to E-Sel decreasing with increasing strain and significantly lower than TNF-α. E-Selectin has been reported on the fibrosa endothelium of sclerotic valves (5), whereas PECAM-1 has been implicated in the activation of eNOS(28). The data obtained by confocal microscopy also showed a protective redox environment in FEC under 10 and 20% strain, evidenced by ROS and eNOS expression. Furthermore, intracellular location of phosphorylated Iκ-B showed an active NF-κB pathway in VEC under 20% strain, resulting in higher VEC expression of ICAM-1. The shift of transcription favored inflammation in VEC under high strains.

Oxidative stress is an indicator of endothelial dysfunction in the vasculature. Balance of reactive oxygen species generation and nitric oxide production maintains a physiological endothelium. NADH/NADPH oxidase activity is responsible for oxidative stress in atherosclerosis, whereas oxidative stress in aortic sclerosis occurs independently of NADH/NADPH oxidase. Instead, oxidative stress occurs as a result of the uncoupling of eNOS, a phenomenon not observed elsewhere in the vasculature(29). Bicuspid valve disease, where mechanical environments promote accelerated calcification, has shown a decrease in eNOS activity(6). We demonstrated that FEC produced eNOS, while keeping ROS generation low at 10 and 20% strain. However, higher levels of eNOS and ROS observed in VEC at 20% strain are indicative of significantly increased oxidative stress

(Figures 25 and 26, respectively). A likely mediator of strain dependent ROS generation in VECs may be the uncoupling of eNOS. Oxidative stress in the valve endothelium can lead to activation of the TGF-β pathway, resulting in fibrosis and calcification. Additionally, Runx2 and MSX2 expression can be increased, causing interstitial cells to de-differentiate into osteoblast-like cells.

Genes demonstrating strong strain magnitude dependence were PECAM-1, E-Selectin, and VCAM-1. FEC expression of E-Selectin and VCAM-1 displayed identical trends; decreasing mRNA levels with increasing strain magnitude. P-Selectin, however, did not demonstrate mechanical dependence in either EC type. P-Selectin proteins in valve ECs reside in Weibel-Palade bodies and are not known to be mechanically sensitive, rather more potently regulated by biochemical stimuli at the transcription level, as we saw with TNF-α(30). A 5% strain resulted in higher CAM expression in FEC, while 10% strain did not result in differential expression of any adhesion molecules. 20% strain resulted in VEC expression to be significantly higher in ICAM-1, displaying a shift of pro-inflammatory gene transcription toward the cells isolated from the ventricularis surface. PECAM-1 transcription levels showed no difference when exposed to TNF-α, and became significantly higher in FEC exposed to 20% strain. This result was not unexpected as it is known that PECAM-1 expression is not induced by TNF-α(31). PECAM-1 plays a complex role in mechanosensation, due to its relationship with the cytoskeleton at the junction of adjacent cells, while also being integral in inflammatory processes(32). PECAM-1 has been shown to be part of a mechanosensitive complex, including VE-Cadherin, and VEGFR2, with PECAM-1 being the primary sensor. PECAM regulates monolayer integrity in addition to leukocyte transmigration. This

would indicate that FEC possess a strain regulated athero-protective mechanism unique from VEC, no doubt contributing to the remarkable longevity of normal healthy valves. These results could also be explained by differential states of oxidative stress seen in the cells at 20% strain. VEC generated much brighter ROS staining, possibly leading to NF-κB activation, resulting in higher inflammatory CAM transcription levels. The mechanism inherent to the fibrosa endothelium could very well serve a protective role, while degenerative processes such as aging, hypotension, and accumulation of oxidized LDL could serve to make the fibrosa endothelium susceptible to leukocyte migration, and eventual calcification. The finding of a more inflammatory state at 5% stretch, as opposed to 10%, follows our previous finding, as well as others (33), that sub-physiological mechanical stimuli results in a pro-inflammatory activated state. 10% strain most accurately mimics the *in vivo* strain levels of an aortic valve EC. Collagen oriented circumferentially has been shown repeatedly to undergo deformations approximating 10% strain (1;25). Hypertensive conditions would impart greater EC strain, even after the lock-up of collagen fibers, as the sub-endothelial membrane most likely continues to deform.

The endothelial cells present on every blood-contacting surface create adhesion molecules critical to the inflammatory response seen in a number of cardiovascular diseases. These transmembrane proteins extend into the blood stream to physically tether circulating monocytes. Adhesion molecules have been known to be present in mechanically defined points in the vasculature, namely bifurcations and regions with oscillatory or disturbed flow patterns(2). The selectin molecules recognize glycoproteins on the surface on circulating leukocytes, which serve to induce rolling of the lymphocytes

on the valve endothelium. The inflammatory adhesion molecules, ICAM-1 and VCAM-1, serve to further bind the leukocytes in the circulating bloodstream, and along with the action of PECAM-1, migrate across the endothelium. ICAM-1, VCAM-1, and E-Selectin have all been detected on excised diseased valves(18).

In conclusion, this study has shown that distinct molecular differences exist between the endothelium of the fibrosa and ventricularis of the porcine aortic valve. The fibrosa was more susceptible to activation by TNF-α than the ventricularis. The ventricularis was more susceptible to oxidative stress at high strain, which led to a significant increase in ICAM-1 gene expression.

Thus, mechanical forces alone, in the form of dynamic cyclic strain, were not sufficient to induce aortic-facing EC susceptibility to mechanisms implicated in degenerative valve disease initiation. Focal activation of valvular ECs may be linked to alterations in other mechanical components (hydrostatic pressure or fluid shear stress), or by a heightened sensitivity to biochemical activation.

3.4 References

(1) Sacks MS, Yoganathan AP. Heart valve function: a biomechanical perspective. Philos Trans R Soc Lond B Biol Sci 2007 Aug 29;362(1484):1369-91.

(2) Davies PF. Hemodynamic shear stress and the endothelium in cardiovascular pathophysiology. Nat Clin Pract Cardiovasc Med 2009 Jan;6(1):16-26.

(3) O'Brien KD. Pathogenesis of calcific aortic valve disease: a disease process comes of age (and a good deal more). Arterioscler Thromb Vasc Biol 2006 Aug;26(8):1721-8.

(4) Hakuno D, Kimura N, Yoshioka M, Fukuda K. Molecular mechanisms underlying the onset of degenerative aortic valve disease. J Mol Med 2009 Jan;87(1):17-24.

(5) Muller AM, Cronen C, Kupferwasser LI, Oelert H, Muller KM, Kirkpatrick CJ. Expression of endothelial cell adhesion molecules on heart valves: up-regulation in degeneration as well as acute endocarditis. J Pathol 2000 May;191(1):54-60.

(6) Aicher D, Urbich C, Zeiher A, Dimmeler S, Schafers HJ. Endothelial nitric oxide synthase in bicuspid aortic valve disease. Ann Thorac Surg 2007 Apr;83(4):1290-4.

(7) Agmon Y, Khandheria BK, Jamil TA, Seward JB, Sicks JD, Fought AJ, et al. Inflammation, infection, and aortic valve sclerosis; Insights from the Olmsted County (Minnesota) population. Atherosclerosis 2004 Jun;174(2):337-42.

(8) Otto CM, Kuusisto J, Reichenbach DD, Gown AM, O'Brien KD. Characterization of the early lesion of 'degenerative' valvular aortic stenosis. Histological and immunohistochemical studies. Circulation 1994 Aug;90(2):844-53.

(9) O'Brien KD, Reichenbach DD, Marcovina SM, Kuusisto J, Alpers CE, Otto CM. Apolipoproteins B, (a), and E accumulate in the morphologically early lesion of 'degenerative' valvular aortic stenosis. Arterioscler Thromb Vasc Biol 1996 Apr;16(4):523-32.

(10) Simmons CA, Grant GR, Manduchi E, Davies PF. Spatial heterogeneity of endothelial phenotypes correlates with side-specific vulnerability to calcification in normal porcine aortic valves. Circ Res 2005 Apr 15;96(7):792-9.

(11) Metzler SA, Pregonero CA, Butcher JT, Burgess SC, Warnock JN. Cyclic strain regulates pro-inflammatory protein expression in porcine aortic valve endothelial cells. J Heart Valve Dis 2008 Sep;17(5):571-7.

(12) Butcher JT, Penrod AM, Garcia AJ, Nerem RM. Unique morphology and focal adhesion development of valvular endothelial cells in static and fluid flow environments. Arterioscler Thromb Vasc Biol 2004 Aug;24(8):1429-34.

(13) Vande Geest JP, Di Martino ES, Vorp DA. An analysis of the complete strain field within Flexercell membranes. J Biomech 2004 Dec;37(12):1923-8.

(14) Sung HJ, Yee A, Eskin SG, McIntire LV. Cyclic strain and motion control produce opposite oxidative responses in two human endothelial cell types. Am J Physiol Cell Physiol 2007 Jul;293(1):C87-C94.

(15) Balachandran K, Konduri S, Sucosky P, Jo H, Yoganathan AP. An ex vivo study of the biological properties of porcine aortic valves in response to circumferential cyclic stretch. Ann Biomed Eng 2006 Nov;34(11):1655-65.

(16) Rozen S, Skaletsky H. Primer3 on the WWW for general users and for biologist programmers. Methods Mol Biol 2000;132:365-86.

(17) Diehl P, Nagy F, Sossong V, Helbing T, Beyersdorf F, Olschewski M, et al. Increased levels of circulating microparticles in patients with severe aortic valve stenosis. Thromb Haemost 2008 Apr;99(4):711-9.

(18) Shahi CN, Ghaisas NK, Goggins M, Foley B, Crean P, Kelleher D, et al. Elevated levels of circulating soluble adhesion molecules in patients with nonrheumatic aortic stenosis. Am J Cardiol 1997 Apr 1;79(7):980-2.

(19) Smith KE, Metzler SA, Warnock JN. Cyclic strain inhibits acute pro-inflammatory gene expression in aortic valve interstitial cells. Biomech Model Mechanobiol 2009 Jul 28.

(20) Maurer BJ, Metelitsa LS, Seeger RC, Cabot MC, Reynolds CP. Increase of ceramide and induction of mixed apoptosis/necrosis by N-(4-hydroxyphenyl)-retinamide in neuroblastoma cell lines. J Natl Cancer Inst 1999 Jul 7;91(13):1138-46.

(21) Konorev EA, Zhang H, Joseph J, Kennedy MC, Kalyanaraman B. Bicarbonate exacerbates oxidative injury induced by antitumor antibiotic doxorubicin in cardiomyocytes. Am J Physiol Heart Circ Physiol 2000 Nov;279(5):H2424-H2430.

(22) Nygard AB, Jorgensen CB, Cirera S, Fredholm M. Selection of reference genes for gene expression studies in pig tissues using SYBR green qPCR. BMC Mol Biol 2007;8:67.

(23) Poggianti E, Venneri L, Chubuchny V, Jambrik Z, Baroncini LA, Picano E. Aortic valve sclerosis is associated with systemic endothelial dysfunction. J Am Coll Cardiol 2003 Jan 1;41(1):136-41.

(24) Davies PF, Passerini AG, Simmons CA. Aortic valve: turning over a new leaf(let) in endothelial phenotypic heterogeneity. Arterioscler Thromb Vasc Biol 2004 Aug;24(8):1331-3.

(25) Yoganathan AP. Fluid mechanics of aortic stenosis. Eur Heart J 1988 Apr;9 Suppl E:13-7.

(26) Goldsmith IR, Blann AD, Patel RL, Lip GY. Plasma fibrinogen, soluble P-selectin, and von Willebrand factor in aortic valve disease: evidence for abnormal haemorheology, platelet activation, and endothelial dysfunction. Heart 2000 May;83(5):577-8.

(27) Guerraty MA, Grant GR, Karanian JW, Chiesa OA, Pritchard WF, Davies PF. Hypercholesterolemia induces side-specific phenotypic changes and peroxisome proliferator-activated receptor-gamma pathway activation in swine aortic valve endothelium. Arterioscler Thromb Vasc Biol 2010 Feb;30(2):225-31.

(28) Dusserre N, L'Heureux N, Bell KS, Stevens HY, Yeh J, Otte LA, et al. PECAM-1 interacts with nitric oxide synthase in human endothelial cells: implication for flow-induced nitric oxide synthase activation. Arterioscler Thromb Vasc Biol 2004 Oct;24(10):1796-802.

(29) Heistad DD, Wakisaka Y, Miller J, Chu Y, Pena-Silva R. Novel aspects of oxidative stress in cardiovascular diseases. Circ J 2009 Feb;73(2):201-7.

(30) Blann AD, Nadar SK, Lip GY. The adhesion molecule P-selectin and cardiovascular disease. Eur Heart J 2003 Dec;24(24):2166-79.

(31) Tzima E, Irani-Tehrani M, Kiosses WB, Dejana E, Schultz DA, Engelhardt B, et al. A mechanosensory complex that mediates the endothelial cell response to fluid shear stress. Nature 2005 Sep 15;437(7057):426-31.

(32) Fujiwara K. Platelet endothelial cell adhesion molecule-1 and mechanotransduction in vascular endothelial cells. J Intern Med 2006 Apr;259(4):373-80.

(33) Thacher T, Gambillara V, da Silva RF, Silacci P, Stergiopulos N. Reduced cyclic stretch, endothelial dysfunction, and oxidative stress: an ex vivo model. Cardiovasc Pathol 2009 Sep 3.

CHAPTER IV

LIVE QUANTITATIVE EN FACE IMAGING OF SOFT TISSUE UNDER MECHANICAL STRESS

Soft tissues, such as tendons, skin, arteries or lung, are constantly subject to mechanical stresses *in vivo*. None more so than the aortic heart valve that experiences an array of forces including shear stress, cyclic pressure, strain, and flexion(1). Anisotropic biaxial cyclic stretch maintains valve homeostasis; however, abnormal forces are implicated in disease progression(2;3). The response of the valve endothelium to deviations from physiological levels has not been fully characterized. Here we show the design and validation of a novel bioreactor capable of applying biaxial stretch to viable heart valve tissue while simultaneously allowing for live *en face* endothelial cell imaging via confocal laser scanning microscopy (CLSM). Concurrently, an image analysis protocol has been developed to process the CLSM data. This program accurately measures cell viability and death, as well as individual cell morphological parameters. Real-time imaging of tissue is possible while undergoing highly characterized mechanical conditions and maintaining the native extracellular matrix. Thus, it provides significant advantages over traditional cell culture or *in vivo* animal models. Planar biaxial tissue stretching with simultaneous live cell imaging could prove useful in studying the mechanobiology of any soft tissue.

4.1 Methods

Table 4 Primary Endpoints for Specific Aim 3.

Primary Endpoint	Methodology	Rationale
Glucose, pH, Sterility	Test media removed from bioreactor	Validate Live Tissue Culture Conditions
Preconditioning, Anisotropy, Hysteresis	Displacement vs Time, Stress-Strain Curves	Validate Soft tissue mechanics
Cellular Morphology	Circularity	Area/Perimeter Metric
	Cell Aspect Ratio	Major/Minor Axis
Endothelium Integrity	Live/Dead Ratio	Porosity indicates damaged endothelium
	Minimum Neighbor Distance	

4.1.1 Design and Construction

The central challenge in the development of the bioreactor was to achieve viable tissue culture conditions on the stage of a confocal microscope, without manipulating the cross-disciplinary confocal setup in a core imaging facility (Electron Microscope Center, Mississippi State, MS). Furthermore, a consistent sample loading and attachment scheme had to provide a viable endothelium under biaxial loading conditions while allowing for fluorescent staining and imaging of cellular processes. The *ex vivo* approach utilizes excised live tissue, while maintaining cellular function with minimal environmental disruption. Control of key tissue culture conditions included regulation of physiological levels of temperature, CO_2 and pH, while maintaining aseptic conditions. In addition, the mechanical environment of soft tissues must be characterized and applied for increased

physiological relevance of experiments. Cardiovascular tissues in particular experience blood pressure dependent tissue deformations. Planar biaxial stretch occurs in the aortic valve due to diastolic transvalvular pressure, or when the valve is mechanically loaded by the pressure gradient experienced between the aorta and left ventricle. Thus, our intended application imposed physiologically relevant mechanical loads on porcine aortic valves. The endothelial monolayer in the vasculature is highly sensitive to mechanics and implicated in a host of disease initiating mechanisms. Study of a fragile cell monolayer is logistically difficult using current tissue level experimental methods due to excessive sample processing for common scanning and transmission electron microscopy applications. Hence, we ventured to visualize a live endothelium without manipulation of biological conditions or mechanical loading.

To achieve these goals, a polycarbonate Lexan well (McMaster-Carr, Elmhurst, IL) was custom milled to the dimensions of the stage insert of the Zeiss LSM 510 laser scanning confocal microscope (Carl Zeiss AG, Oberkochen Germany). CAD drawings and the bioreactor on the stage of the confocal microscope can be seen in Figure 27 and Figure 28, respectively. Aseptic conditions were maintained by combining a sealed environment with materials that could easily be sterilized via UV radiation or autoclave. A lid was designed to be sealed with medical grade silicone adhesive and integrated with an injection port for the using disposable sterile membranes (Suba-Seal 8.0mm, Sigma) for both fluorescent and tissue culture medium control (Figure 29). The *ex vivo* stretch bioreactor uses digital mini servo rotary steppor motors (HiTec, Poway, CA) as the mode of applying planar translation. Digital capabilities provide for ease of programming, and the size of the servos (weighing less than 32 grams and occupying only 1.092 in^2 of

space) provides for ideal use on the cramped microscope stage. The servos operate with a stall torque of approximately 5 kg*cm. The controller has a rotary step resolution of 0.11°, translating to a linear position resolution of 34.5µm. The motors are controlled using a Labview program (Appendix I) run by a laptop (Dell Latitude X1) computer with LabView Version 8.0. The SSC-32 (LynxMotion, Perkin, IL) servo controller is used to position the motors based on its high resolution (1 µS, 0.09^{o}) for accurate positioning and smooth movements. Position, speed, and time data can be sent to the controller using ACII characters in LabView 8.0 (National Instruments, Austin, TX). The commands are passed to the controller from a computer through a USB port and through a USB/RS232 serial port converter. The motors are sent commands to move backward and forward repeatedly, simulating the cyclic distension of a valve constantly opening and closing in systole and diastole, respectively. The sliding Teflon translation arms and Teflon tracks provide a low friction system well within the operating torque of the servo motors. The excised soft tissue specimen attaches to the translation arms via 12 (3 per side) custom 22 gauge stainless steel hooks on removable hooking arms. The hooks are sutured to the hooking arm, which is pinned to the Teflon translation arm using a custom milled lock and pin system. The hooks that puncture the tissue are located on the same plane as the thin film bending beam load cells (Futek, Irvine, CA) that are mounted on the stretching frame. The attachment frame enables for repeatable sample loading of a 10mmX10mm specimen of live tissue. Previous experiments show that only about 80 grams of force are needed for a 2 mm stretch in aortic heart valves [6]. In order to closely simulate a heartbeat, the motors must spend approximately 857 milliseconds on each cycle. During the cycle about 2/3 of the time is spent in diastole (a condition simulated by elongating

the tissue) and 1/3 of the time in systole (a condition simulated by letting the tissue relax). As the leaflet is stretched, tissue stresses are generated by the distension of the load bearing fibrous components of the valve, predominantly elastin and collagen type I. To characterize the stresses, forces are measured using thin film bending beam load cells (Futek, Irvine CA) manufactured for reading forces up to 0.25 lb (113.4 grams). Voltage values produced by the load cells are passed through the 1B31 Wide Bandwidth Strain Gauge Signal Conditioners (Analog Devices, Norwood MA). The signal conditioners are wired to produce a differential gain of 335 and a low cutoff frequency of 100Hz. The values output by the signal conditioners are read by the NI USB6008 Data Acquisition (DAQ) Module (National Instruments) and converted to an analog signal. Figure 29 shows this detailed connection setup. Maintaining cell viability requires precisely controlled temperature conditions. In order to maintain 37°C in the bioreactor, a LabView controlled temperature system was created. To measure the temperature of the well, an NTC 10KOhm (Digikey, Thief River Falls, MN) thermistor is used. A resistor network is adhered to the bottom of the sample well on the stage and maintains a predetermined set temperature.

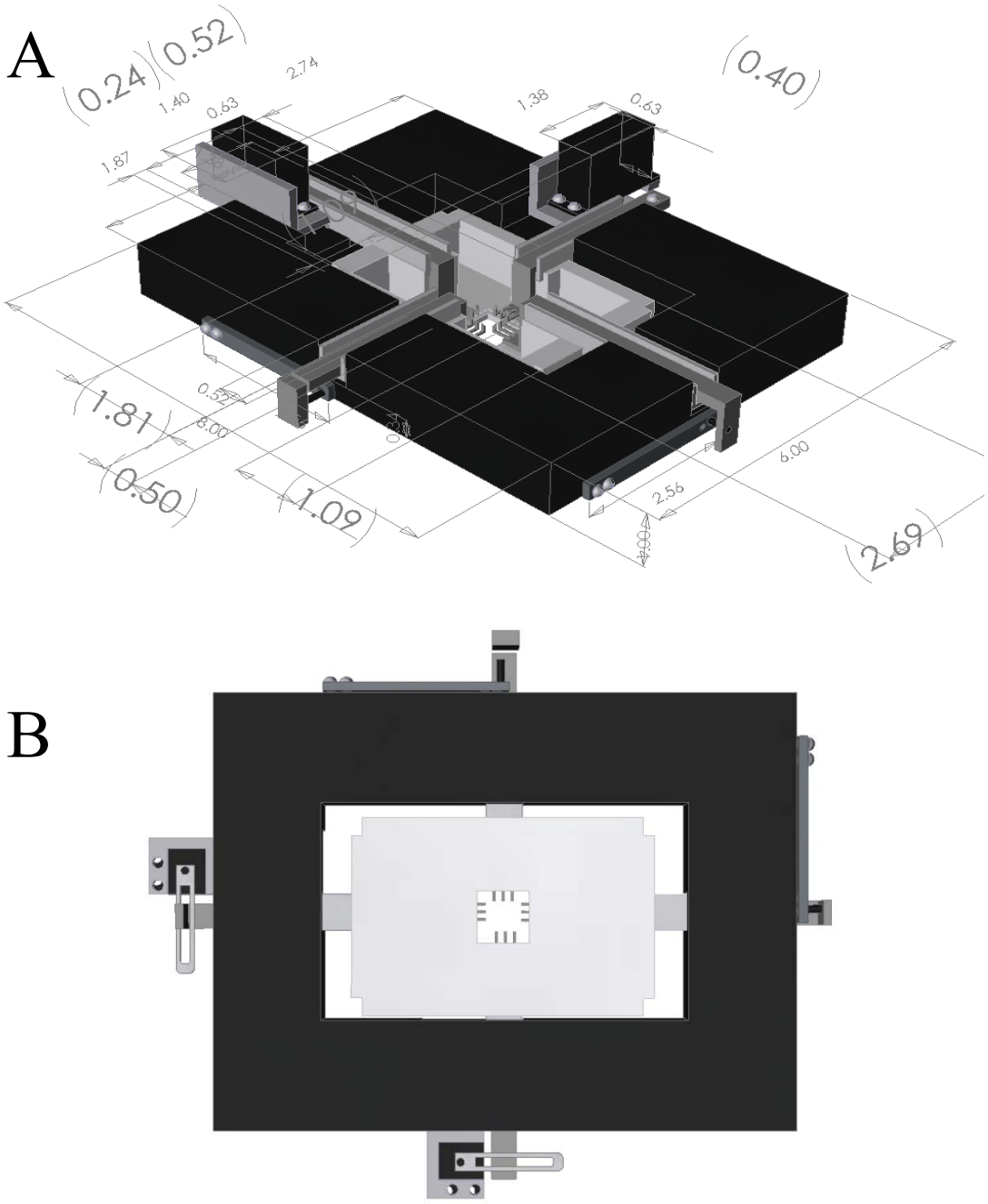

Figure 27 CAD representation of stretch bioreactor (Solidworks). Isometric View of Bioreactor Well and Frame, dimensions in inches. B) View from objective of inverted microscope.

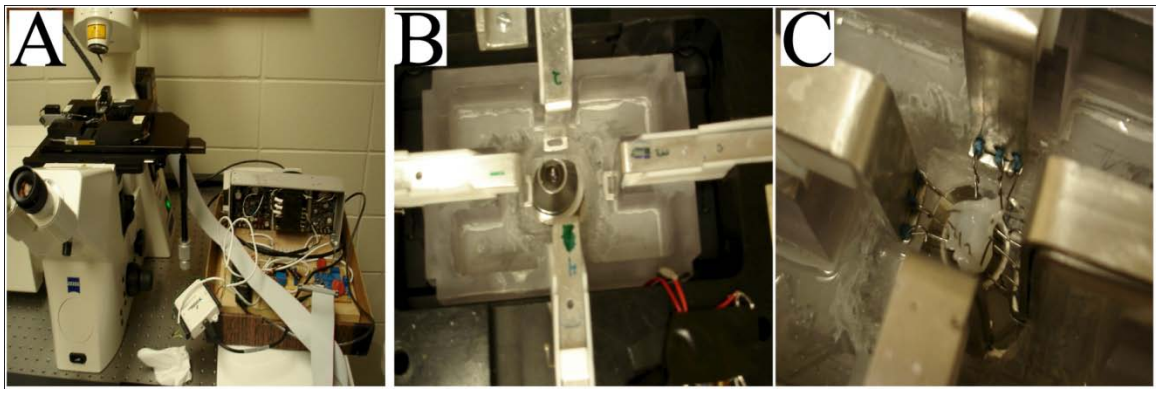

Figure 28 The stretch bioreactor on the stage of the Zeiss LSM 510 (A), the tissue culture well inserted into the stage insert with the microscope objective visible (B), and the microscope objective visible under the coverslip with an AV leaflet attached (C).

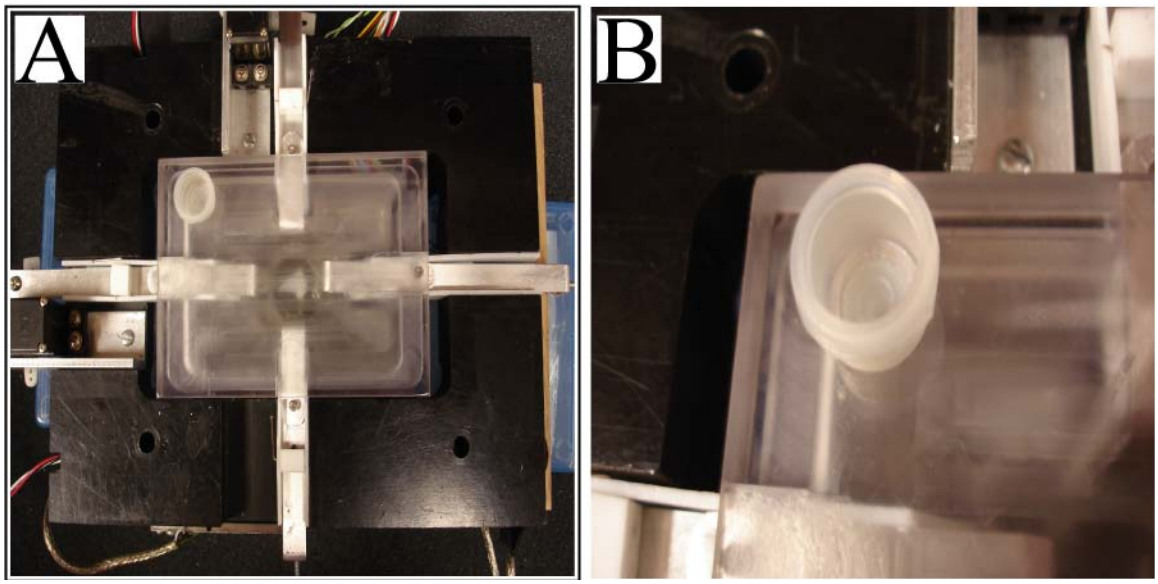

Figure 29 Stretch bioreactor shown with lid attached via medical grade silicone adhesive (A), media exchange port (B) is autoclavable and self-sealing when punctured with a syringe needle.

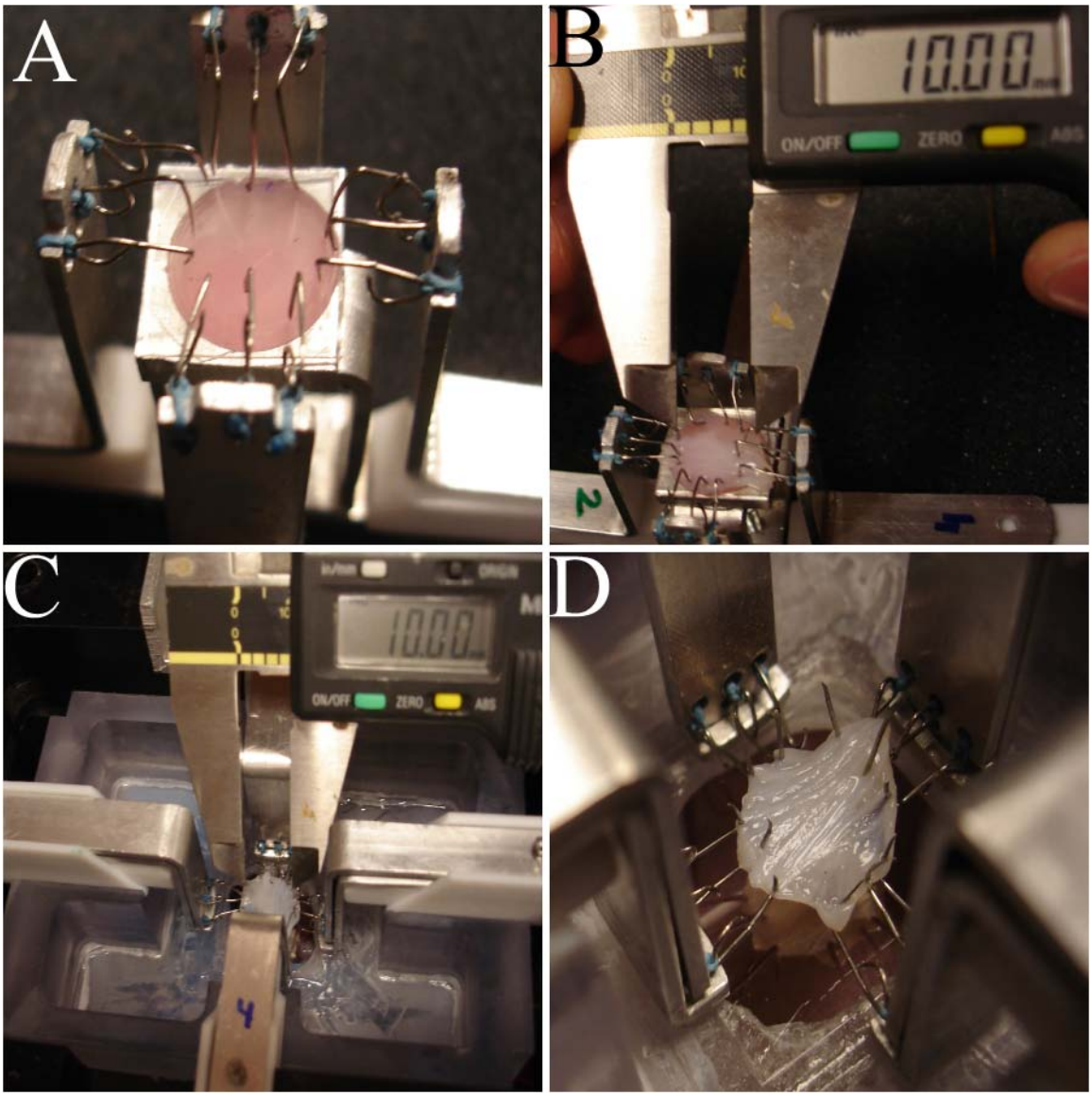

Figure 30 Sample attachment scheme. Attachment frame is set to consistently pierce tissue at a distance of 10mm (A). Pierced AV leaflet showing 10mm hook to hook distance (B), and is constant once introduced into the stretching well (C). Attached AV leaflet is shown in the absence of stretching or imaging media for contrast (D).

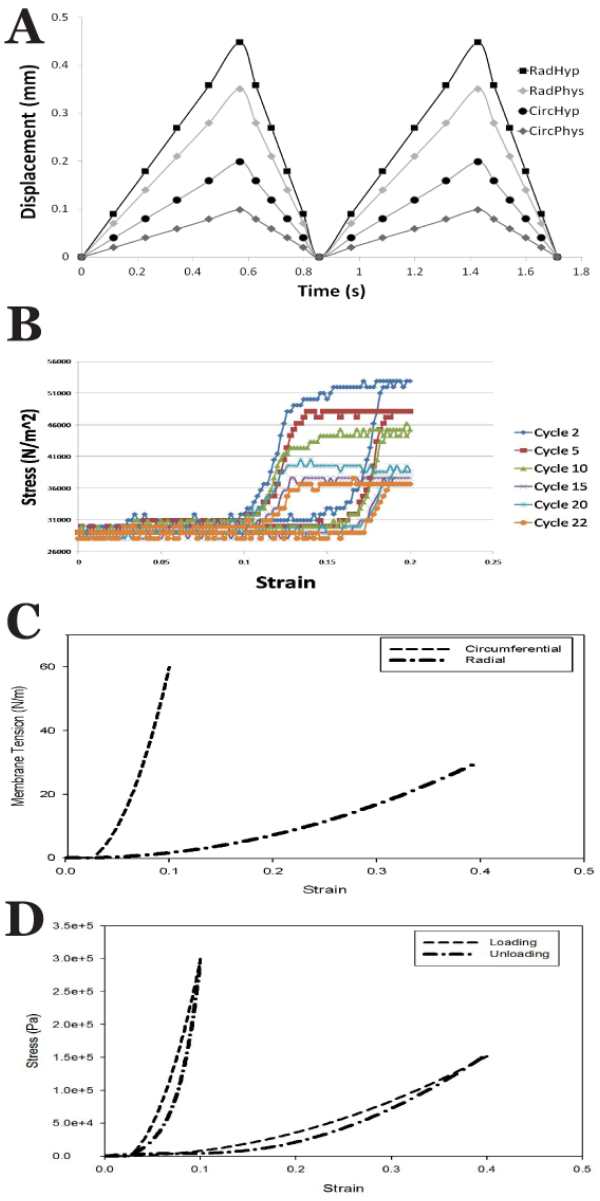

Figure 31 Mechanical Validation of bioreactor. (A) Displacement(mm) vs time(s) graph of sample loading under physiological and hyperphysiological conditions in the radial and circumferential directions. (B) Stress-strain curve depicting preconditioning of a valve leaflet in the radial directions, with a repeatable loading curve achieved after 15 cycles. (C) Membrane tension (N/m) vs strain curve in the radial and circumferential directions. (D) Stress (Pa) strain curves for an aortic valve under physiological stretch depicting the hysteresis of soft tissue, or difference in stress response when loading or unloading a tissue.

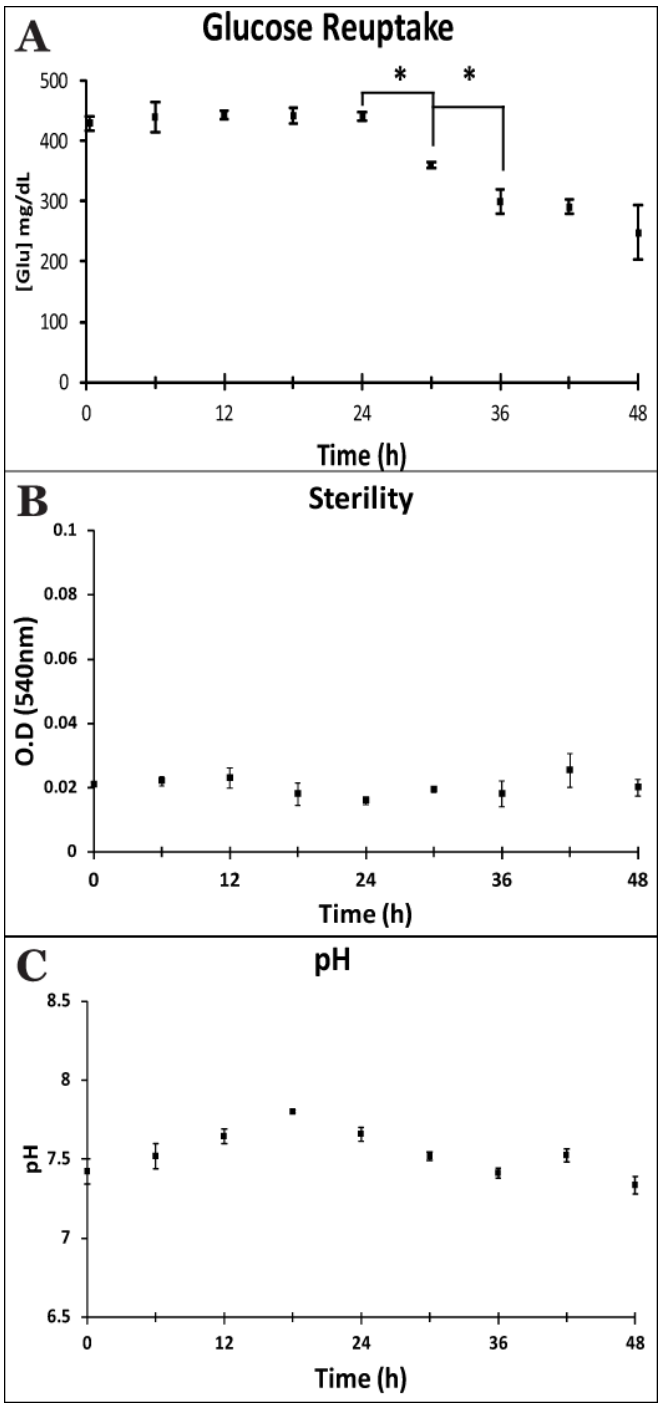

Figure 32 Biological performance of bioreactor, depicting (A) Glucose levels of media, which were found to significantly decrease after 24h and 30h (B) sterility as determined by the optical density of the media taken at 540nm, and (C) pH levels.

4.1.2 Live Cell Imaging

Fluorescence microscopy on living cells requires an intimate working knowledge fluorophore excitation and emission, digital image acquisition, and biological response to laser exposure. Optimization of live cell imaging parameters followed accepted principles and guidelines(7;8). Briefly, temperature, CO_2, and pH are crucial variable that must be controlled. Temperature regulation was carried out by a series of resistors with a thermistor feedback loop. The bioreactor easily operates in an incubator at 37°C and 5%CO_2. However, maintenance of cell viability becomes logistically difficult on the microscope. Complete cell culture medium supplemented with 25mM HEPES buffer maintains cell viability following CO_2 removal for up to 10hr. The bioreactor was designed to be retrofitted to the stage insert of a Zeiss LSM 510 laser scanning confocal microscope (Carl Zeiss AG, Oberkochen Germany). Following stretching, samples were stained with calcein-AM (5μM), ethidium homodimer (5μM) and Hoechst 33342 (1μM, all Invitrogen) for 15 minutes before image acquisition. The Zeiss LSM 510 has adjustable pinholes for each channel to allow for detection of only in-plane focused light. Imaging cells on live tissue however, introduces substantial out of focal plane fluorescence. Thus, the pinholes were experimentally determined and set to 86, 61, and 70 μm for the blue, green, and red channels, respectively. This allowed for maximum fluorescence detection while optimizing the balance between pixel saturation and laser strength. Laser strengths were set as low as possible to minimize tissue damage during live cell image acquisition. Laser strengths were 25%, 50%, and 50% for blue, green, and red channels respectively. Two images in distinct regions of each layer were captured to give approximately ~1000 cells for analysis. As seen in Figure 367, endothelial viability

and integrity was maintained under no load, physiological load and hyper-physiological load conditions. Aortic valve leaflets were freshly excised from a porcine heart directly following slaughter (Sansing Meat Service, Maben, MS) and transported in cold sterile phosphate buffered saline (D-PBS, Sigma). The leaflets were then cut with a razor blade into circumferential and radial strips aseptically in a sterile hood. The strips were then separated into three treatment groups: fresh, static, and stretched. The fresh leaflets were stained with calcein-AM (5μM), ethidium homodimer (5μM) and Hoechst 33342 (1μM, all Invitrogen) for 15 minutes and transported immediately to the confocal microscope (EM Center, MSU) for image acquisition. Leaflet strips were rinsed twice in PBS and placed on a 1 mm thick glass slide. A 22x22mm 1 oz glass coverslip was gently placed on the tissue and held on by capillary action. The slip aided in providing a more planar cellular surface where a large enough region of interest could be analyzed while maintaining a relatively uniform focal plane. Static leaflet strips were submersed in modified eagles medium (DMEM, Sigma) supplemented with fetal bovine serum (FBS, Atlanta Biological) and incubated at 37°C in 5% CO_2 for 72 hours. Following stretching or static incubation, samples were stained and imaged identically to the fresh samples. The Zeiss LSM 510 confocal microscope was used in the plane scanning mode to acquire each image at a single focal z-plane. 3D image stacks were not created due to the additional processing required. Plane scanning mode was used to create a 1024X1024 8-bit image with a scale of 0.9μmX0.9μmX1.0 μm. The objective used was an EC Plan-Neofluar 10X, with a numerical aperture (NA) of 0.30. Beam splitters split the laser lines at 405, 488, and 543 nm for the red, green, and blue channels, respectively. Filters for fluorescent detection were a band pass 420-480 (blue), band pass 505-530 (green) and a

long pass 615 nm (red channel). Selection of fluorophores maximized use of the electromagnetic spectrum to minimize channel crossover and allow for a user-friendly distinction between live and dead cells.

4.1.3 Image Handling

Adobe Photoshop CS4 (Adobe Systems Incorporated, San Jose, CA) was used to post-process images according to guidelines from the Microscopy Association of America (John Mackenzie, NC State, Confocal Microscopy Workshop). This method is used to avoid data manipulation from conventional "brightness/contrast" methods that have become abundantly abused. Light and dark levels are set using the histogram of pixel values of individual channels. For instance, the dark levels of the blue channel are set at the level where individual nuclei outlines are first seen, hence, the first relevant pixels in the blue channel are set in the histogram and all background not indicating nuclei is set to a histogram level of zero, or "true black". Light levels, or saturation point, a level of 255 in an 8-bit image or 4095 in a 12-bit image, is set to the first discernible pixels in each channel individual. This assures that the brightest pixel level is now set to the saturation point. This is a process known as histogram stretching, a method that spreads your data from each channel across the 256 or 4096 level spectrum, enhancing contrast of your data, while taking care not to over-represent bright spots, or have data on the dark side of the spectrum set to black artificially. Next, gamma levels are set sequentially in the red, blue, and green channels. Identical gamma levels are used for the green channel to give a proper comparison between images. Images are then saved in the TIFF format to avoid any loss of image quality due to compression.

4.1.4 Image Analysis

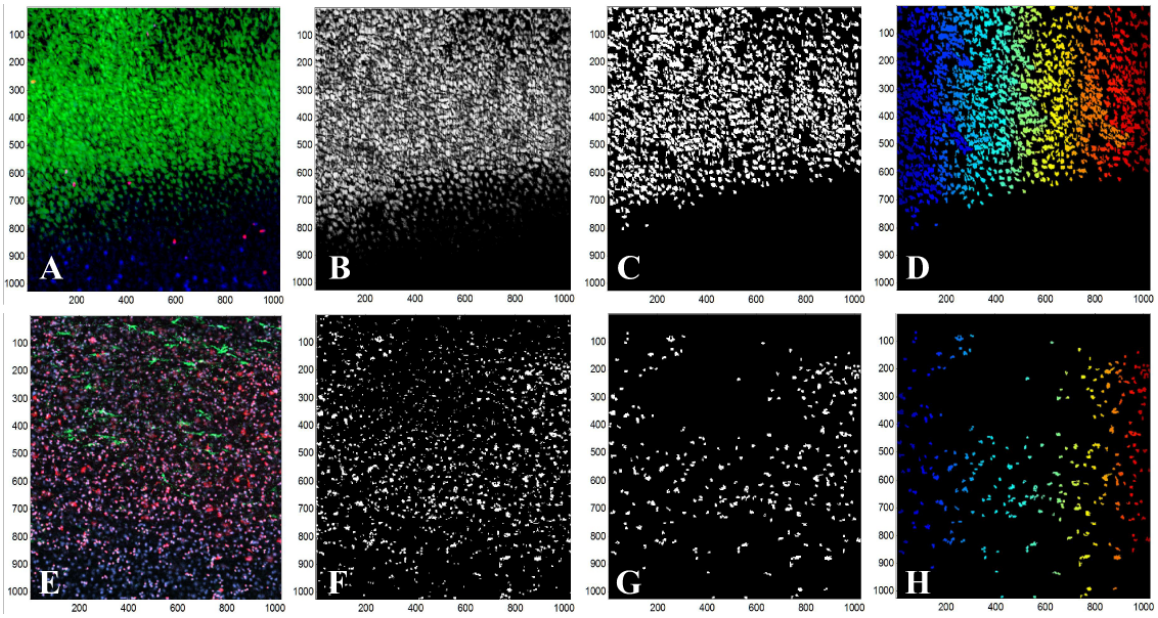

Figure 33 Image post-processing using custom code for Digital Image Processing Toolbox in Matlab. A representative particle analysis workflow is shown for live (A-D) and dead (E-H) cells. Raw images (A,E) are thresholded using Otsu's method(B,F), segmented(C,G), and labeled (D,H) for morphological analysis.

The preprocessing step was composed of background subtraction, channel image subtraction, and transformation to a binary image. Background subtraction involves first constructing the background image using block processing and subtracting the result from the channel image. Channel image subtraction was performed to subtract nuclei information from each channel image. Due to the fact that nuclei are present in all cells, and the fluorescent stain is highly permeable, precise determination of the origin of nuclei fluorescence was unattainable. Therefore, the nuclei components were subtracted and ignored for live and dead cell statistical analysis. Channel image subtraction was carried

out by subtracting the blue channel, including nuclei information, from the red or green channel image using equation 1.

$$I_{channel} = I_{channel} - \lambda \cdot I_{blue} \tag{1}$$

where I is the weighting factor, $0 < \lambda \leq 1$, depending on the channel. A thresholding technique was used to change the image into a binary image. To determine the individual thresholds, Otsu's method was employed (5). The sequence of image processing for live cells and predominantly dead cells is shown in the Appendix.

Information was extracted from processed images using a custom Matlab program. Number of live cells, dead cells, area, perimeter, circularity, aspect ratio, orientation, and the minimum neighbor distance were calculated. This information was used to calculate live/dead cell ratio, which is defined in equation 2.

$$Cell\ Ratio = \frac{Cell_{live}}{\left(Cell_{live} + Cell_{dead}\right)} \tag{2}$$

Cell circularity was measured with equation 3.

$$Circularity = \frac{4\pi \cdot Area}{Perimeter^2} \tag{3}$$

The post processing of samples for electron microscopy retains many of the biological interactions, however, are rendered useless for observing native cell size, shape, and interactions. The goal of this particular segment of the study is to visualize the

native AV endothelium with minimal sample processing and the ability to quantify endothelial morphological parameters. Electron microscopy has been carried out with all available imaging modalities including standard scanning electron microscopy, variable pressure environmental scanning electron microscopy, and transmission electron microscopy. The relationship between the strain level of the underlying extracellular matrix and the morphology of the endothelium will be investigated. The limitations due to processing of valves for electron microscopy have been overcome through the use of laser scanning confocal microscopy. Fluorescence microscopy is a valuable tool for biological imaging, especially in regard to live cell imaging. The inherent autofluorescence of biological tissue and underlying cell populations can be corrected for in live tissue *en face* preparations. The use of pinholes to collected only fluorescence emitted from a single plane has been instrumental in imaging of the endothelium. We have designed a method to visualize the aortic valve endothelium and analyze the properties of monolayer integrity and cellular morphology.

The aortic valve endothelium is a highly mechanosensitive monolayer involved in the initiation of calcific aortic valve disease. Valvular pathogenesis begins due to an endothelial injury, where the endothelial cells are removed. The mechanism is not currently known as to how the AVECs are removed. We have performed a study to analyze the AVEC response to cyclic stretch in the radial or circumferential directions. An automated image analysis program was designed to characterize confocal fluorescence microscopy images. The images were segmented and features were extracted in order to calculate the cell ratio, minimum neighbor distance, and circularity. There are several key limiting factors in our design. Though the overall goal of the

stretch bioreactor is to mimic *in vivo* condition, this is not completely possible. First, the native heart valve leaflet is subject to harsh fluid shear stresses and flexural stresses that are mostly absent while the tissue is stretching in the bioreactor. Also heart valves are attached to the aortic wall through connective tissue that is severed when the leaflets are excised from the pig. As a result, the tensile strength possessed by the leaflet may be diminished. The bioreactor is designed to impart planar biaxial stresses; however, the heart valve leaflet is subject primarily to radial and circumferential stress. One axis closely approximates the radial direction, whereas the other serves as a pseudo-circumferential stretch. The measurement of these stresses also poses some limitation on the final results. Our strain calculations are based experimental values that are only accurate one hundredth of a millimeter. The force calculations are also based on experimental values determined from converting voltage to mass. When stress is calculated from these force values, any small error is amplified when dividing by the cross-sectional area and multiplying by the force of gravity.

The third limitation of the bioreactor is its ability to be used on all objectives of the LSM. Because it is important for the endothelial layer to be within the working distance or focal plane, some high powered objectives (above 40x) cannot get close enough to the tissue because of the depth of the well. High magnification objectives are most likely too destructive on the endothelial surface, due to reactive oxygen species created from the focused laser at substantial enough power to make the fluorophores emit fluorescence. The goal of this section of the study is to design, construct, and validate a method to relate physiological forces with an endothelium response. Given that aortic valve sclerosis may be initiated by an endothelial injury, denudation, and/or activation,

the method chosen will observe endothelial cells on a freshly excised porcine aortic valve. The methods defined here will serve as a functional methodology to use a truly integrative approach that fuses the fields of live fluorescence imaging, applied tissue level mechanics, and ex vivo tissue culture. The design phase consists of requirements to visualize the aortic valve endothelium on a single cell scale, while applying physiologically relevant tissue level forces. Live cell imaging will utilize the Zeiss LSM 510 Confocal Laser Scanning Microscope.

4.1.5 Fluid Shear Stress Calculation

$$\tau_\omega = U_0 * \sqrt{\rho\omega\mu} * \sin\left(\omega t - \frac{\pi}{4}\right) \quad (4)$$

Shear stress at the wall of an oscillating plane is given by τ_ω, which is in the units of Pa. Briefly, shear stress at the wall of an oscillating plane below a viscous fluid is defined by the initial velocity, in our case, the instantaneous velocity of the servo motor arm, multiplied by the square root of the product of the density of the liquid,ρ, the plate frequency,ω, and the dynamic viscosity,μ, multiplied by the phase of sin of the frequency. For calculation purposes, we have used the density of water, 1g/cm^3, and used the dynamic viscosity of water at 40°C. since the AV leaflet will be stretching in either an optically clear imaging media composed of HEPES buffered phenol red free culture media, a saline solution, or tissue culture with media. The shear stress at the wall, or membrane, which would be the endothelial cell surface, was calculated for maximum shear stress during the loading phase, which lasts for 2/3 of the cycle and simulates diastole, as well as the unloading phase, lasting 1/3 of the cycle, and simulates systole.

Peak shear stress would be seen during the unloading phase, as the membrane moves the same magnitude in half the time.

Shear stress is critical to a normal functioning endothelium. We calculated a shear stress of less than 2 dynes cm^{-2}. This is consistent with a CFD computed for a bioreactor that pulled AV leaflets uniaxially to the same strains and at similar strain rates(19). Full calculations can be found in the Appendix.

4.2 Results

4.2.1 Soft Tissue Mechanics

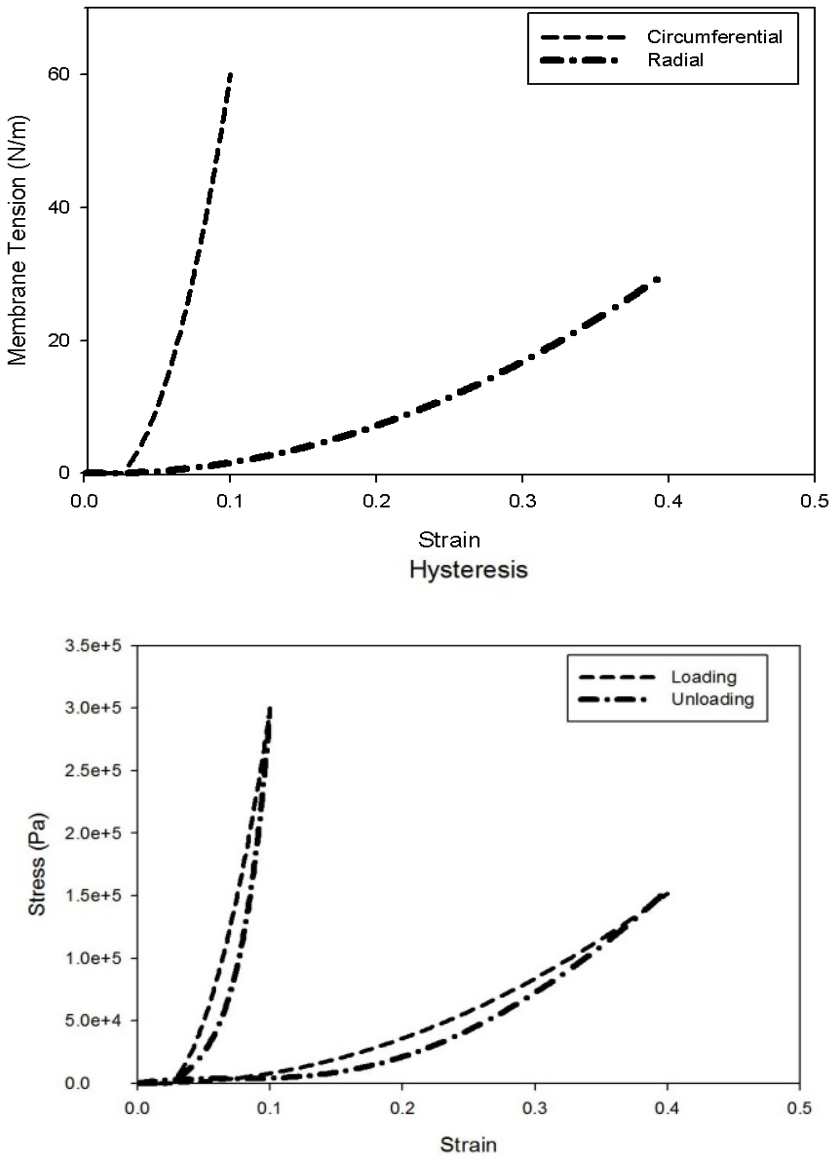

Figure 34 AV tissue response to strain in the radial and circumferential directions. Hysteresis (A) displayed in as well as a (B) membrane tension vs strain graph. Note the circumferential direction reaches a peak of 60N/m at a strain of 10%.

4.2.2 Endothelial Specific Visualization

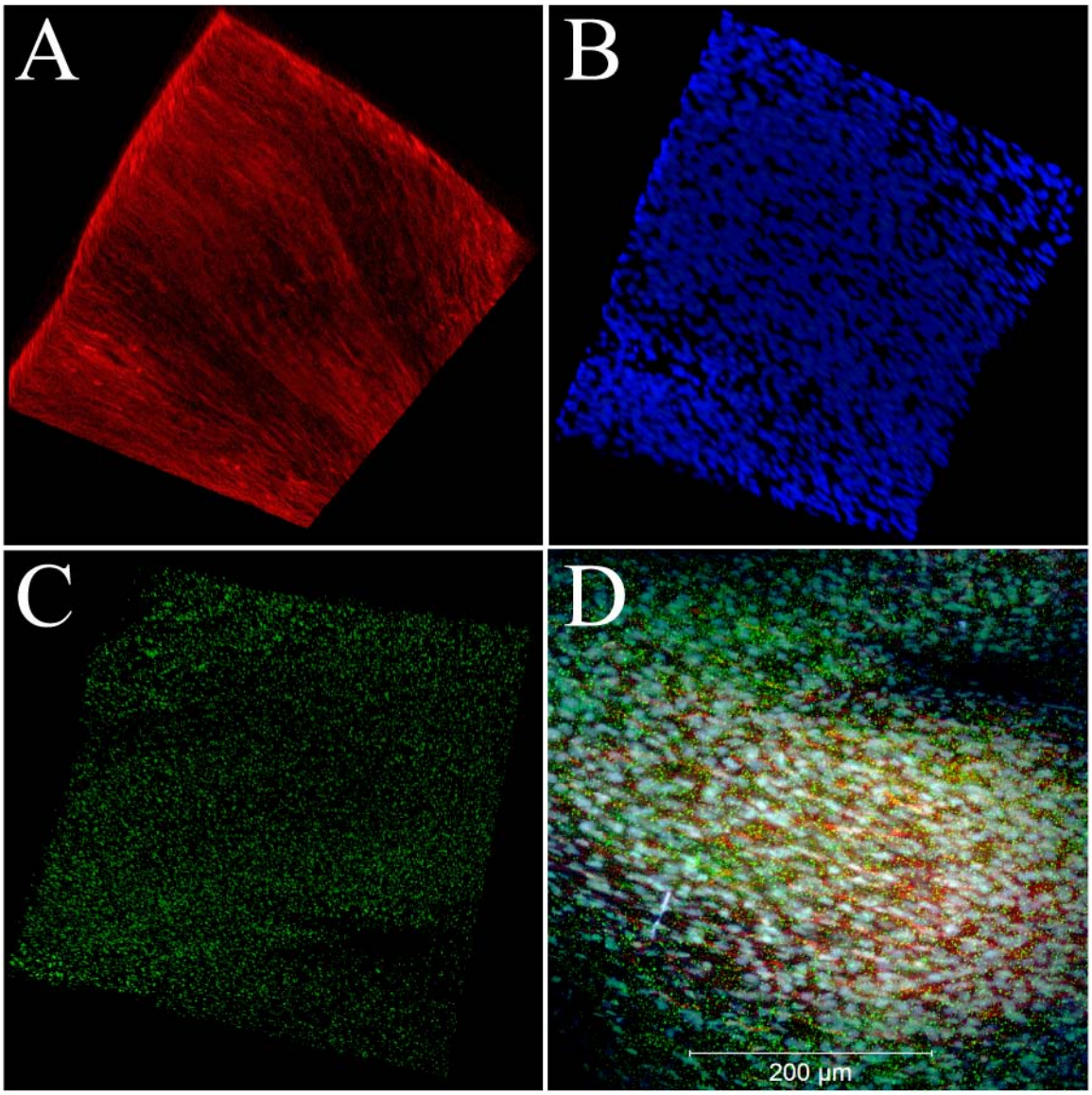

Figure 35 *En Face* preparation of AV endothelium. 3D reconstructions of nuclei (Hoechst 33358, A), F-Actin stained with (AlexaFluor 635, B), and EC marker vonWillebrand Factor (Mouse Anti-Human vWF IgG1 and Goat Anti- Mouse IgG1 Alexa Fluor 488, green). 3D reconstructions (A-C) are merged into a single projection image (D).

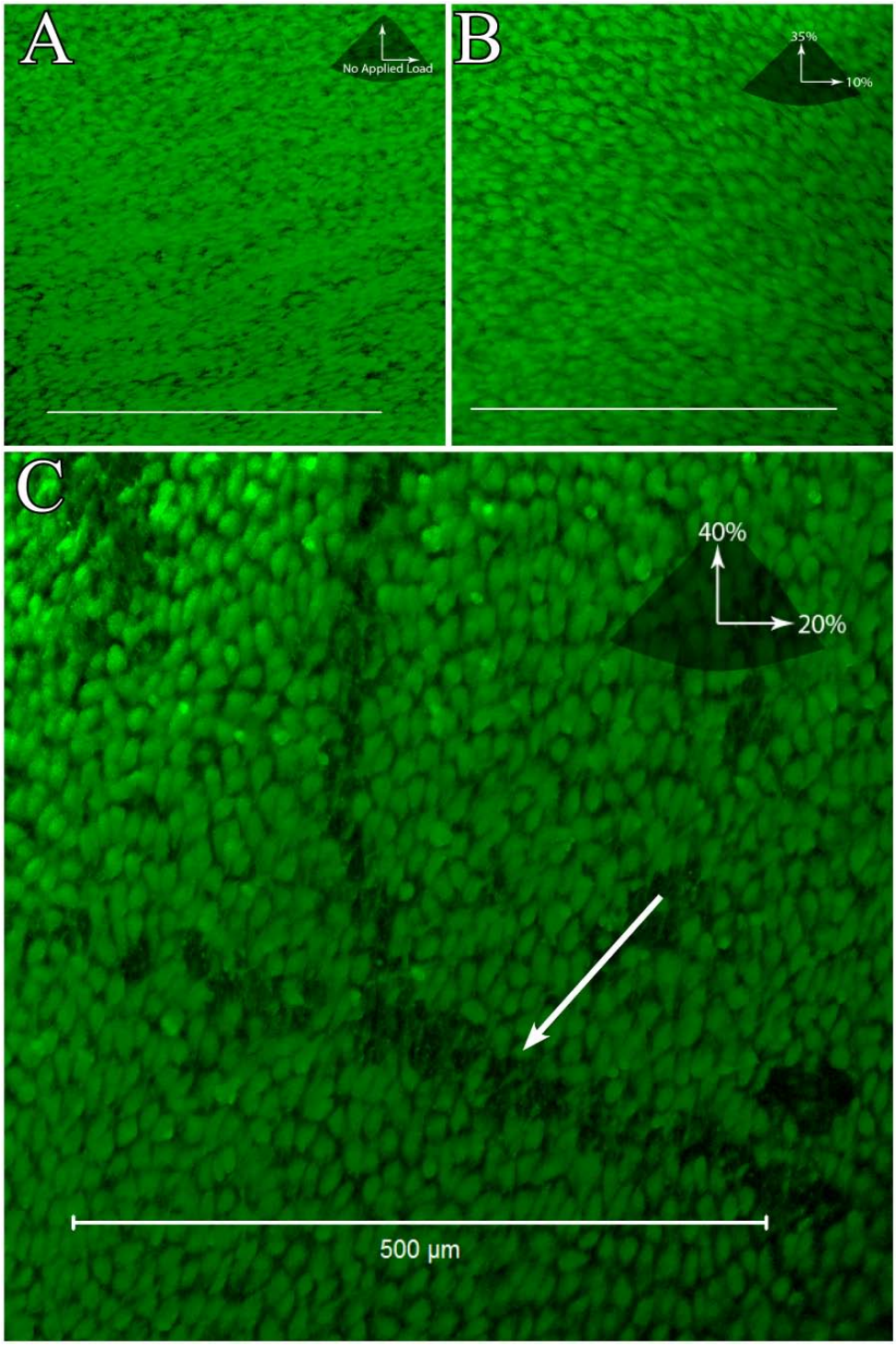

Figure 36 Fresh AV leaflet under no applied load (A), physiological stretch (B) and hyper-physiological stretch (C). Scale bars indicate field of view is approximately 3600µm^2.

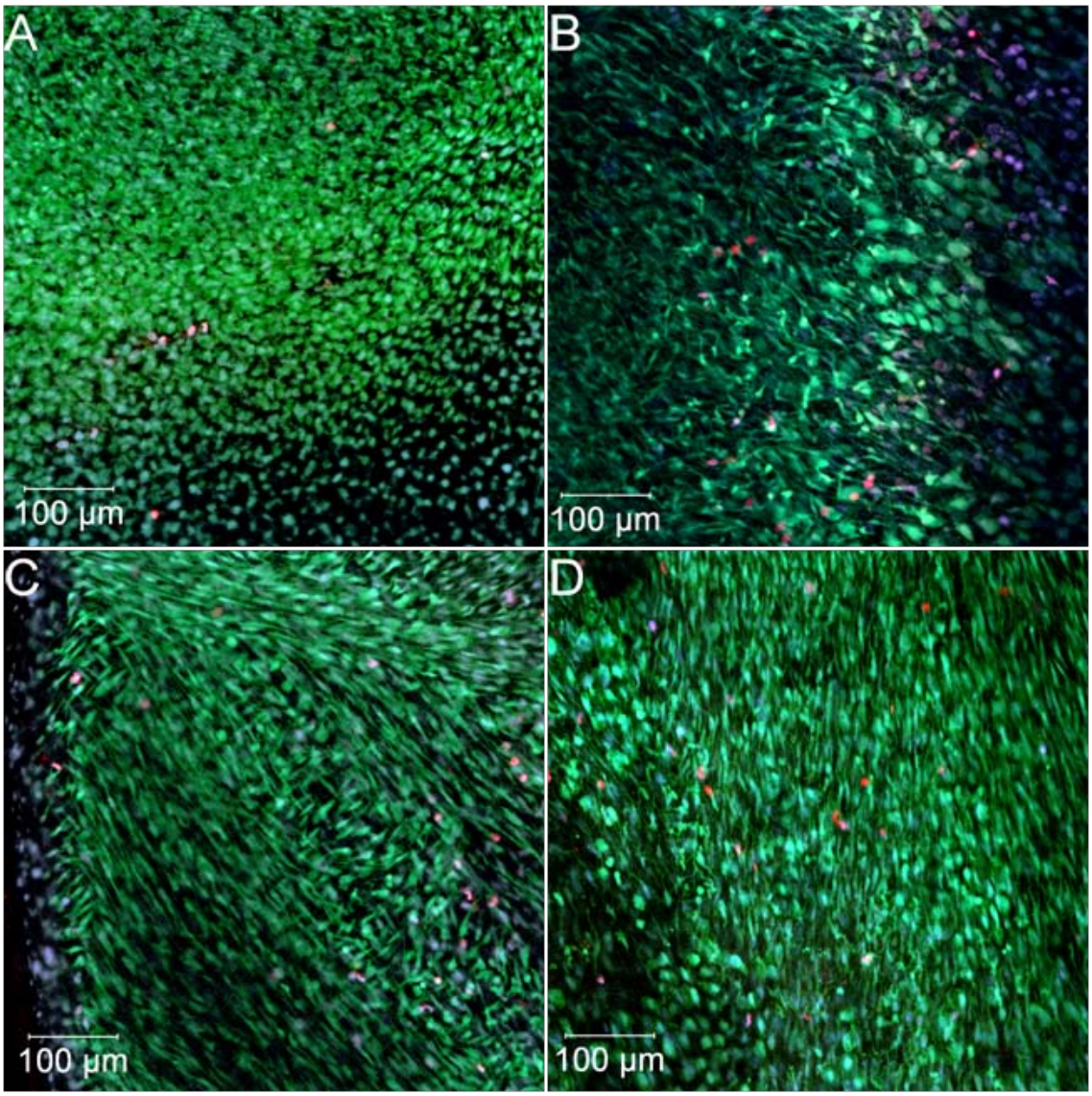

Figure 37 Live aortic valve endothelial cells on the aortic (A,B) or ventricularis (C,D) facing surface immediately imaged after excision in the radial (A,C) or circumferential (B,D) direction. Live cells (calcein, green) dead cells (ethidium homodimer, red) and nuclei (Hoechst 33342) are shown with scale bars of 100 µm.

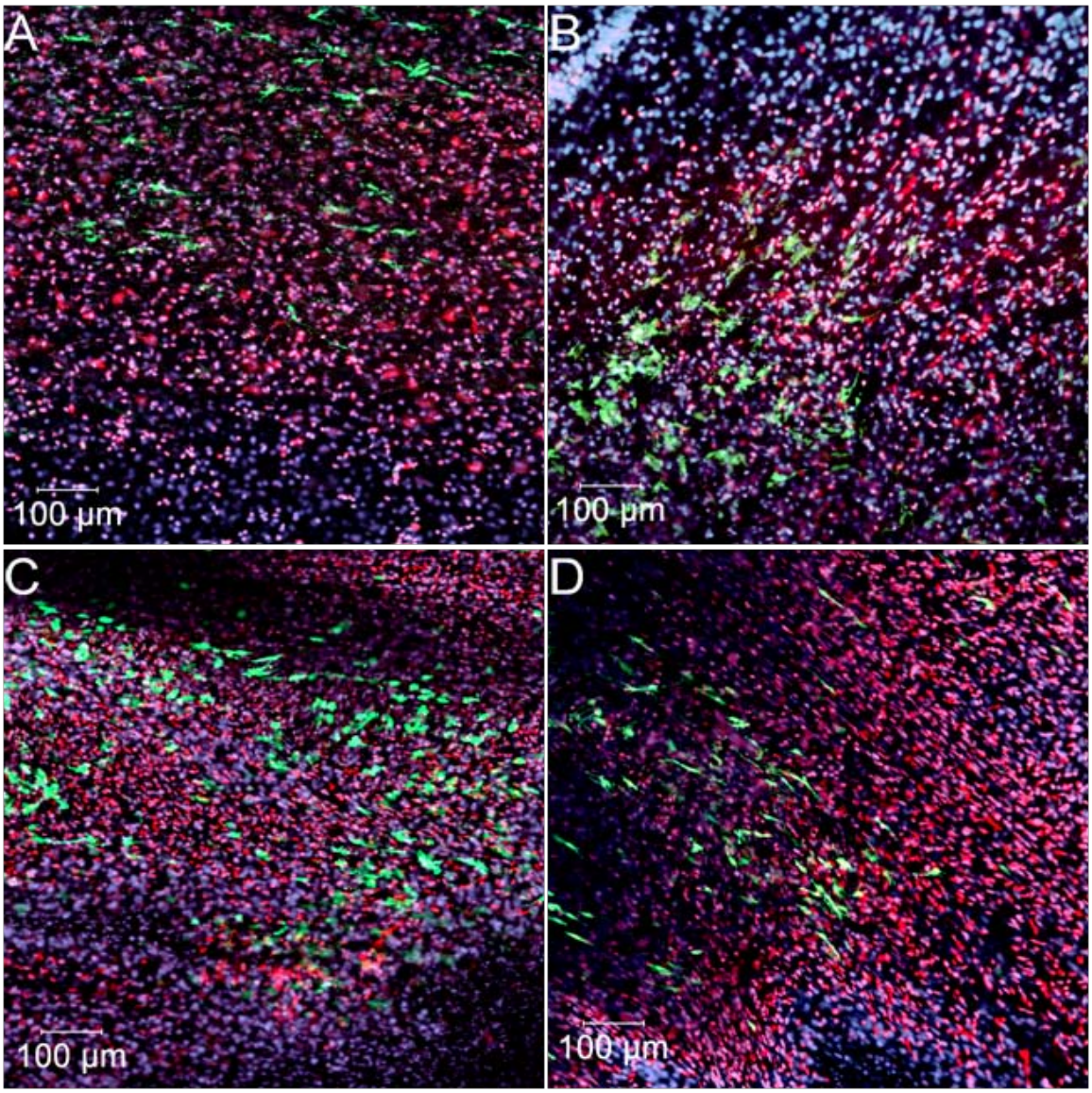

Figure 38 Live aortic valve endothelial cells on the aortic (A,B) or ventricularis (C,D) facing surface following 72h static incubation in the radial (A,C) or circumferential (B,D) direction. Live cells (calcein, green) dead cells (ethidium homodimer, red) and nuclei (Hoechst 33342) are shown with scale bars of 100 µm.

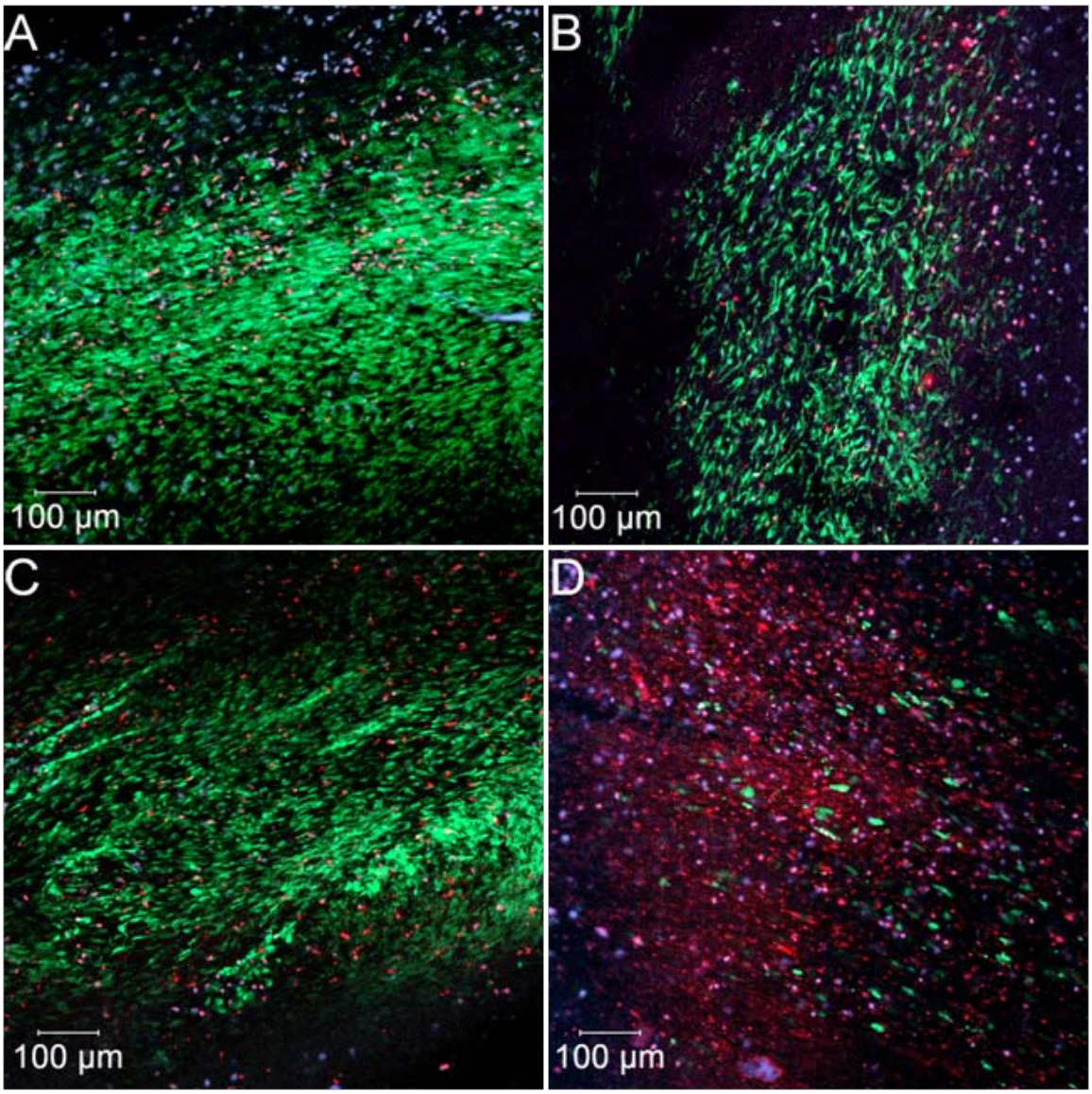

Figure 39 Live aortic valve endothelial cells on the aortic (A,B) or ventricularis (C,D) facing surface following 72h stretch applied in the radial (A,C) or circumferential (B,D) direction. Live cells (calcein, green) dead cells (ethidium homodimer, red) and nuclei (Hoechst 33342) are shown with scale bars of 100 µm.

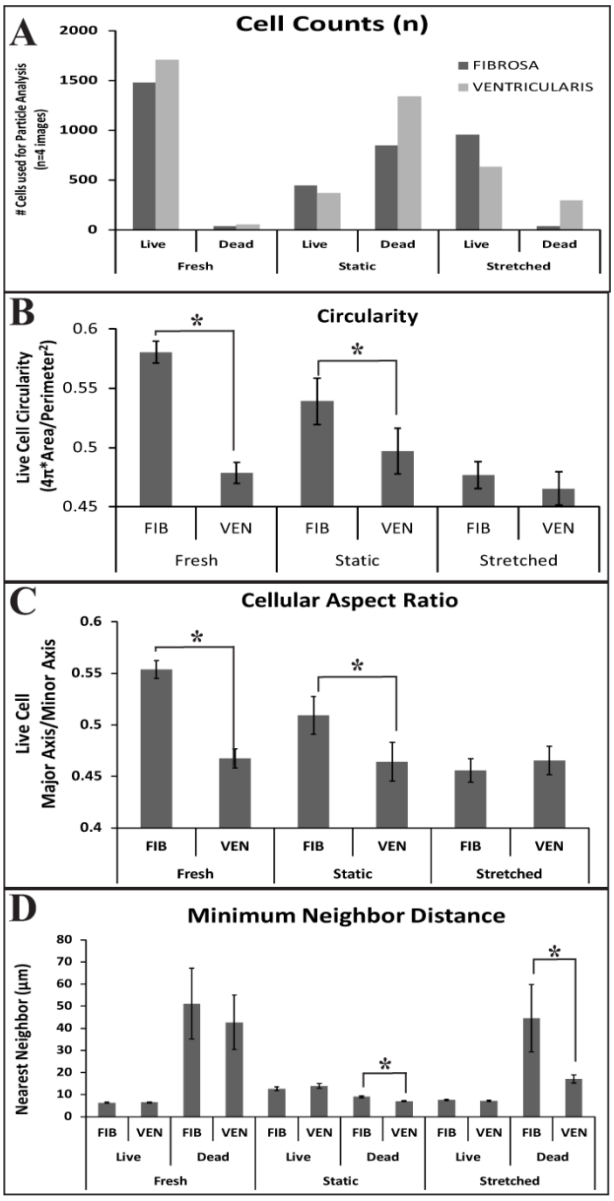

Figure 40 Results from particle analysis of live cell cytoplasm (calcein-AM) and dead cell nuclei (ethidium homodimer). (A) Live cell ratio was expectedly significantly higher in live tissue, with nearly 100% of cells analyzed staining positively for calcein, while the leaflets with no mechanical stimulation showed significant cell death. The stretched leaflets showed a much more viable endothelium of the fibrosa surface. (B) Circularity of live cells was greatest in fresh cells. (C) Monolayer integrity can be assumed from the nearest distance of an endothelial cell to a neighboring cell.

4.3 Discussion

The cyclic stretch bioreactor demonstrated here combines the ability to maintain tissue and cellular viability on a microscope stage without modification to the microscope system. The ex vivo approach to cellular mechanobiology represents a time and cost effective model, when compared to animal models, as well as increased physiological relevance, when compared to in vitro studies. We have demonstrated the ability to reproduce physiologically relevant planar biaxial loads on a freshly excised porcine aortic valve leaflet. Visualizing the AV endothelium on a Zeiss LSM 510 confocal microscope was verified with a 3D reconstruction of f-actin, cell nuclei, and vonWillebrand factor staining. The real time mechanical data was correlated to images of live endothelial cells stained with fluorescent calcein, a marker for cellular viability. Furthermore, the valvular endothelium showed an inverse correlation of monolayer integrity with increased applied biaxial load.

We anticipate the ability of the bioreactor to apply mechanical loads to soft tissue while allowing for live cell imaging will be useful to the study of a wide range of interdisciplinary approaches to cellular mechanobiology, particularly in cardiovascular research, or tissue with mechanically regulated pathogenesis. Potential applications include retro-fitting the device for a two-photon and spinning disk confocal microscope for deeper tissue penetration and prolonged live imaging studies, respectively. Pharmaceutical applications on cardiovascular tissues could easily be carried out by engaging the chemical makeup of the tissue culture medium.

Technological advances in biological fluorescence microscopy in recent decades have been nothing short of remarkable. The breadth of microscopy applications is equally

astounding, including but by no means limited to research on cancer, cardiovascular disease, and endocrinology.

The goals were met by custom fabricating a tissue culture well that fits on the stage of a Zeiss LSM 510 confocal microscope. The well was designed to be capable of sterile incubation of a freshly excised aortic valve leaflet under regulated tissue culture conditions. The bioreactor must also allow for repeatable sample attachment and subsequent characterization of strain state, and application of cyclic stretch at physiologically simulating levels. The in vivo strains experienced by the AV have been estimated using a variety of uniaxial and biaxial methods(9-14) Mechanics of soft tissue exhibit highly non-linear stress-strain, large deformations, complex viscoelasticity and axial coupling behaviors. Due to the changes in internal structure with strain, with collagen its due to rotating towards stretch axis and fiber uncrimping. Collagen crimp has been shown to be regulated up to 20mmHg TVP with no significant differences past 20mmHg. Decrease in circumferential extensibility has been attributed to locking of the collagen fibers. Adamcysk and Vesely showed in situ strains, showed that there might be a different internal structure of the non-coronary cusp due to the fact that they saw negative strains(10). Constitutive models have been developed to characterize the AV leaflet mechanical response, most notably the fiber architecture which has been characterized as the total energy of the leaflet due to the sum of the individual fiber strain energies(11;15;16). Membrane tension is often used due to complications with variable layer thickness heterogenous layer structure. The structural method does well to characterize the biaxial behavior due to the extreme anisotropy and strong mechanical coupling between the axes. Membrane tension has drawbacks though, most notably the

inability to account for layer specific mechanical contributions. The mechanical role of the load bearing layers, the fibrosa and ventricularis was investigated by Stella and Sacks (17). They found what vesely proposed, that the ventricularis contributes to the radial tension of the ventricularis. Strain rate is also a crucial mitigating factor in testing soft tissue. Strain rate dependencies were negligible, hysteresis was invariant with strain rate. The AV leaflet can thusly be modeled as a quasi-elastic material, MVAL showed significant stress relaxation but negligible creep over 3h. Heart valves are an anisotropic quasi-elastic material, which may be unique in their ability to withstand significant loading without respect to time dependent effects. Radial length does not change during systole, however increases drastically during diastole(9). *In vivo* strains were seen at 10 and 30 in radial and circumferential directions, and the corresponding strain rates are 440 and 1240 respectively. A biaxial strain analysis of porcine aortic valves by Lo and Vesely showed a radial strain of 23.0% and a circumferential strain of 10.1% at a transvalvular pressure of 20mmHg. This was defined as the transition point. They also showed significant lock-up of the valve as pressures increased to 80mmHg, there was not a significant increase in strain(12). Preconditioning is a necessity for soft tissue mechanical testing. AV have been shown to take 15-20 cycles to give a repeatable loading curve(18).Shear stress is critical to a normal functioning endothelium. We calculated a shear stress of less than 2 dynes cm^{-2}. This is consistent with a CFD computed for a bioreactor that pulled AV leaflets uniaxially to the same strains and at similar strain rates(19).

In conclusion, we have designed a bioreactor capable of replicating the mechanical loading state of an aortic heart valve. Maintaining the mechanical

environment was accomplished while allowing for live quantitative *en face* endothelial cell imaging. The potential applications of this device are widespread. The endothelium is an exquisitely sensitive monolayer, studied most commonly in vitro, or viewed microscopically by cross section. An en face approach has given us the quantitative measures needed to conduct studies measuring the morphological response to appropriate mechanical stimulation.

4.4 References

(1) Thubrikar M. The Aortic Valve. Boca Raton: CRC; 1990.

(2) Giddens DP, Zarins CK, Glagov S. The role of fluid mechanics in the localization and detection of atherosclerosis. J Biomech Eng 1993 Nov;115(4B):588-94.

(3) David MW. Mechano-potential etiologies of aortic valve disease. J Biomech 2010 Jan 5;43(1):87-92.

(4) L.Bruce. Lecture Notes from ECE 8473 Digital Image Processing. 2008.

(5) A Threshold Selection Method from Gray-Level Histograms. Systems, Man and Cybernetics, IEEE Transactions on 1979;9(1):62-6.

(6) Inai T, Mancuso MR, McDonald DM, Kobayashi J, Nakamura K, Shibata Y. Shear stress-induced upregulation of connexin 43 expression in endothelial cells on upstream surfaces of rat cardiac valves. Histochem Cell Biol 2004 Nov;122(5):477-83.

(7) Frigault MM, Lacoste J, Swift JL, Brown CM. Live-cell microscopy - tips and tools. J Cell Sci 2009 Mar 15;122(Pt 6):753-67.

(8) Pawley J. Handbook of Biologcial Confocal Microscopy. New York: Springer; 2006.

(9) Thubrikar MJ, Aouad J, Nolan SP. Comparison of the in vivo and in vitro mechanical properties of aortic valve leaflets. J Thorac Cardiovasc Surg 1986 Jul;92(1):29-36.

(10) Adamczyk MM, Vesely I. Characteristics of compressive strains in porcine aortic valves cusps. J Heart Valve Dis 2002 Jan;11(1):75-83.

(11) Billiar KL, Sacks MS. Biaxial mechanical properties of the natural and glutaraldehyde treated aortic valve cusp--Part I: Experimental results. J Biomech Eng 2000 Feb;122(1):23-30.

(12) Lo D, Vesely I. Biaxial strain analysis of the porcine aortic valve. Ann Thorac Surg 1995 Aug;60(2 Suppl):S374-S378.

(13) Sacks MS, Smith DB, Hiester ED. The aortic valve microstructure: effects of transvalvular pressure. J Biomed Mater Res 1998 Jul;41(1):131-41.

(14) Thubrikar M, Piepgrass WC, Bosher LP, Nolan SP. Cyclic changes in aortic valve leaflet length and their relationship to flexion stresses in natural and trileaflet prosthetic valves. Surg Forum 1978;29:287-8.

(15) Billiar KL, Sacks MS. A method to quantify the fiber kinematics of planar tissues under biaxial stretch. J Biomech 1997 Jul;30(7):753-6.

(16) Billiar KL, Sacks MS. Biaxial mechanical properties of the native and glutaraldehyde-treated aortic valve cusp: Part II--A structural constitutive model. J Biomech Eng 2000 Aug;122(4):327-35.

(17) Stella JA, Sacks MS. On the biaxial mechanical properties of the layers of the aortic valve leaflet. J Biomech Eng 2007 Oct;129(5):757-66.

(18) Lee TC, Midura RJ, Hascall VC, Vesely I. The effect of elastin damage on the mechanics of the aortic valve. J Biomech 2001 Feb;34(2):203-10.

(19) Balachandran K, Konduri S, Sucosky P, Jo H, Yoganathan AP. An ex vivo study of the biological properties of porcine aortic valves in response to circumferential cyclic stretch. Ann Biomed Eng 2006 Nov;34(11):1655-65.

CHAPTER V

CARDIOVASCULAR HEALTH OUTREACH: BULLDOGS FOR HEART HEALTH

Overweight children have nearly tripled in number over the past 30 years worldwide, reaching epidemic levels(1;2). Several risk factors for cardiovascular disease; hyperlipidemia, hypertension, and diabetes, occur more frequently in obese children and young adults(4-8). Preventing the early onset of obesity reduces the risk of children and adolescents developing coronary heart disease later in life(9). The American Obesity Association defines the term "overweight" as children, ages 2 to 19 years, with a BMI between the 85th and 94th percentile; whereas, the term "obese" refers to children with a BMI at or above the 95th percentile(3). Within the last decade, an increasingly sedentary lifestyle has sent childhood obesity levels skyrocketing; therefore, to combat the disease, children must boost their physical activity(10;11). Overall poor nutrition and increased consumption of various forms of high fructose corn syrup, mainly in the youth targeted marketing of soft drinks, have contributed to excessive weight gain among children and adolescents. The need for children to learn the principles of a balanced diet, portion size, and regular physical activity has never been more dire (12-16).

The state of Mississippi leads the nation in obesity and cardiovascular disease mortality(17). Over half of the state (53%) is classified as rural, known to be a contributing factor in health disparities. Lower socioeconomic status is correlated to poor

health. Mississippi, being the poorest state in the nation (highest proportion of citizens below the poverty level), undoubtedly experiences synergistic effects of low income households and poor overall health(18;19). While financial burdens are not easily alleviated, health education and physical activity must be promoted to help reduce the risk of obesity and heart disease. Mississippi clearly requires additional programs to help educate and motivate the community to adopt a heart healthy lifestyle. Changes must be facilitated in the mental attitude towards food options and exercise. The primary focus should be to educate children and adolescents to help prevent the onset of obesity before a dangerous progression occurs later in life. As the third most overweight college in the nation, Mississippi State University requires motivation to adopt a heart healthy lifestyle while inspiring the state of Mississippi to get fit, stay active, and make positive food choices.

The specific aim of this chapter is to develop a cardiovascular health curriculum and outreach program to assist in the awareness and prevention of cardiovascular disease. A cardiovascular health outreach program has been initiated and a heart healthy curriculum has been developed to educate kids, parents, and college students in the prevention of heart disease.

5.1 Methods

5.1.1 Initiation of Outreach Organization

Bulldogs for Heart Health (BH^2, or informally, BH "squared") was founded by a group of biomedical engineering students working on mechanisms of heart valve disease at Mississippi State University(Scott Metzler, Kimberly Schipke, Katie Culpepper, and

Steven Waller). After researching heart disease on a daily basis and studying the state's heart disease and obesity crisis, the students decided to form an organization to address these issues, and attempt to reverse the declining health trends. Bulldogs for Heart Health became an official campus organization in November 2007. According to its constitution, the primary purpose of the organization shall be to educate and inform the Mississippi State community on issues relating to cardiovascular health and research through interactive and motivational methods. BH² aims to improve the lives of Mississippians by traveling to schools across the state to educate students and parents about the state's heart disease crisis, encourage positive lifestyle changes, present realistic healthy food options, and teach a simple and effective exercise regimen. The long term goal of the proposed plan is to improve the quality of life in Mississippi by creating healthier, more active citizens.

Cardiology Associates of North Mississippi, through the work of Jack Foster M.D, was the first sponsor of the organization. Their generous donation gave the organization an opportunity to start planning an interactive curriculum for K-12 outreach projects as well as on campus activities. The Smart Balance© corporation sent several hundred coupons to BH² to give financial assistance for Mississippi citizens when buying their healthy butter alternatives. Also, Blue Diamond© Almonds donated hundreds of samples of their new smokehouse flavored almonds to use in outreach projects. In addition, the founders were able to find several other local sponsors such as the Veranda Restaurant, McAlister's Deli, The Savvy Grape, Movie Gallery, MAK B & Co., City Bagel Café, Tokros, Aspen Bay Candles, Bulldog Lanes, and The Lodge. The support

from the community strengthened the resolve of the founders pursue a far reaching health education approach.

5.1.2 Outreach Methodology

Bulldogs for Heart Health initially focused on outreach to K-12 students and provide preventative heart health education. When designing a curriculum for elementary through high school students, BH² founders wanted to include three main education points (1) heart anatomy and physiology, (2) exercise techniques, and (3) nutrition. Teaching students the elegant design and intuitive function of the heart helps them internalize many of the health principles. The correlation between exercise and heart function is not difficult to draw for young students, particularly when they are holding a porcine heart in their hands, and can feel the impressive musculature of the ventricles, the elasticity of the atria, and tracing the path of the coronary arteries from the aorta back to the heart. By incorporating exercise into learning activities, the students will strengthen both their minds and their hearts. To prevent excessive weight gain and maintain their strong hearts, nutrition was integrated into the lesson plans. By explaining portion size and the benefits of healthy eating habits, the students will learn not what appropriate quantities are, but what types of foods in particular best benefit the body and the mind.

The students, faculty, and staff at Mississippi State University were the next focus, to address the high rank among overweight universities. To increase awareness about the organization, BH² organized an event at State Theatre to raise money and recruit new members. BH² then researched local cardiovascular conferences and invited its members to attend for free health screenings. Bulldog for Heart Health's main event to

inspire heart healthy choices on campus was GET FIT MSU, where students, faculty, and staff competed to lose weight and get fit.

After designing the curriculum for several different age groups, the founders then designed a webpage and posters to allow fellow students, faculty, staff, and other Mississippi citizens to become aware of the organization and get involved. The website created for Bulldogs for Heart Health can be found at: www.bh2.org.msstate.edu. A logo for BH², seen in Figure 42 was also created by the founders to be used on the BH² website and posters. In the future, the logo can be used for t-shirts for members to wear and advertise the organization.

Figure 41 Bulldogs for Heart Health Logo

5.2 Results

5.2.1 K-12 Outreach

5.2.1.1 Nora Davis Magnet School (3rd) – Laurel, MS

The first outreach project for Bulldogs for Heart Health occurred in Laurel, MS. A group of biomedical engineers visited the 3rd grade classroom of MSU alumni Andrea Schipke at Nora Davis Magnet School. First, a pig heart was dissected to explain how the heart works and why it is important to keep the heart healthy, as seen in Figure 43. Students wore gloves and were able to touch the fixed porcine heart, put their fingers through the aorta, compare the thickness of the right and left side, touch the valves, etc. Following the heart anatomy lesson, students made hand weights out of water bottles using the infield turf of their favorite professional sports teams as filler. Profile Products donated five different colors of clay used by professional baseball and football teams. Students were able to layer their weights using their favorite sports teams' colors. To incorporate exercise with learning, students were instructed to hold the weight with their arms outstretched and draw the alphabet, as well as practice their spelling word list and multiplication tables. The instructors also suggested students hover a few inches over their seats during TV commercials to help get their hearts pumping and get a mini work-out from the couch. Lastly, the students made a personal trail mix out of almonds, Craisins, soy nuts, pumpkin seeds, sunflower nuts, peanuts, and dark chocolate and learned all of the health benefits associated with each item. These foods have all been recommended by the AHA as heart healthy, and are obscure enough that most kids had not experienced them. The students were sent home with health information for their

parents to help to educate the people responsible for monitoring eating habits. Information was distributed from the American Heart Association regarding the dangers and prevention of diabetes and obesity. Coupons for Smart Balance products were also provided to allow parents to try a healthier alternative to butter or shortening. Members of Bulldogs for Heart Health and Mrs. Schipke's class can be seen in Figure 43.

Figure 42 Cardiovascular health instruction at a local elementary school. Heart anatomy and physiology is presented in an interactive hands-on approach. The author of this dissertation (left) is showing students a porcine heart prior to a group dissection.

Figure 43 Bulldogs for Heart Health members at Nora Davis Magnet School in the most obese city in North America, Meridian, MS.

5.2.1.2 Overstreet Elementary School (3rd)

The curriculum presented at Nora Davis Magnet School was well received, upon hearing feedback from teachers that reported students referencing the heart presentation in the following weeks. Bulldogs for Heart Health used the same curriculum to inspire students at Overstreet Elementary School to maintain a healthy heart. By the end of the fall semester of 2008, the organization visited every 3rd grade classroom in Starkville, MS. The children were extremely responsive to the lessons excited to use their personalized hand weights to practice their spelling lists and multiplication tables. The teachers noted the weights were a great way to incorporate exercise with learning, which validated the efforts of Bulldogs for Heart Health. The kids also enjoyed trying snacks that not only tasted good but were good for their heart as well. It is important to teach that

eating healthy can really be delicious and satisfying. All in all, a positive, healthy lesson was brought to several hundred children in the Starkville area.

5.2.1.3 Sudduth Elementary School (1st) - Meridian, MS

During the spring of 2009, Bulldogs for Heart Health attended a health fair at Sudduth Elementary School in Meridian, MS to reach out to more elementary students across the state. After learning about the message that BH² brings to classrooms, a 1st grade teacher requested BH² visit her students so they can benefit from the material presented. The successful curriculum taught at Nora Davis and Overstreet Elementary was also taught at Sudduth Elementary School in Starkville, MS. Afterwards, the students took the time to sign and mail a thank you note to Bulldogs for Heart Health to show their appreciation for the information provided to them.

5.2.1.4 Armstrong Middle School (8th)

On April 17, 2009, Bulldogs for Heart Health visited Armstrong Middle School in Starkville, MS. To kick off the event, a pig heart was dissected to educate the students about the anatomy of the heart. Following the dissection, a presentation was given on proper nutrition and portion size. To effectively teach portion size, examples were given in terms of items the students are familiar with to make it easier to recognize how much food they should consume. For example, six dice are equal to a serving of cheese and a deck of cards is equivalent to a serving of meat. Next, lard was weighed out to illustrate the saturated fat content in a Bloomin' Onion™ from Outback Steakhouse©, a Quarter Pounder with Cheese™, a regular size French fries, and a six piece Chicken McNugget™

from McDonald's©. Also, the amount of sugar in a two liter of Coca-Cola was compared with a 32 oz. Gatorade and a 20 oz. Monster energy drink. Actually seeing the mounds of lard and sugar in foods and drinks people consume on a daily basis had quite an impact on the students. After the event was over, Nicki Marooney, an 8th grade teacher from Armstrong Middle School, invited Bulldogs for Heart Health to come back every year to bring heart health awareness and education to the students. Needless to say, the lesson was well received and Bulldogs for Heart Health can start preparing for next year's event.

5.2.1.5 Distribution of AHA material

The American Heart Association was contacted by Bulldogs for Heart Health to create a connection between the two organizations so they can work together and help the state of Mississippi. AHA donated numerous educational materials to BH² to facilitate classroom learning. A portion of the material was kept for BH² to use during outreach, but the majority of the material was given to Dr. Margaret Pope in the Department of Education at Mississippi State University. The intent of the donation was for future educators from MSU to use the educational material during their semester of student teaching. In the spring of 2009, eighteen educator candidates utilized the AHA material in their life science lesson plans. By incorporating heart health education into their curriculum, the lessons were taught in classrooms statewide, thereby increasing the impact of BH²'s message in concert with the American Heart Association.

5.2.2 MSU Campus Outreach

5.2.2.1 Fundraising Efforts

On April 9, 2008, Bulldogs for Heart Health arranged for The People's Party to perform a benefit show at State Theatre in Starkville, MS. The People's Party is an amazing band from Venice Beach, CA with an infectious social conscience in the midst of a cross country tour. The band has played at the Super Bowl in Phoenix, AZ, a New Year's Eve show at Pier No. 2 in San Francisco, as well as Washington, D.C. for Rock the Vote. With the help of The People's Party and local businesses, Bulldogs for Heart Health was able to raffle off prizes and raise almost $500 for our organization. The event was a great success and helped raise enough money for several classroom visits. The concert also allowed fellow Mississippi State students to learn more about the new organization on campus and sign up to help with future events and classroom outreach.

5.2.2.2 Weston Reed Cardiovascular Conference – Tupelo, MS

In the fall of 2008, Bulldogs for Heart Health organized for a group of MSU students to attend the Weston Reed Cardiovascular Conference in Tupelo, MS. The conference had several stations along the concourse to evaluate individual risk factors for heart disease. The cardiologists and nurses at the conference gave free screenings and counseling for participants. The screenings provided by the staff included cholesterol, blood pressure, body mass index, electrocardiogram, and echocardiogram. The students who attended the event were able to evaluate their health and learn about the importance of knowing your numbers. The conference was a great way to learn about heart disease and raise awareness of one's own health.

5.2.2.3 GET FIT MSU

To address Mississippi State University's ranking as the 3rd most overweight university in the nation, Bulldogs for Heart Health hosted a fitness challenge during the spring semester of 2009 in collaboration with Jason Townsend, Laura Walling, and the Sanderson Center. Over 100 students, staff, and faculty from Mississippi State University participated in the event, which helped make the fitness challenge a success. The fitness challenge began February 5th and the participants had 12 weeks to shed pounds and get fit. Trainers from the Sanderson Center helped participants lose weight and participants were also given information about making positive eating habits. The top four losers in weight loss, body fat turnover, and overall increase in fitness were invited to the final "weigh in" and grand prize drawing. As an incentive to get healthy, Bulldogs for Heart Health presented the winner, Dave Aurich who lost 25lbs and nearly 10% body fat, with both a Nintendo Wii and a Wii Fit to keep the weight off and maintain an active lifestyle. The three runner ups, Melanie Walsh, Jacquie Myers, and Laura Anderson, received $50 gift cards for Hibbett Sports to spend on new shoes, apparel, or exercise equipment. Melanie Walsh lost nearly 70lbs and dropped over 10% body fat, Jacquie Myers lost 12lbs and 10% body fat, and Laura Anderson lost 11inches from her waist and more than 5% body fat.

5.2.2.4 Total Estimated Outreach

Table 5 Outreach totals Bulldogs for Heart Health Nov 2007-June 2009.

Nora Davis Magnet School	20 students
Overstreet Elementary	300 students
Sudduth Elementary	25 students
Armstrong Middle School	120 students
AHA Material Distribution	450 students
The People's Party	50 students
Weston Reed Conference	5 students
GET FIT MSU	100 students
TOTAL	**1070 students**

5.3 Discussion

According to the Guidelines for Child Obesity Prevention Programs: Promoting Healthy Weight in Children developed by the Society for Nutrition Education (SNE), it is important for health programs to set goals for health, not weight, in addition to healthy eating and physical activity within a nurturing environment. SNE also focuses on community involvement to help support children in their fight for fitness. Bulldogs for Heart Health has met all requirements set by the Society for Nutrition Education and is a model for other heart health programs. BH² introduces more than just nutrition and exercise to students, the organization most importantly provides information about the heart while relaying concrete examples on why proper maintenance is crucial. BH² has created numerous different activities for all age groups so the entire community can participate in getting healthy through multiple avenues.

After reaching over a thousand students since its inception in 2007, Bulldogs for Heart Health continues to strive for a healthier, active Mississippi. Besides BH², the state has introduced several different programs to help reduce the risk of obesity and

cardiovascular disease. For instance, Health is Academic: Nutrition Integrity Project where deep fat frying kitchen equipment is replaced with economical alternatives such as baking equipment. Another great program provided to Starkville city schools is the Safe Routes to School Project whose goals are to reduce traffic congestion, improve air quality, and increase physical activity. The most recognized statewide initiative, however, is Blue Cross and Blue Shields's Let's Go Walkin' Mississippi Campaign, which provides free pedometers, tracking logs, and other resources to the public. According to the American Heart Association's Heart Disease and Stroke Statistics – a 2008 Update, the estimated direct and indirect cost of cardiovascular disease is $156.4 billion dollars. If the same amount of money were spent on education and preventative care, the state would be in much better shape, both literally and figuratively. Mississippi citizens should continue to request more legislation and funding for outreach programs to put a stop to the obesity trends.

The hypothesis of Bulldogs for Heart Health, cardiovascular health education and motivation will result in positive lifestyle changes and a healthier Mississippi, will not be measured immediately. The effects of BH² and other state funded programs will take some time to produce results; therefore, it is difficult to measure their effectiveness. Future studies could be conducted to investigate the involvement of Bulldogs for Heart Health in several different classrooms throughout a semester to measure differences in fitness levels before and after the organization's involvement. BH² currently has over 125 members who are determined to make an impact on the health of Mississippi and ensure that the organization endures throughout the years.

5.3.1 Future outreach programs

In the future, BH² intends to reach out to the high school level students in the local area and across the state. Dr. Holly Wiley, instructor in the Department of Kinesiology at MSU, is planning to have her secondary health education students create a curriculum for BH² and future educator candidates to use in outreach and lesson plans, respectively. With this win-win arrangement, a group of college students will get practice creating lesson plans while hundreds of K-12 students will benefit from the information presented by BH² and future educators. Also, Bulldogs for Heart Health and the Food Science Department of MSU would like to host cooking demonstrations to teach high school students how to cook at least one healthy meal for themselves before they leave for college. In addition, BH² would like to organize a group of MSU football and basketball players, as well as, cheerleaders and pom squad members to come talk to students about what it took for them to get where they are and demonstrate different exercises and techniques they use to stay in shape.

Since GET FIT MSU was so successful, Bulldogs for Heart Health has already made arrangements with the Sanderson Center to host another fitness challenge in the near future to motivate students to lose weight and get healthy. Dr. Vivien Miller, a statistics professor at MSU, is using the American Heart Association's Heart Disease and Stroke Statistics: a 2008 Update to create homework and test problems to raise awareness among college students about the heart disease epidemic sweeping the country. BH² would also like to organize a circuit training day and have students perform different exercises at several stations spread out across the drill field for prizes. The organization

would like to join other campus groups to organize a triathlon so students can participate in a demanding exercise event and push themselves to build a stronger heart.

In the future, Bulldogs for Heart Health members should join the American Heart Association's Community Action Network so they can present AHA's message to their community about healthy eating and exercise. BH² should also work together with the PTA so they can talk to parents and teachers about promoting a healthy lifestyle both at school and at home. Parents need to be educated about what types of foods they should feed their children and should also be given AHA's healthy recipe book for cooking ideas. Bulldogs for Heart Health would like to reach out to every member of the community to make Mississippi a leader in health awareness and fitness.

In order to implement the hands-on approach to childhood obesity prevention, a model must be laid out with quantifiable metrics to assess the potential physiological impacts of BH^2. Before too much more outreach is carried out, a strategic plan of action should be devised. The plan of action should include well-defined parameters to observe previous to, during, and after, a Bulldogs for Heart Health initiative. Factors that could be tracked for efficacy of the program are BMI, eating habit shifts, a short quiz or questionnaire on cardiovascular health, IRB approval would most likely be needed to obtain data from students, in the hopes of developing a tried and proven cardiovascular outreach model.

5.4 References

(1) Wang Y, Lobstein T. Worldwide trends in childhood overweight and obesity. Int J Pediatr Obes 2006;1(1):11-25.

(2) Ogden CL, Carroll MD, Curtin LR, McDowell MA, Tabak CJ, Flegal KM. Prevalence of overweight and obesity in the United States, 1999-2004. JAMA 2006 Apr 5;295(13):1549-55.

(3) Philipsen NM, Philipsen NC. Childhood Overweight: Prevention Strategies for Parents. J Perinat Educ 2008;17(1):44-7.

(4) Rees A, Thomas N, Brophy S, Knox G, Williams R. Cross sectional study of childhood obesity and prevalence of risk factors for cardiovascular disease and diabetes in children aged 11-13. BMC Public Health 2009;9:86.

(5) Lauer RM, Connor WE, Leaverton PE, Reiter MA, Clarke WR. Coronary heart disease risk factors in school children: the Muscatine study. J Pediatr 1975 May;86(5):697-706.

(6) Lauer RM, Lee J, Clarke WR. Factors affecting the relationship between childhood and adult cholesterol levels: the Muscatine Study. Pediatrics 1988 Sep;82(3):309-18.

(7) Lauer RM, Clarke WR. Childhood risk factors for high adult blood pressure: the Muscatine Study. Pediatrics 1989 Oct;84(4):633-41.

(8) Berenson GS, Srinivasan SR, Bao W, Newman WP, III, Tracy RE, Wattigney WA. Association between multiple cardiovascular risk factors and atherosclerosis in children and young adults. The Bogalusa Heart Study. N Engl J Med 1998 Jun 4;338(23):1650-6.

(9) Smoak CG, Burke GL, Webber LS, Harsha DW, Srinivasan SR, Berenson GS. Relation of obesity to clustering of cardiovascular disease risk factors in children and young adults. The Bogalusa Heart Study. Am J Epidemiol 1987 Mar;125(3):364-72.

(10) Dugan SA. Exercise for preventing childhood obesity. Phys Med Rehabil Clin N Am 2008 May;19(2):205-16, vii.

(11) Anderson SE, Economos CD, Must A. Active play and screen time in US children aged 4 to 11 years in relation to sociodemographic and weight status characteristics: a nationally representative cross-sectional analysis. BMC Public Health 2008;8:366.

(12) Troiano RP, Briefel RR, Carroll MD, Bialostosky K. Energy and fat intakes of children and adolescents in the united states: data from the national health and nutrition examination surveys. Am J Clin Nutr 2000 Nov;72(5 Suppl):1343S-53S.

(13) Nicklas TA, Yang SJ, Baranowski T, Zakeri I, Berenson G. Eating patterns and obesity in children. The Bogalusa Heart Study. Am J Prev Med 2003 Jul;25(1):9-16.

(14) Linardakis M, Sarri K, Pateraki MS, Sbokos M, Kafatos A. Sugar-added beverages consumption among kindergarten children of Crete: effects on nutritional status and risk of obesity. BMC Public Health 2008;8:279.

(15) Dennison BA, Rockwell HL, Baker SL. Excess fruit juice consumption by preschool-aged children is associated with short stature and obesity. Pediatrics 1997 Jan;99(1):15-22.

(16) Berkey CS, Rockett HR, Field AE, Gillman MW, Colditz GA. Sugar-added beverages and adolescent weight change. Obes Res 2004 May;12(5):778-88.

(17) Mokdad AH, Bowman BA, Ford ES, Vinicor F, Marks JS, Koplan JP. The continuing epidemics of obesity and diabetes in the United States. JAMA 2001 Sep 12;286(10):1195-200.

(18) Davy BM, Harrell K, Stewart J, King DS. Body weight status, dietary habits, and physical activity levels of middle school-aged children in rural Mississippi. South Med J 2004 Jun;97(6):571-7.

(19) Polhamus B, Dalenius K, Thompson D, Scanlon K, Borland E, Smith B, et al. Pediatric nutrition surveillance. Nutr Clin Care 2003 Oct;6(3):132-4.

CHAPTER VI

SUMMARY AND CONCLUSIONS

6.1 Major Findings and Improvements

The hypothesis of this dissertation was that an altered mechanical environment has a causal relationship with AVEC activation. Testing this hypothesis fell into three specific aims. Each specific aim resulted in furthering the understanding of the aortic valve endothelium, of which surprisingly little is known. The results of this dissertation have shown us that 1) cyclic strain regulates pro-inflammatory adhesion molecule expression in aortic valve endothelial cells and 2) cyclic strain activates aortic valve endothelial cells in a side-specific manner. The take home message being that mechanical stress in the aortic valve has direct implications on the AVEC mediated initiation of degenerative AVD. The endothelium on the aortic facing and load bearing layer demonstrated anti-oxidant and athero-protective behavior under applied strain, indicating an inherent sensitivity to mechanical loading. The third specific aim successfully completed the construction of a cyclic stretch bioreactor, capable of real time imaging of the aortic valve endothelium under mechanical stress. This machine is the first of its kind and drastically improves upon the field of endothelial mechanobiology. In addition, Bulldogs for Heart Health, a cardiovascular outreach program, has made a significant impact on the education and motivation of heart healthy lifestyles in greater Mississippi and especially the Mississippi State community. The specific aims are revisited below.

Specific Aim 1) Elucidate the role of in vitro cyclic strain on pro-inflammatory adhesion molecule expression in aortic valve endothelial cells. Specific Aim 1 found that adhesion molecule expression is regulated by cyclic stretch in AVECs. Cyclic stretch magnitudes of 5 and 20% showed a significant increase in adhesion molecule expression, as evidenced by flow cytometry and confocal laser scanning microscopy. Adhesion molecule expression was found to be inhibited by a 10% cyclic stretch. The results from this study indicate the AVEC may sense and respond to particular magnitudes of cyclic strain by becoming activated or maintaining a quiescent EC phenotype. The strain response of AVEC at 10% strain led to the hypothesis that AVECs sense strain in the circumferential direction, which would be along the alignment of the underlying collagen fibers. These results have been published in the Journal of Heart Valve Disease(1). The use of AVEC pooled from both surfaces of the valve prevented elucidation of side specific mechanisms of strain response. Investigation of strain dependent EC activation on side or layer specific isolated AVEC was conducted in specific aim 2.

Specific Aim 2) Investigate the cyclic-strain dependent activation of side-specific aortic valve endothelial cells. The results from Specific Aim 2 demonstrated for the first time that AVECs have a side specific response to *in vitro* cyclic stretch. Microarray profiles have shown AVEC gene expression to be highly side specific *in vivo*. However, the AVEC are in unique mechanical environments and inherent mechanoresponsive mechanisms have never been tested *in vitro* to elucidate whether differential gene expression is due to AVEC sub-phenotype or mechanical environment. The results from this study suggest a more complex relationship in AVEC response to strain from the fibrosa and ventricularis endothelial cells. Genes involved in strain regulated

mechanosensing are magnitude dependent in FEC only (PECAM-1). Adhesion molecule gene expression was significantly downregulated by stretch in FEC when compared to positive controls. These findings suggest the FEC may be an inherently strain responsive cell type, while the VEC is more likely to be regulated by laminar fluid shear stress.

Specific Aim 3) Develop a novel biaxial stretch bioreactor to investigate endothelial cell response to tissue level anisotropic biaxial cyclic strain. Specific Aim 3 was completed successfully, the cyclic stretch bioreactor was able to reproduce physiological stress-strain behavior of freshly excised porcine AV leaflets with desired levels of accuracy. The method to image the AV endothelium under well-defined loads represents a dramatic improvement upon previous methods. The ability to reproduce physiological stress states while directly observing endothelial cell response is the first of its kind to this authors knowledge. The bioreactor was able to reproduce the characteristic soft tissue response to applied loads. This was demonstrated by the hysteresis curves presented, as well as the non-linear biaxial stress-strain curve. The observation of the AV endothelium under an array of stress states was produced with single cell resolution. The bioreactor represents a significant improvement in valvular endothelium studies. The results shown have demonstrated that the AV endothelium is exquisitely sensitive to its strain environment.

In summation, the study of aortic valve disease necessitates a complex, multi-disciplinary approach to fully appreciate and understand the mechanisms involved. The AV functions in a highly dynamic environment, thus, the role of fluid shear stress, pressure, and mechanical stretch cannot be underestimated in relation to both physiological and pathophysiological processes. AV mechanics have been extensively studied and in far greater capacity than the cell types of the AV(2). Given that AVD was

seen as a passive and degenerative process well into the 1990's, cell-mediated models of valve pathology have only recently been accepted. The field of vascular biology has seen such incredible progression over the span of more than three decades. Increasing prevalence of heart attack and stroke dictated much of this research and has led to the common use of a number of cardiovascular related pharmaceuticals (low dose aspirin, statins, ACE inhibitors, vasodilators, beta blockers, etc). Historically, valvular biology has not received nearly the amount of funding or attention. Valvular biology will always be categorically associated with the field of vascular biology, however previous assumptions on parallel cellular behavior have recently been disproven. Valvular cells are a distinct phenotypical entity in the body. Valvular interstitial cells are not vascular smooth muscle cells, and valvular ECs are most certainly not vascular ECs. Phenotypic differences, at times subtle, need to be fully investigated to understand valvular disease processes. AVD has also seen many parallels with atherosclerosis, and the assumption has been made that the cell types behave similarly in disease progression. Alterations in mechanical environment have been shown to accelerate the progression of atherosclerosis, yet the mechanical determinants of valvular disease have only recently been investigated.

This study is the first to investigate the valvular endothelium response to cyclic stretch. While cyclic stretch has been investigated with respect to the ECM components and its effect on interstitial cells, the valve endothelium has gone previously unstudied. This is possibly due to the technical difficulty involved with studying a monolayer on a tissue under constant mechanical stimulation. Technical limitations have been overcome,

while a novel method was developed to directly observe the valvular endothelium in response to mechanical environment.

6.2 Endothelial Cell Mechanical Response

As this work has progressed, the study of the valve endothelium has made remarkable strides. We now know that the valvular endothelium has a direct impact on the mechanical properties of the aortic valve(3). The study on biaxial stretch and endothelial regulation of mechanical properties validates the need to construct the bioreactor in specific aim 3. The study also underscored the importance of endothelial integrity on physiological valve function. An adult swine model study has also recently examined the effects of a risk factor for valve disease, in the form of hypercholesterolemia, on the integrity of the AV endothelium(4). The study used a microarray analysis to find a more sensitive phenotype on the side susceptible to degenerative AVD. However, the profile on the aortic surface was not of a dysfunctional phenotype, but rather a protective cell type. Hypercholesterolemia can influence both, the mechanical and the biochemical environment in aortic valves, an example of the complex interplay of a multitude of factors in valve disease. The biochemical and mechanical environments are highly correlated.

6.3 Future Directions

Aortic valve biology, mechanobiology, and pathogenesis research have all made impressive strides in the 21st century. We learned valvular endothelial cells are phenotypically different from vascular ECs, with sub-phenotypes present on either valve

surface. We have steadily crept closer to a full mechanical characterization of AV structural components. As knowledge of pathogenesis of degenerative valve disease progresses the complex interplay of mechanical, biochemical, lifestyle, and aging factors are highlighted. Genetic factors are only recently being elucidated(5). Surgical replacement of heart valves has progressed rapidly to accommodate the tens of thousands of valve surgeries a year. The first percutaneous valve was recently approved by the FDA. This means the prospect of valve replacement without open heart surgery may not be too far from routine. Yet, recent progress withstanding, we still lack a single pharmaceutical intervention that targets the specific molecular biology of degenerative AV disease. As the cellular biology of AV phenotypes becomes more defined in response to humoral stimuli, pharmaceutical intervention to delay the onset and progression of AVD will be crucial. As valve surgeries are focused on the young and the elderly, avoiding open heart surgery poses a significant increase in quality of life for those afflicted with valve disease. What is not currently known is the effect of pharmaceuticals prescribed for the treatment of coronary artery disease on the physiological function of heart valves. The coronary vasculature has a tendency to become constricted, and most drug interventions work, in a sense, to open the arteries. Heart valves, on the other hand, have the opposite function, preventing retrograde blood flow and maintaining well defined fluid profiles. As the cellular and molecular biology of valvular and vascular structures are quite different, pharmaceutical agents beneficial to the vasculature could have destructive effects on valvular structure.

6.4 Publications and Presentations

6.4.1 Peer-Reviewed Journal Publications

1. Metzler, S. A., Digesu, C. S., Howard, J. I, Kalluri, H., Mun, S.K., Bruce, L., To, F., Warnock, J. N Live Quantitative En Face Imaging of Soft Tissue under Mechanical Stress. Nature Methods. Submitted March 2010.

2. Metzler, SA., Digesu, CS., Howard, JI., Warnock, JN. Cyclic Strain Activates Aortic Valve Endothelial Cells in a Side Specific Manner. American Journal of Physiology Heart and Circulatory Physiology. Submitted March 2010.

3. Metzler SA, Pregonero CA, Butcher JT, Burgess SC, Warnock JN. Cyclic Strain Regulates Pro-inflammatory Protein Expression in Porcine Aortic Valve Endothelial Cells. J Heart Valve Dis 2008 Sep;17(5):571-7.

4. Smith, K. E., Metzler, S. A., Warnock, J.N. Cyclic Strain Inhibits Acute Pro-Inflammatory Gene Expression in Aortic Valve Interstitial Cells. Biomech Model Mechanobiol. 2010 Feb;9(1):117-25.

5. Warnock, J. N., Pregonero Gamez, C. A., Metzler, S. A., Chen, J., Liao, J. Vasoactive Agents Alter the Biomechanical Properties of Aortic Heart Valve Leaflets in a Time-dependent Manner. J Heart Valve Dis. Accepted for Publication May 2009.

6. Pregonero CA, Metzler SA, Warnock JN. Elevated Pressure Modulates Osteogenic De-Differentiation of Aortic Valve Interstitial Cells. AJP Heart and Circulatory Physiology. Re-submission. March 2010.

6.4.2 Platform Presentations

1. Metzler, SA., Digesu, CS., Howard, JI., Warnock, JN. Cyclic Strain Activates Aortic Valve Endothelial Cells in a Side Specific Manner. Fourth Biennial Heart Valve Biology and Tissue Engineering Meeting. Hilton Head, SC March 7-10, 2010

2. Metzler, S. A., Digesu, C. S., Howard, J. I., To, F., Warnock, J. N. "A Novel *ex vivo* Bioreactor with Live Cell Imaging Analysis for Characterizing the Strain-Based Initiation of Degenerative Valve Disease" 2009 Annual Meeting of the Southeastern Microscopy Society, Athens, GA 27th-29th May, 2009

3. Metzler, S. A., Waller S. C., Weed B., Liao J., Warnock, J. N. "Layer Dependent Aortic Valve Endothelial Cell Response to Uniaxial Cyclic Stretch". Presented at the 2008 Annual Meeting of the Southeastern Microscopy Society, Pensacola, FL, 16th-18th April, 2008.

4. Metzler, S. A., Burgess, S. C., Warnock, J. N. "Cyclic Strain Regulates Pro-Inflammatory Gene Expression in Porcine Aortic Valve Endothelial Cells. Presented at the 4th Biennial Meeting of the Society for Heart Valve Disease, New York, NY, 15th-18th June, 2007.

6.4.3 Poster Presentations

1. Metzler, S. A., Digesu, C. S., Howard, J. I., To, F., Warnock, J. N. "A Novel *ex vivo* Bioreactor with Live Cell Imaging Analysis for Characterizing the Strain-Based Initiation of Degenerative Valve Disease" 2009 Frontiers of Biomedical Imaging Science, Vanderbilt University, Nashville, TN 2nd-5th June, 2009

2. Waller S. C., Metzler, S. A., Elder, S. H., Liao J., Warnock, J. N. "Evaluation of Chitosan Scaffolds for a Tissue Engineered Aortic Heart Valve". Presented at the 2008 Annual Meeting of the Biomedical Engineering Society, St. Louis, MO, October 2nd-4th, 2008.

3. Metzler, S. A., Waller S. C., Weed B., Liao J., Warnock, J. N. "Layer Dependent Aortic Valve Endothelial Cell Response to Uniaxial Cyclic Stretch". Presented at the 2008 Annual Meeting of the Biomedical Engineering Society, St. Louis, MO, October 2nd-4th, 2008.

4. Metzler, S. A., Waller S. C., Sacks M.S, Liao J., Warnock, J. N. "Characterization of Aortic Valve Endothelial Cell Response to Global Tissue Stretch". Presented at the 2007 Annual Meeting of the Biomedical Engineering Society, Los Angeles, CA, 26th-30th September, 2007.

5. Pregonero Gamez, C. A., Kothari, P., Metzler, S. A., Warnock, J. N. "Cyclic Strain Inhibits Inflammatory Activation of Valvular Interstitial Cells via the Actin Filaments". Presented at the Annual Meeting of the Institute of Biological Engineering, St. Louis, MO, 30th March-1st April 2007.

6. Pregonero Gamez, C. A., Kothari, P., Metzler, S. A., Warnock, J. N. "Cyclic Strain Inhibits Inflammatory Activation of Valvular Interstitial Cells via the Actin Filaments". Presented at the Annual Hilton Head Workshop, Hilton Head Island, SC, 7th-11th March 2007.

6.5 References

(1) Metzler SA, Pregonero CA, Butcher JT, Burgess SC, Warnock JN. Cyclic strain regulates pro-inflammatory protein expression in porcine aortic valve endothelial cells. J Heart Valve Dis 2008 Sep;17(5):571-7.

(2) Sacks MS, Yoganathan AP. Heart valve function: a biomechanical perspective. Philos Trans R Soc Lond B Biol Sci 2007 Aug 29;362(1484):1369-91.

(3) El-Hamamsy I, Balachandran K, Yacoub MH, Stevens LM, Sarathchandra P, Taylor PM, et al. Endothelium-dependent regulation of the mechanical properties of aortic valve cusps. J Am Coll Cardiol 2009 Apr 21;53(16):1448-55.

(4) Guerraty MA, Grant GR, Karanian JW, Chiesa OA, Pritchard WF, Davies PF. Hypercholesterolemia induces side-specific phenotypic changes and peroxisome proliferator-activated receptor-gamma pathway activation in swine aortic valve endothelium. Arterioscler Thromb Vasc Biol 2010 Feb;30(2):225-31.

(5) Bosse Y, Mathieu P, Pibarot P. Genomics: the next step to elucidate the etiology of calcific aortic valve stenosis. J Am Coll Cardiol 2008 Apr 8;51(14):1327-36.

APPENDIX A

PROTOCOL

A.1 mRNA Isolation Post-Flexercell

1. Aspirate media from the edge of wells
2. Rinse each well with 2 ml of PBS (add onto the edge), let marinate, and aspirate
3. Add 500 µL of Trypsin to each well and incubate for 5-10 minutes (until cells detach)
4. Add 500 µL of 10% FBS media to each well to neutralize Trypsin
5. For every plate, pipette both wells of the same cell type into a 15 mL conical tube
6. Spin the tubes down for 8 minutes at 1000 rpm
7. Gently remove tubes from centrifuge and aspirate media (avoid removing cell pellet)
8. Prepare a solution of RLT/B-ME using the amounts given for your plate count
9. Add 350 µL of RLT/B-ME mixture to each tube
10. Homogenize tubes for 30 seconds
11. Prepare a solution of 70% Ethanol using DEPC water and 200 Proof Biological Grade Absolute Ethanol
12. Add 350 µL of prepared 70% ethanol solution to each tube
13. Pipette all 700 µL in each 15 mL conical tube into an RNeasy mini spin column inside a collection tube
14. Spin the columns for 15 seconds at an rpm above 10,000
15. Empty the collection tubes and add 700 µL of RW1 to each spin column
16. Spin the columns for another 15 seconds and replace the collection tubes afterwards
17. Add 500 µL of RPE to each column and spin for 15 seconds
18. Empty the collection tubes and add another 500 µL of RPE

19. Spin for 2 minutes and empty the collection tubes

20. Spin for 1 minute dry

21. Remove the RNeasy mini spin column and place it in 1.5 mL conical collection tubes

22. Add 50 µL of RNase-free water to each column, and spin for 1 minute

23. Discard the spin columns and store the 1.5 conical collection tubes in a -80 □C freezer.

Notes: RNA degrades in < 1 hr, so isolation must be done as quickly as possible and with a limited number of samples to avoid lag time between steps

A.2 Total mRNA Integrity

1. Use NanoDrop ND-1000 Spectrophotometer to determine quality of RNA
2. Apply 1 drop of ddH20 10% Clorox to Nanodrop pedestal and lower sample arm until it clicks
3. Wait 1 minute.
4. Rub the upper and lower pedestals thoroughly with a kimwipe and repeat 2 more times with ddH20 10% Clorox.
5. Repeat 3 more times using a drop of ddH20
6. Blank until Nanodrop reads ±0.5
7. Place 1.5 µl of Total RNA on pedestal and run.
8. Clean pedestal with 1 drop of ddH20 after each run.
9. Run each RNA sample in duplicate.

A.3 Confocal Microscopy Of Collagen Membranes

1. Carefully remove Flexcell plates from the Flexercell and aspirate media.
2. (Start here for Coverslips) Rinse 2X for 5 min in Sterile D-PBS.
3. Fix for 30 min in the dark in fresh 4%PFA with slight agitation(4°-37°C has been cited for all rinse steps, gentle agitation is preferred on belly dancer in incubator or fridge, keep covered to avoid drying out of cells).
4. Rinse for 30 min at 4°C with PBS/0.01M Glycine/0.1%Triton-X.
5. Rinse for 15 min PBS/1%BSA.
6. Block non-specific binding for 15 min with PBS/5%NGS/1%BSA
7. Incubate overnight(12-18hr) at 4°C with gentle agitation in primary antibody solutions (for Ik-B 1:1000)Enough to submerge coverslip (i.e~2µl in 2mL PBS/1%BSA for 4-5 coverslips in wells)
8. Rinse for 2X 5min with PBS/1%BSA
9. Incubate 15 min PBS/1%BSA/1%NGS
10. Incubate 2hr w/ Goat Anti-Rabbit AF488 (1:100 or 20µl in 2ml in PBS w/1%BSA) cover with foil from here on out
11. Rinse 15min PBS/1%BSA
12. Rinse 15min PBS
13. Incubate at 4°C for 30min in (1:20-1:200 has worked well, w/varied strength of staining) AlexaFluor 635 phalloidin or Rhodamine phalloidin. Stock is 300U/1.5ml =200U/ml. 1:250 is 8µl in 2ml, final 1-10U/ml)
14. Rinse 2X 5min in PBS

15. Mount w/ Vectashield w/DAPI Place 1 drop (~25µl) carefully on coverslip surface, allow to spread evenly, excess should be wicked off the side w/ kimwipe or paper towel, invert onto coverslide, take care not to compress or shear cells, seal with clear nail polish. Store in the fridge in the dark until image acquisition.

Table 6. Reagents for Fluorescent Staining

Reagents	Company	Catalog Number	Location
Paraformaldehyde	EMS	RT-157-4	Tissue Culture Rm Fridge
Triton-X 100	Sigma		Biomedical Lab Reagent Wall
Phosphate Buffered Saline	Sigma		Tissue Culture Rm Fridge
Vectashield Mounting Media with DAPI	Vector	H-1200	Tissue Culture Rm Fridge
Normal Goat Serum	Invitrogen	PCN-5000	Tissue Culture Rm Freezer
Rhodamine Phalloidin	Molecular Probes		Tissue Culture Rm Freezer
AlexaFluor 635 Phalloidin	Molecular Probes	A34054	Tissue Culture Rm Freezer
Hoechst 33342	Molecular Probes	H21492	Tissue Culture Rm Freezer
Hoechst 33358	Molecular Probes	H1398	Tissue Culture Rm Freezer
Bovine Serum Albumin	Sigma	A 7906	Tissue Culture Rm Freezer
Dimethyl Sulfoxide (DMSO)	Sigma	D2650	Biomedical Lab Reagent Wall
Glycine	Sigma	G7126	Biomedical Lab Reagent Wall

A.4 Seeding Flexercell Plates

1. Aspirate media from flask.
2. Rinse with PBS.
3. Add enough Trypsin to submerge the bottom surface of the container and incubate for 5 minutes.
4. Add an equal amount of DMEM 10% FBS %1 ABAM and place solution in a centrifuge tube. Centrifuge for 5 min at 1000 rpm and aspirate in a supernatant.
5. Re-suspend in enough media to allow for 1 million cells/well.
6. Gently pipette 1 ml of solution into the center of each well.
7. Let incubate for 1 hour, then add 2 ml DMEM 10% FBS %1 ABAM to each well.

Table 7. Reagents for Cell Culture and Cryopreservation

Reagent	Company	Catalog Number	Location
Dulbecco's Modified Eagle's Medium	Sigma	D5796	Tissue Culture Rm Fridge
Fetal Bovine Serum	Sigma	D5652-50L	Tissue Culture Rm Freezer
Anti-biotic/Anti-mycotic	Invitrogen	15240-062	Tissue Culture Rm Freezer
Dimethyl Sulfoxide	Sigma	D2650	Tissue Culture Rm
Trypsin EDTA	Mediatech	25-053-Cl	Tissue Culture Rm Freezer
Collagenase D	Roche Diagnostics	11 088 858 001	Tissue Culture Rm Fridge
Low Temperature Freezer Vials	VWR International	16001-100	Tissue Culture Rm

A.5 Live Reactive Oxygen Species Kit

Reagents

Image-IT LIVE Green Reactive Oxygen Species Kit

Hanks Balanced Salt Solution GIBCO

Fluorophores

Carboxy-H2DCFDA 495/529

Hoechst 33342

1. Gently aspirate media or stretching medium from plates and rinse 2X 5min in PBS. Rinsing should be done with slow gentle agitation on a Belly Dancer (Stovall Life Science, Greensboro, NC) placed in an incubator for 37°C rinses or incubations, or in the refrigerator for 4°C rinses.

Notes: Prepare all reagents and antibody dilutions prior to the end of stretching experiments. AVECs may be loosely adhered at to the Collagen Type I at the conclusion of the stretching experiments, depending on duration and magnitude. Cells should never be allowed to dry out. Aspiration and rinsing steps should be done gently to prevent loss of cells from membrane.

A.6 Ex Vivo Bioreactor

Sample Harvesting and Attachment

Materials to be Autoclaved:

Forceps

Scissors

Phosphate Buffered Saline

Attachment Frame with Paraffin Wax

Well

Lid

Attachment Pins

Hooking Arms

Procedure:

1. Leaflets should be excised on-site at the slaughterhouse (Sansing Meat Service, Maben MS) directly following slaughter.
2. To ensure endothelial cell health, pigs should ideally be ~6 months old and have a post slaughter weight of no more than 120 lbs.
3. Ventricles should be cut off halfway up the heart.
4. Remove both atria.
5. The mitral ring should be cut open exposing the anterior mitral valve.
6. Observe a commissure point by looking down the aortic valve conduit and make an imaginary line following down the aorta.

7. Using this line as a guide, cut vertically straight up exposing the three aortic valve cusps. If needed, note the three leaflets as non-coronary, left and right coronary. The left and right coronary leaflets will have a coronary ostia initiating a coronary artery directly behind them.
8. Carefully grab the free hanging edge of the leaflet with the forceps, and with scissors, or a scalpel blade if preferred, cut the leaflets free one third up from the basal attachment region. Scalpels can be used, however, tend to dull very quickly while cutting through the thick pieces of tissue. The process is very time sensitive and a sharp pair of scissors should suffice, and avoid having to change razor blades in the middle of the procedure.
9. Rinse the leaflet well in Tissue solution before placing it into cold Transport solution.
10. Repeat steps 8-9 for the other two leaflets.

    Sample Attachment
11. Cut a sterile 15mmx15mm collagen membrane from a Flexcell Collagen type 1 plate.
12. Remove the leaflet from PBS and place it on the collagen square in the center of the attachment frame. Note side facing up will be side to be visualized on the LSM 510. Ventricular surface will always attempt to wrap around the fibrosa surface, which will curl up. This phenomenon is due to the natural expansion of the elastin fibers normally in compression *in vivo*.
13. Align leaflet so that circumferential direction is parallel to arms 1 and 3, and the radial direction is parallel to arms 1 and 4.

14. Pin in attachment arms, which have been premeasured to pierce the leaflet in a 10mmX10mm square. Pierce the tissue with each sample hook, making sure to pierce through the collagen membrane and into the paraffin wax. This ensures that the collagen membrane will hold the leaflet in place when transferring to the bioreactor. Hooks should be placed in order, from hook 1 to hook 4.
15. Keep tissue hydrated with PBS, ensuring the leaflet never dries out.
16. Remove locking pins holding hook arms to attachment frame.
17. While holding hooking arms to attachment frame, invert attachment frame over the well and frame, being sure to line up arms 1-4 with their corresponding spots on the translation arms. Insert locking pins into the holes that will secure the hooking arms to the translation arms.

APPENDIX B

BIOREACTOR SUPPLEMENTAL INFORMATION

B.1 Bioreactor Wall Shear Stress

$$\text{Revolutions} := \frac{1}{4}$$

$$\text{time}_{dias} := \frac{2}{3}$$

seconds

$$\text{time}_{sys} := \frac{1}{3}$$

seconds

$$\omega_{dias} := 2 \cdot \pi \cdot \left(\frac{\text{Revolutions}}{\text{time}_{dias}} \right) = 2.356$$

Hz

$$\omega_{sys} := 2 \cdot \pi \cdot \left(\frac{\text{Revolutions}}{\text{time}_{sys}} \right) = 4.712$$

Hz

Systolic Release

$$\text{radius} := 0.018$$

m

$$\rho := 1000$$

$$\frac{kg}{m^3}$$

$$\mu := 0.653 \cdot 10^{-3}$$

$$\frac{N \cdot s}{m^2}$$

$$U_{o\_sys} := \text{radius} \cdot \omega_{sys} = 0.085$$

$$\frac{m}{s}$$

$$\tau_{sys} := U_{o\_sys} \cdot \sqrt{\rho \cdot \omega_{sys} \cdot \mu} \cdot \sin\left(\omega_{sys} \cdot time_{sys} - \frac{\pi}{4}\right)$$

$$\tau_{sys} = 0.105$$

Pa

$$\tau_{sys} := 1.05$$

$$\frac{dyn}{cm^2}$$

Diastolic Release

$$U_{o\_dias} := radius \cdot \omega_{dias} = 0.042$$

$$\frac{m}{s}$$

$$\tau_{dias} := U_{o\_dias} \cdot \sqrt{\rho \cdot \omega_{dias} \cdot \mu} \cdot \sin\left(\omega_{dias} \cdot time_{dias} - \frac{\pi}{4}\right)$$

$$\tau_{dias} = 0.037$$

Pa

$$\tau_{dias} := 0.37$$

$$\frac{dyn}{cm^2}$$

B.2 Digital Imaging Workflow

Sample Image Analysis

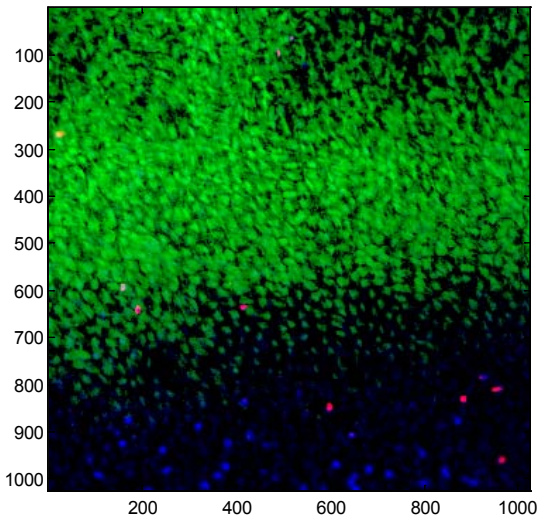

Figure 44 CLSM Image of Live (calcein, Green) and dead (ethidium homodimer, red) endothelial cells on an aortic valve leaflet.

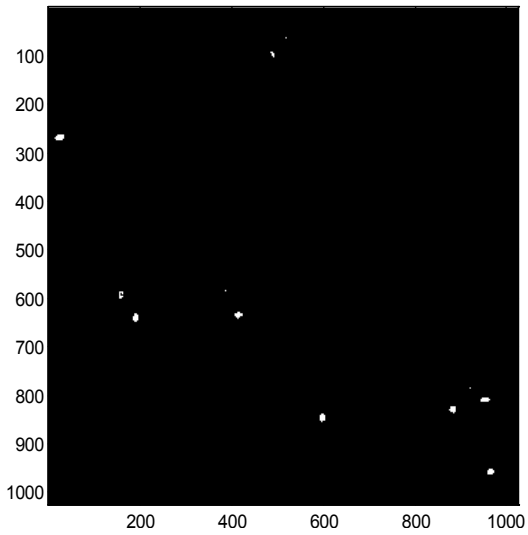

Figure 45 CLSM Image of Live (calcein, Green) and dead (ethidium homodimer, red) endothelial cells on an aortic valve leaflet. Image thresholded into Red Channel, for dead cell analysis only.

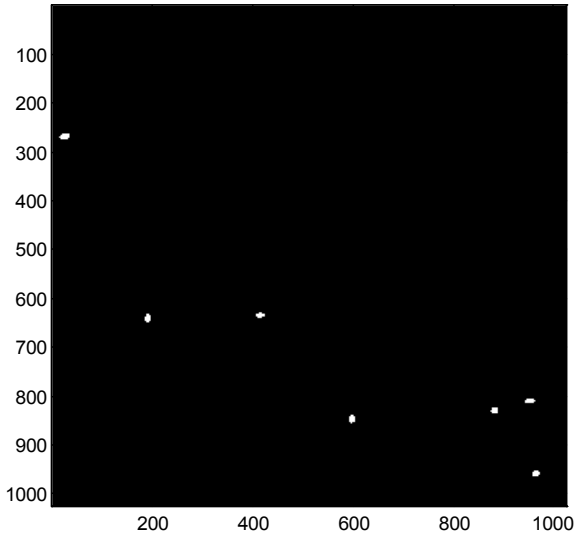

Figure 46 Red channel image of dead cells, following segmentation and 1-step erosion and dilation.

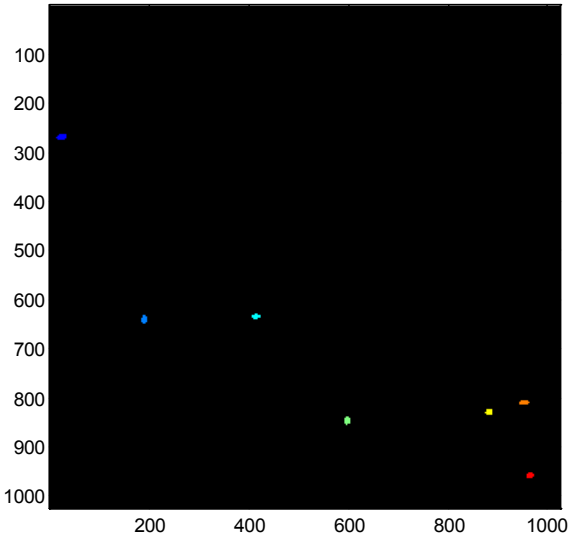

Figure 47 Final image of dead cells used for particle analysis

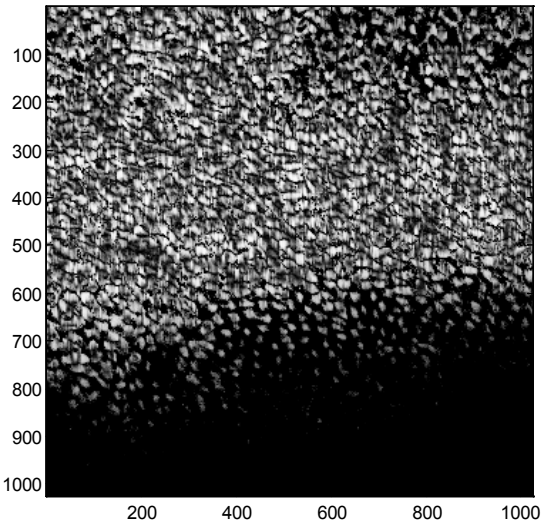

Figure 48 CLSM Image of Live (calcein, Green) and dead (ethidium homodimer, red) endothelial cells on an aortic valve leaflet. Image thresholded into Green Channel, for live cell analysis only. Image of live cells thresholded using Otsu's method.

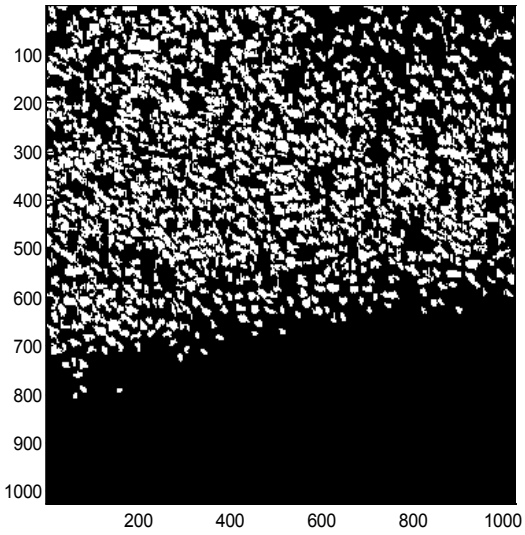

Figure 49 Live cells following segmentation and processing.

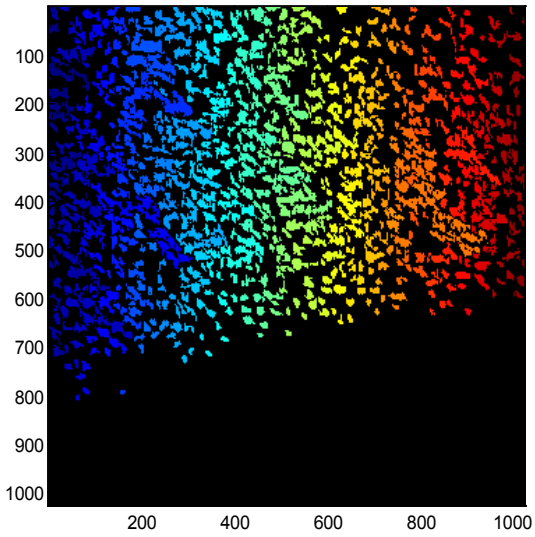

Figure 50 Matlab Image Processing Toolbox Output Image of processed and labeled Live Cells used for Particle Analysis.

B.3 Image Processing Toolbox Code

```
function [INFO channel_morph,N] = redsegment(original_image, figures)
%
%function [INFO channel_morph] = redsegment(original_image, figures)
%
% A function to segment out the (red colored) dead cells from an image
% which is 3 dimensional (RGB) data. Image usually has all red, green and
% blue content with red indicating dead cells and blue indicating nuclei.
%
%INPUTs:
%       original_image : the image for which segmentation is to performed. A
%                [1024 X 1024 X 3] sized image for this project
%       figures : boolean, shows the figures such as
%
%OUTPUTs:
%        N : gives a count of the total number of dead cells( red cells)
%        INFO : gives the needed info of the cell. A matrix with the
%                 needed info like the 'FilledArea','MajorAxisLength',
 %               'MinorAxisLength', 'Orientation', 'BoundingBox', 'centroid' etc.
%                A [cell_number X 6] matrix
%        channel_morph : binary image after cleaning up ( for ratio of area)
%

image_red = original_image(:,:,1);
image_green = original_image(:,:,2);
image_blue = original_image(:,:,3);

MINIMUM_SIZE = 75/2;
MAXIMUM_SIZE = 300/2;

channel_image = image_red;

weight_factor = 0.5;
% subtract background component from image
func1 = @(x) min(x(:,:));
channel_image_min = blkproc(channel_image,[16,16],func1);
channel_image_min = imresize(channel_image_min,[1024,1024],'bilinear');
diff_channel_image = channel_image - channel_image_min*weight_factor;

weight_factor = 0.6;
% subtract nuclei from channel image
diff_channel_blue = diff_channel_image - image_blue*weight_factor;
channel_BW = im2bw(diff_channel_blue, graythresh(diff_channel_blue));

if figures == 1
  figure,imagesc(uint8(channel_BW)),colormap(gray),axis image
  title('After blue channel and background subtraction ')
end

channel_morph = bwmorph(channel_BW,'open',1);

% erase the area smaller than minimum area
channel_morph = bwareaopen(channel_morph,MINIMUM_SIZE*2,8);
[channel_label N] = bwlabel(double(channel_morph));

% for comparison
if figures == 1
    figure,imagesc(uint8(channel_morph)),colormap(gray),axis image
    title('After mophological processing ')
end

%%% Data Analysis %
stats = regionprops(channel_label,'Area','Perimeter','Orientation',...
    'MajorAxisLength','MinorAxisLength','Centroid');
area = [stats.Area]/2;
```

```
perim = [stats.Perimeter]/sqrt(2);
circularity = 4*pi*area./(perim.^2);
orientation = [stats.Orientation];
length_major = [stats.MajorAxisLength];
length_minor = [stats.MinorAxisLength];
ratio_major_minor = length_minor./length_major;
centroid = [stats.Centroid];
cent_x = centroid(1:2:end);
cent_y = centroid(2:2:end);

% calculating minimum distance of all entries
K = length(cent_x);
mat_cent_x = repmat(cent_x,K,1) - repmat(cent_x',1,K);
mat_cent_y = repmat(cent_y,K,1) - repmat(cent_y',1,K);
mat_dist =  abs(mat_cent_x.*mat_cent_x - mat_cent_y.*mat_cent_y);
mat_dist(mat_dist == 0) = inf;
min_dist = sqrt(min(mat_dist')/2);

% putting together all information for normal size of cell( overlapped
% cells are ignored
index = find(area <= MAXIMUM_SIZE);
INFO = [ index' area(index)' perim(index)' circularity(index)' ...
   orientation(index)' length_major(index)' length_minor(index)' ...
   ratio_major_minor(index)' min_dist(index)'];

num_cell = length(INFO(:,1));
% average
INFO(num_cell+1,:) = [ 1 sum(INFO(1:num_cell,2:end))/num_cell];
% variation
INFO(num_cell+2,:) = [ 2 std(INFO(1:num_cell,2:end)) ];
%%%%%%%%%%%%%%%%%%%%%%%%%%%%%%%%%%%%%%%%%%%%%%%%%%%%%%%%

if figures == 1
   % Lable
   RGB = label2rgb(channel_label, @jet, 'k');
   figure,imagesc(RGB),colormap(gray),axis image
   title('Labeled Image')

   % Original_image with Mask
   dead_cell = double(original_image());
   dead_cell(:,:,1) = dead_cell(:,:,1) + (double(channel_morph)*255);
   dead_cell(:,:,2) = dead_cell(:,:,2) + (double(channel_morph)*255);
   dead_cell(:,:,3) = dead_cell(:,:,3) + (double(channel_morph)*255);
   figure,imagesc(uint8(dead_cell)),colormap(gray),axis image
   title('Final result on the original image')
end

function [cell_number,cell_info, live_cell] = greensegment(RGB_Image,threshold_param,parameter)
%
%function [cell_number,cell_info] = greensegment(RGB_Image,threshold,parameter)
%
% A function to segment out the (green colored) live cells from an image
% which is 3 dimensional (RGB) data. Image usually has all red, green and
% blue content with red indicating dead cells and blue indicating nuclii.
%
%INPUTs:
%       RGB_Image : the image for which segmentation is to performed. A
%                   [1024 X 1024 X 3] sized image for this project
%       threshold_param : This is to increase or decrease the gray_threshold
%                         values for red,green, blue images while converting
%                         it to a B/W image. A [1 X 3] vector in the order of
%                         [ red, green, blue]
%       parameter : This a value used for increasing or decreasing the
%                   value of the threshold applied to the histogram_equalized image
%                   when trying to convert it to a B/W image. A [1 X 1]
%                   element.
%
%OUTPUTs:
%       cell_number : gives a count of the total number of live cells( green cells)
```

```
%       cell_info : gives the needed info of the cell. A matrix with the
%                   needed info like the 'FilledArea', 'MajorAxisLength',
%                   'MinorAxisLength',  'Orientation', 'BoundingBox', 'centroid' etc.
%                    A [cell_number X 6] matrix
%

MIN_AREA = 90;
MAX_AREA = 300;
MAX_MAJ_AXIS = 30;
MAX_MIN_AXIS = 20;
image_red = RGB_Image(:,:,1);
image_green = RGB_Image(:,:,2);
image_blue = RGB_Image(:,:,3);

thre_red = graythresh(image_red); % 110
bw_red = im2bw(image_red,thre_red + threshold_param(1));

thre_green = graythresh(image_green); % 130
bw_green_1 = im2bw(image_green,thre_green + threshold_param(3));

thre_blue = graythresh(image_blue); % 125
bw_blue = im2bw(image_blue,thre_blue + threshold_param(3));

fun1 = @(x) min(x(:,:));
image_green_min = blkproc(image_green, [16,16],fun1);
image_green_min = imresize(image_green_min,[1024,1024],'bilinear');

image_green_diff = image_green - image_green_min;

image_green_diff_hist = adapthisteq(image_green_diff);

image_hist_diff = image_green_diff_hist - image_red;

thre_level = graythresh(image_hist_diff);
bw_green = im2bw(image_hist_diff,thre_level + parameter);

bw_green = bw_green - bw_blue;

 [row,col] = find(bw_green == -1);
for j = 1:length(row)
   bw_green(row(j),col(j)) = 0;
end;
bw_green_clean = bwmorph(bw_green,'clean');
bw_green_open = bwmorph(bw_green_clean,'open');
bw_green_morphed = bwmorph(bw_green_clean,'majority');

bw_green_final = bwareaopen(bw_green_morphed,MIN_AREA,8);

live_cell = bw_green_final;

[Labelled_image,num_label] = bwlabel(bw_green_final,4);
Labelled_image_RGB = label2rgb(Labelled_image, @jet, 'k');

cell_number = num_label;

STATS = regionprops(Labelled_image,'FilledArea','Area','Perimeter','Orientation',...
   'MajorAxisLength','MinorAxisLength','Centroid');
for i = 1:num_label
   if(STATS(i,1).FilledArea > MAX_AREA)
      if(STATS(i,1).MajorAxisLength > MAX_MAJ_AXIS | STATS(i,1).MinorAxisLength > MAX_MIN_AXIS)
          cell_number = cell_number + 1;
       end;
   end;
   if(STATS(i,1).FilledArea < MIN_AREA/2)
      cell_number = cell_number - 1;
   end;
end;
area = [STATS.Area]/2;
perim = [STATS.Perimeter]/sqrt(2);
```

```
circularity = 4*pi*area./(perim.^2);
orientation = [STATS.Orientation];
length_major = [STATS.MajorAxisLength];
length_minor = [STATS.MinorAxisLength];
ratio_major_minor = length_minor./length_major;
centroid = [STATS.Centroid];
cent_x = centroid(1:2:end);
cent_y = centroid(2:2:end);

% calculateing minimum distance of all entries
K = length(cent_x);
mat_cent_x = repmat(cent_x,K,1) - repmat(cent_x',1,K);
mat_cent_y = repmat(cent_y,K,1) - repmat(cent_y',1,K);
mat_dist =  abs(mat_cent_x.*mat_cent_x - mat_cent_y.*mat_cent_y);
mat_dist(mat_dist == 0) = inf;
min_dist = sqrt(min(mat_dist')/2);

% putting together all information for normal size of cell( overlapped
% cells are ignored
index = find(area >= MIN_AREA/2 & area <= MAX_AREA/2);
INFO = [ index' area(index)' perim(index)' circularity(index)' ...
   orientation(index)' length_major(index)' length_minor(index)' ...
   ratio_major_minor(index)' min_dist(index)'];


num_cell = length(INFO(:,1));
% average
INFO(num_cell+1,:) = [ 1 sum(INFO(1:num_cell,2:end))/num_cell];
% variation
INFO(num_cell+2,:) = [ 2 std(INFO(1:num_cell,2:end)) ];
%%%%%%%%%%%%%%%%%%%%%%%%%%%%%%%%%%%%%%%%%%%%%%%%%%%%%%%%

cell_info = INFO;


function [ratio Num_dead_cell Num_live_cell]  = extractInfo(output_file_name,file_name)
%
%function [ratio Num_dead_cell Num_live_cell]  =
%extractInfo(output_file_name,file_name)
%
% A function that runs the redsegemnt and greensegment to collect essential
% data such as area, perimeter, and live-dead cell ratio
%
%INPUTs:
%       output_file_name : file name for output
%       file_name : input file name
%
%OUTPUTs:
%        ratio : live-dead cell ratio based on area (pixel count)
%        Num_dead_cell : number of dead cells
%        Num_live_cell : number of live cells
%

close all;
addpath(genpath('./ECE8473TIFFs'))
file_name_image = [ file_name '.tif' ];
original_image = imread(file_name_image);

FIGURES = 0;
ISGREEN = 1;

if FIGURES == 1
   figure,imagesc(original_image),colormap(gray),axis image
end

tic
[INFO_red dead_cell N] = redsegemant(original_image, FIGURES);
toc
Num_dead_cell = N;
```

```
Area_Dead_Cell = sum(dead_cell(:));parameter = 0.15;
threshold_param = [0.25 0.24 0.35];

% the result should be binary image so that we can calculate the number
% of pixels.
tic
[cell_number,INFO_green, live_cell] = greensegment(original_image,threshold_param,parameter);
toc
Num_live_cell = cell_number;
Area_Live_Cell = sum(live_cell(:));

ratio = Area_Live_Cell/(Area_Live_Cell + Area_Dead_Cell);

red_file_name = [file_name '_red'];
xlswrite(output_file_name,INFO_red,red_file_name);
green_file_name = [file_name '_green'];
xlswrite(output_file_name, INFO_green,green_file_name);
```

B.4 Labview Subvi For Bioreactor

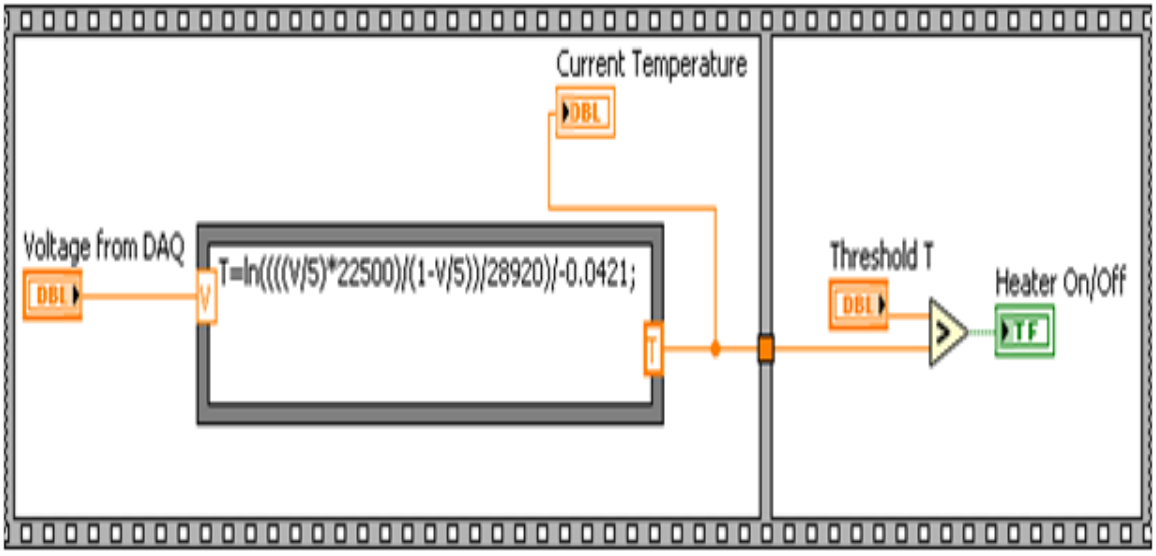

Figure 51 Labview Subvi Temperature control. Heater is turned on and off if the current temperature is outside the range specified by the threshold temperature.

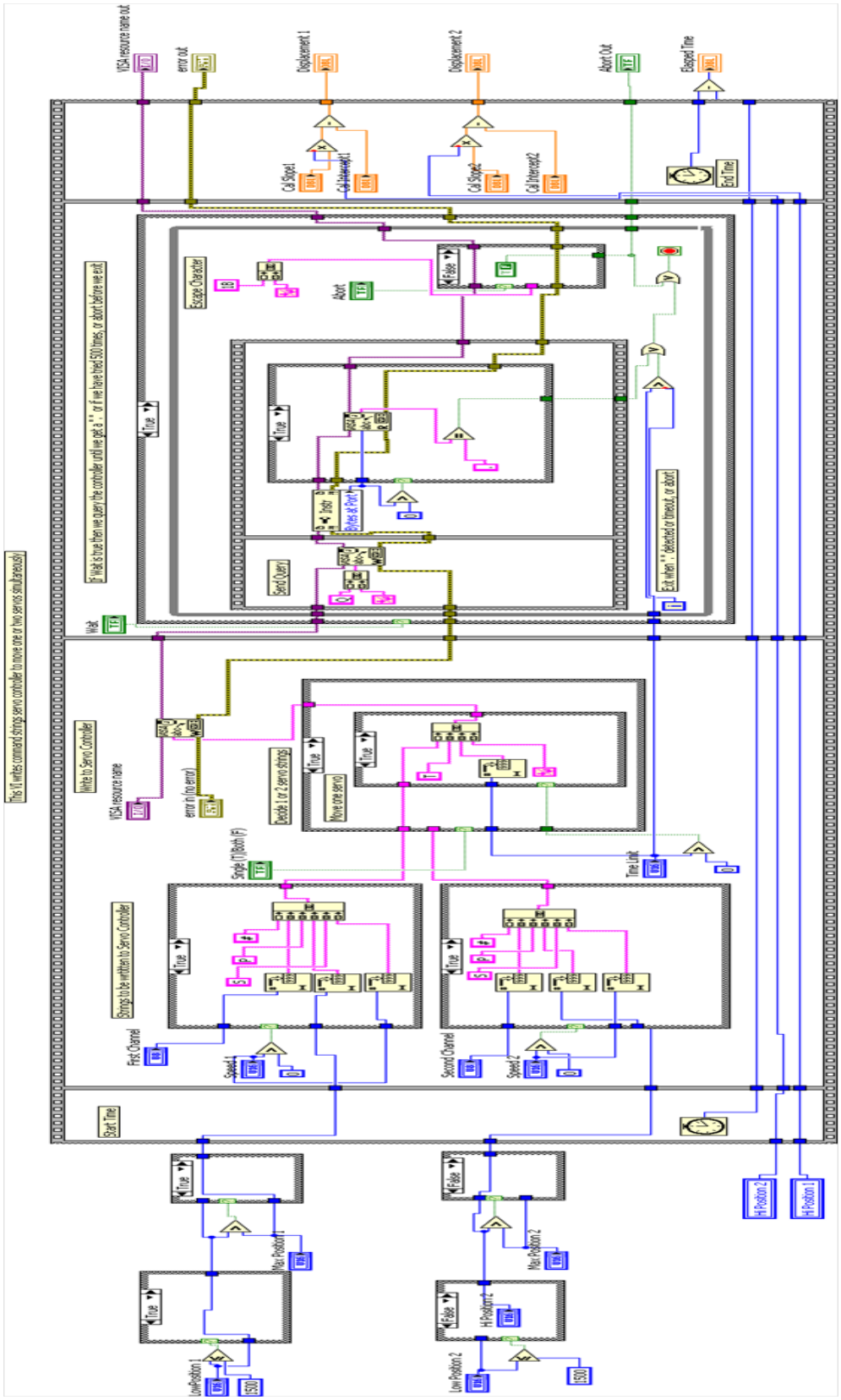

Figure 52 Labview Subvi for Servo motor positioning, note the outputs on the right of displacement and time.

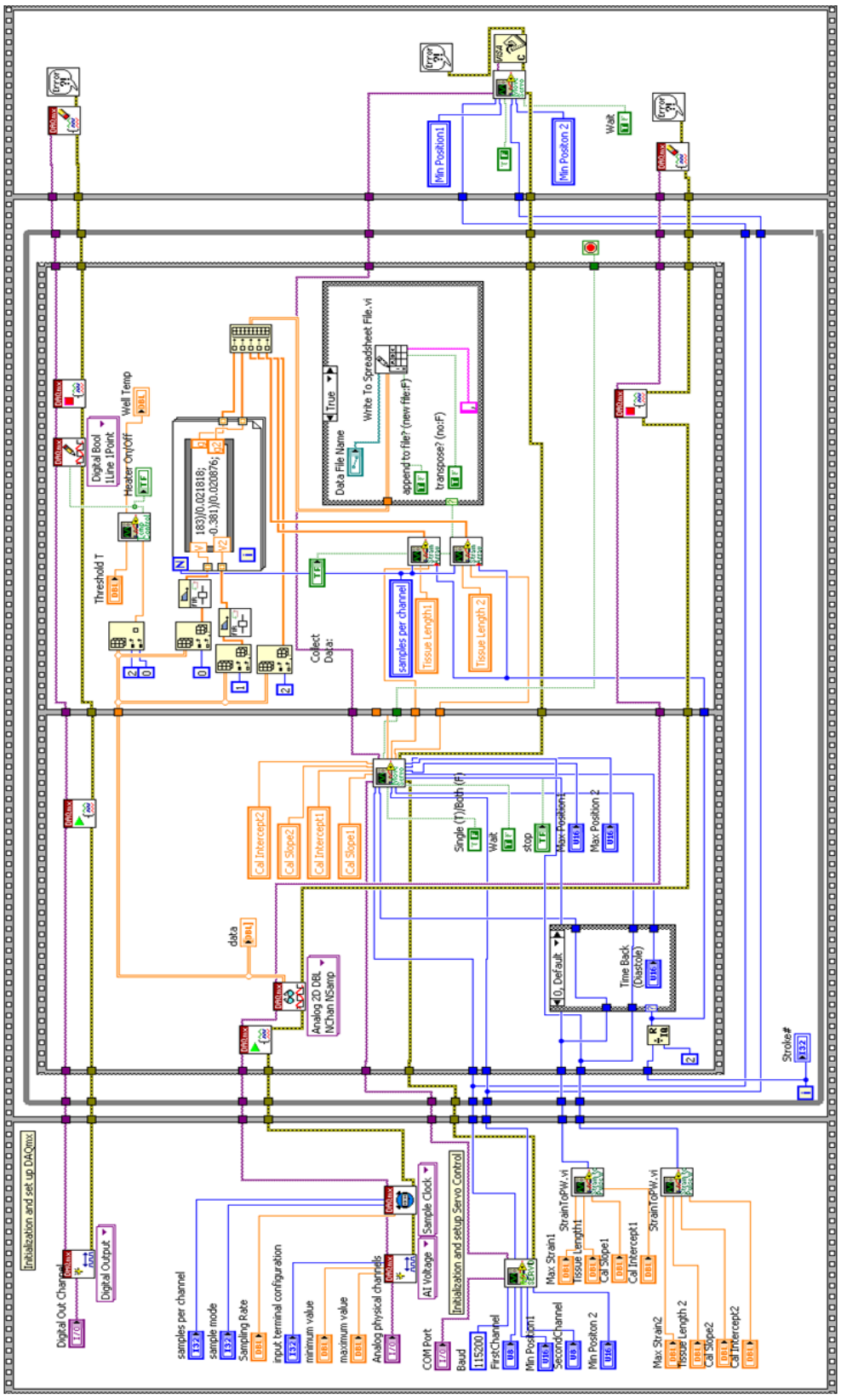

Figure 53 Labview Subvi for data collection. Note the inputs of strain and tissue length and output writing to an excel file in the center.